3-10-2010

Thrust and Performance Study of Micro Pulsed Plasma

Jeremy J. Selstrom

THRUST AND PERFORMANCE STUDY OF MICRO PULSED PLASMA THRUSTERS

THESIS

Jeremy J. Selstrom, Captain, USAF

AFIT/GAE/ENY/10-M21

DEPARTMENT OF THE AIR FORCE
AIR UNIVERSITY

AIR FORCE INSTITUTE OF TECHNOLOGY

Wright-Patterson Air Force Base, Ohio

AFIT/GAE/ENY/10-M21

THRUST AND PERFORMANCE STUDY OF MICRO PULSED PLASMA THRUSTERS

THESIS

Presented to the Faculty

Department of Aeronautics and Astronautics

Graduate School of Engineering and Management

Air Force Institute of Technology

Air University

Air Education and Training Command

In Partial Fulfillment of the Requirements for the

Degree of Master of Science in Aeronautical Engineering

Jeremy J. Selstrom

Captain, USAF

March 2010

AFIT/GAE/ENY/10-M21

THRUST AND PERFORMANCE STUDY OF MICRO PULSED PLASMA THRUSTERS

Jeremy J. Selstrom

Captain, USAF

March 2010

Approved:

_____/Signed/_____	5 March 2010
Lt Col Richard D. Branam, USAF (Chairman)	date
_____/Signed/_____	5 March 2010
Lt Col Richard E. Huffman (Member)	date
_____/Signed/_____	5 March 2010
Dr. William A. Hargus, III (Member)	date

Abstract

Currently there is a need for precision pointing, station keeping, orbital insertion and attitude control on small satellites on the scale of 1-100kg. For satellites of this size a need exits for small devices capable of producing small impulse bits that will not overwhelm such a small satellite. Chemical propulsive devices are too large and cannot produce the small impulse bits needed for these satellites. The answer to this problem appears to be electric thrusters. This type of propulsive device turns electrical power into thrust. These thrusters can be made very small and also have I_{sp}'s much larger than chemical devices. This allows electric devices to be used on even the smallest of satellites due to their small size and almost as important the less fuel they require due to their high I_{sp}'s. For the smallest of satellites or for precision control the device of choice is the micro-Pulsed Plasma Thruster (µPPT). These devices are extremely small, only 20mm in diameter and a few centimeters long. The propellant is polytetraflouroethylene (PTFE), also known as PTFE™, which is contained entirely within the thruster, reducing the complexity of the device, eliminating the need for propellant tanks or feed lines. The operation of the thruster is also less complex than other electric thrusters and chemical devices. By creating an arc between an imbedded cathode within the propellant to the anode which surrounds the PTFE, pieces of the PTFE can be ablated and ionized from the surface. The electromagnetic forces present due to the arc then accelerate the propellant creating very small impulse bits, on the order micro-Newtons. Originally developed at the Propulsion Directorate of the Air force Research Laboratory located at Edwards AFB, CA, as a smaller version of the widely tested Pulsed Plasma thruster, the µPPT has not been tested as extensively as the PPT. This research is focused on several areas of the

µPPT performance. An important idea studied is the effect of lifetime use on the performance. The thruster is fired for a simulated lifetime of use to see if there is an impact on the thrust of the thruster later in life. Also vital is the efficiency of the thruster. A µPPT performing at max efficiency will ionize all ablated material; however, we know that not to be the case. In this research the effort is made to collect these non-ionized particles in order to measure their mass post-test. With this collected mass and a knowledge of how much the thruster has ablated, it can be determined what percentage of the propellant has been ionized. With the non-ionized particles also comes a concern about contamination. Knowing the amount of particles that can collect at the end of a lifetime of use allows a better understanding of what contamination issues a spacecraft may have and what precautions need to be made.

Acknowledgements

My name may be on the cover of this paper, but without the help and support of a large group of people, the paper would not exist. First I would like to thank Lt Col Richard Branam who stuck with me through thick and thin (to include every piece of lab equipment I touched breaking except an oscilloscope) and gave countless hours to help me troubleshoot equipment and solve several analysis and conceptual issues. The AFIT laboratory staff, Jay Anderson, Chris Zickafoose, Sean Miller, Barry Page, John Hixenbaugh and Wilbur Lacy from ENY and Greg Smith from ENP, provided countless hours and effort to help me complete this research. I have yet found a problem these gentleman cannot solve and trust me, I tried. I would also like to thank my family who put up with all the phone calls and random emails venting about my thesis. They truly provided a lot of support and an escape from the world of µPPTs. Lastly, I would like to thank the Air Force for once again teaching me to be careful for what I wish for.

Table of Contents

Page

List of Figures

Page

List of Tables

List of Symbols

Symbol	
A	Plate Area
A_r	Ratio of LDS and Thruster Radii
B	Magnetic Field Strength (T)
C	Capacitor
C	Dampening Coefficient
D	Plate Diameter
d	Plates Separation Distance
E	Applied Electric Field (V/m)
E'	Effective Electric Field (V/m)
F	Farad
$F(t)$	Forcing Function
g	gram
g_o	Gravity, 9.81 m/s^2
I	Impulse Bit, Moment of Interia
Hz	Hertz
I_{sp}	Specific Impulse (s)
J	Current (A)
K	CV_o^2 Conversion factor, 96485 (A*s/F)
L	Inductor
M_t	Mass Lost by the Thruster
M_b	Mass Gained by the Collection Bowl
m	milli
$\dot{m}$	Mass Flow (kg/s)
N	Newton
N	Number of capacitors
Q	Charge of the Plates
q	Charge of the Moving Particles (C)
R	Given Ratio for Arm Movement to Distance Moved (V/m)
R_a	Radius of the Anode
R_c	Radius of the Cathode
r_{LDS}	Radius to LDS Tip (m)
r_t	Radius to Thruster (m)
S	Switch
T	Tesla
torr	Pressure
V	Volts
V_{in}	Input Voltage
V_{LDS}	Measured Voltage (V)
V_{out}	Output Voltage
ε_o	Permittivity of Free Space
η	Efficiency
η_f	Frozen Flow Efficiency
η_{heat}	Heat Loss Efficiency

η_o	Overall Efficiency
η_{ppu}	Power Processing Unit Efficiency
η_{prop}	Propellant Efficiency
η_{sh}	Sheath Efficiency
η_{trans}	Transfer Efficiency
Γ	Dampening Coefficient
θ	Motion of arm (rad)
Φ	Late-term Ablation Factor
μ	micro, Torsional Spring Constant
μ_o	Material Permittivity
ν	Fire Rate (Hz), Particle Velocity (m/s)
ω	Natural Frequency (Hz)
$w_r.$	Frequency Response

List of Abbreviations

Abbreviation	
AFIT	Air Force Institute of Technology
AFRL	Air Force Research Laboratory
BNC	Coaxial Connector
CCD	Charge Coupled Device
DAQ	Data Acquisition System
DC	Direct Current
GNAT	Geo-orbital Nano-thruster Analysis and Testing Lab
LC	Inductor/Capacitor Circuit
LDS	Laser Displacement System
PPT	Pulsed Plasma Thruster
TVAC	Temperature Vacuum Chamber
uPPT	Micro-Pulsed Plasma Thruster
XPPT-1	Thruster used at AFRL

Thrust and Performance Study of Micro Pulsed Plasma Thrusters

I. Introduction

I.1 Background

An increasing need for propulsion devices for precision pointing, station keeping, orbital insertion and attitude control of small satellites exists. These satellites have been classified as mini-satellite (100 - 500 kg), micro-satellite (10 - 100 kg), nano-satellites (10 - 100 kg) and pico-satillites (1 - 10 kg). Chemical propulsion devices are ideal for larger satellites, but have several drawbacks for satellites of these sizes. Chemical devices have an I_{sp} of around 200-400s. The lower I_{sp} is acceptable for launch and large satellites because chemical rockets produce large amounts of thrust, but require large amounts of propellant. In addition, chemical rockets cannot create the very small impulse bits required for small satellites; large impulse bits would simply overwhelm the satellite, placing it in the wrong orbit. So another type of device is needed, one that has a high I_{sp} in order to be more fuel efficient and yet create small impulse bits for the precise maneuvers required by the small satellites. One type of propulsive device fitting the unique set of criteria is electric propulsive devices. Electric devices have extremely high I_{sp}'s, in the range of 5,000 s and higher, are physically small and create impulse bits anywhere from hundreds of Newtons down to micro-Newton levels. These characteristics make them the best choice for the emerging small satellite arena.

I.1.1 Electric Propulsion

Unlike chemical devices (solid or liquid) which heat a gas to create thrust, electric devices produce thrust by several different methods. There are three main types of electric devices. The first are electro-thermal, such as Resistojets and Arcjets, which use electricity to heat a gaseous propellant. The next type is electro-magnetic, for example Ion and Hall Effect thrusters. Electro-dynamic devices ionize and electrodynamically accelerate a propellant. The last kind is electro-dynamic and magnetodynamic thrusters, most common of which are the Pulsed Plasma Thruster (PPT) and the micro-Pulsed Plasma Thruster (μPPT). The electro-magnetic devices use an arc to ablate and ionize a solid propellant.

I.1.1.1 Electro-Thermal

Arcjets and Resistojets, used successfully in flight for station keeping, have I_{sp}'s[1] on the order of 1000 s, thus proving to be extremely fuel efficient. The higher specific impulse allows them to have a small propellant tank, even for long duration missions. Being relatively large for electric devices (on the order of a few kilograms and 10 to 20 cm in length) makes them very useful for mini-satellites and some micro-satellites, but would not fit on smaller satellites.

The arcjet uses an arc between a cathode, located just prior to a constrictor, and an anode, located in the nozzle. The arc passes through the constrictor section superheating a gas which then expands through the nozzle.

Although the arcjet and resistojet are electrical devices, using electric current to heat a gas, they also expand the heated gas through a nozzle to produce thrust, relating them to chemical propulsion systems. As the gas expands through the nozzle, the gas

pressure increases accelerating the flow through a momentum transfer, creating thrust. There is no use of electromagnetic fields to ionize, or accelerate the flow. This aerodynamic process makes these devices slightly different from other electric devices using the electromagnetic field for thrust.

I.1.1.2 Electro-Magnetic

Ion and Hall Effect thrusters have also flown on several orbital missions as both station keeping and orbit insertion devices. Ion thrusters have also been used as the main engine on deep space missions, the most well known being DEEP SPACE-1. The size can vary based on the needs of the satellite, from small, just a few Watts of power to the extreme of several thousand-watt sizes. These devices use a gaseous propellant and therefore require a fuel tank in order to operate. However, with an I_{sp}[1] in the range of 1500-3000 s, they too can carry a smaller tank providing the propellant for long missions. Due to the versatile size, these types of device are perfect for use on micro- to mini-satellites or even larger satellites.

These devices work very differently from the arcjet and resistojets discussed above. For ion thrusters, the gas is ionized rather than heated. Injected gas into the chamber passes through an electric field, introducing the neutral atoms to high-energy free electrons. These electrons collide with the neutral gas, ionizing most of the gas. The electrons are contained within this chamber by a charged set of grids at the opening. One grid, held at high potential, with the other grid at ground, creates a potential difference. A force due to the potential difference, repels the electrons, but attracts the ions, accelerating them through the opening of the grids. The acceleration produces a momentum exchange, thus providing thrust. Another stream of electrons being emitted

by an external cathode neutralize the ions after leaving the thruster. This neutralization is necessary so the ions do not travel back to the satellite damaging the other systems onboard.

As the high potential grid is charged, it will want to expand and can move closer to the ground and cause an arc to form. The curve biases the grids to bend in a certain way, reducing the likelihood of them expanding towards each other.

Hall Effect thrusters also ionize a propellant gas; however, in a much different way. An electromagnet surrounds the chamber creating a magnetic field in the radial direction inside the chamber. The magnetic field attracts some of the free electrons emitted from a cathode external to the chamber. The magnetic field eventually captures these electrons and due to their charge, they begin to spin along the magnetic field lines inside the chamber, in motion known as the Hall Effect. Injected into the chamber, a neutral gaseous propellant ionizes as it passes through the free electrons caught in the Hall Effect. The electric and magnetic fields present in the chamber then accelerate the newly formed ions out of the chamber, as described by the Lorentz force. The momentum exchange produces the thrust. The electrons emitted by the cathode and not attracted by the magnetic fields, combine with the emitted ions to form a quasi-neutral plasma.

I.1.1.3 Electro-Dynamic

PPTs, extremely small propulsion devices, are only a few centimeters to a few millimeters in size. Unlike the other electric devices using a gaseous propellant, PPTs typically use a solid propellant (i.e. polytetraflouroethylene (PTFE), more commonly known as Teflon™). Using a solid propellant requires the propellant be stored inside the

thruster itself, eliminating the need for a storage tank as well as all the complexity it adds to the device. With a thrust in the range of milli- to micro-Newtons, PPTs are best used for nano- and pico-satellites. Having an I_{sp}[1] near 1000 s, makes PPTs slightly less desirable than other devices, but small size and rather simplistic design more than make up for any disadvantage they may have requiring more fuel for a similar velocity change.

PPTs and µPPTs use the same mechanism to produce thrust. These devices also use an electro-magnetic force to accelerate ions, much differently than the ion and Hall Effect thruster. Here, an arc forms from a cathode to an anode across the surface of the propellant. This arc heats and ablates the top surface of the propellant. The particles pass through the arc, ionize into plasma, and accelerate away from the thruster by the induced electromagnetic field created by the arc itself. The Lorentz force again explains how the thruster produces thrust, as in this case the ions are pushing on the electro-magnetic field. The formation of the electromagnetic field accelerates both the free electrons and ions away from the thruster in the same direction, although they are spinning in opposite directions forming a quasi-neutral plasma. Although inside the plasma, there are regions of differing charge, outside the plasma the net charge is very close to zero. The quasi-neutral plasma removes the need to have a second emitter of free electrons to neutralize the plasma like in the Hall thrusters.

PPTs and µPPTs are structurally different due to their differing sizes. The PPT, being larger, can afford to be more complex. This size thruster typically has a breech or spring fed propellant system. This design keeps the surface of the propellant collocated with the igniter used to create the arc between the cathode and anode. The µPPT, however, is structurally much simpler than the PPT due to its extremely small size. The

cylindrical shape of μPPT stores the propellant inside the tube between the inner and outer electrodes. Some μPPTs have three electrodes with an intermediate cathode set to ground, very close to an inner high voltage anode, imbedded inside the propellant, forming an inner cylinder. The inner cylinder forms an improvised spark igniter. μPPTs do not need to feed the propellant to the tip of the thruster. The electrodes erode during the arc formation, due to the small size, keeping spark level with the electrodes and the propellant.

I.1.2 μPPTs for use on small satellites

These devices are widely proposed on pico-satellites (1 – 100 kg) due to their small size, large I_{sp} and low impulse bit, creating on the order of micro-Newtons of thrust. Their size makes them easily integrated into even the smallest of satellites. They have extremely long lifetimes due to the high I_{sp} and their low thrust levels will not overwhelm small satellites and negatively interfere with their orbit.

I.1.3 History of PPTs and μPPTs

I.1.3.1 PPTs

The first PPT was flown on the Zond-2 spacecraft in 1964 launched by the former Soviet Union[2]. The first US launched PPT was onboard the LES-6 mission in 1968. In 1976 the LES-8 and LES-9 satellites tested PPTs for use as station-keeping devices. The Transit Improvement Program (TIP) used PPTs for drag correction in the TIP II and TIP III satellites in 1975 and 1976 respectively. The first satellite navigation system, the Navy Navigation System (NNS) had three satellites using PPT for drag corrections in the

1980s. More recently, the Earth observing satellite (EO-1) uses a dual-axis PPT for pitch control as well as momentum management.

μPPTs were developed by the Air Force Research Laboratory, Propulsion Directorate at Edwards AFB CA. They were created to fill a need for smaller thrusters to provide small impulse bits on nano- and pico-satellites. One such spacecraft is the Dawg-Star. Falcon Sat-III demonstrated the use of a 3-axis μPPT for orbit stabilization. However, the μPPT falls well behind the PPT in terms of time in space. μPPTs require added missions and time in space to become a trusted space propulsion device used on more important missions.

I.2 Problem Statement

μPPTs, being a new variation on the PPT, have not completed rigorous studies of their performance unlike the large amount of research completed on the PPT. Most work has been limited to the short-term function of the thruster to determine I_{sp}, thrust and propellant efficiency. However, these parameters may change throughout the lifetime of a thruster as it ablates more and more propellant. Therefore, a major focus of this paper will be determining the lifetime performance of a thruster and any changes occurring throughout. The PPT gives off solid particulates from the failure to ionize all of the propellant and the erosion of the electrodes. These particles are very small, but over the lifetime of the thruster can add up and heavily contaminate the satellite and other nearby objects. These same phenomena happen in μPPTs. Yet to be determined directly is the total mass of these particles. Knowing the total mass of the emitted particles can give a better understanding of the efficiency of the thruster. Additionally, by measuring the

mass lost periodically through the lifetime of the thruster, any performance fluctuations over time can be identified.

I.3 Objectives

This research has many objectives all related to the overall life performance of μPPTs. The main characteristic of the device will be the overall thrust the device is capable of providing over the lifetime of the thruster. The idea is to see if a μPPT coming to the end of its expected life will suffer any change in the thrust it is capable of producing. Another effect on the performance of the thruster is the efficiency loss due to the propellant ablated but not ionized. By measuring the thruster pre- and post-test, an average mass ablated can be found. Knowing ablated mass and the thrust produced gives propellant efficiency of the thruster. The total efficiency of the thruster to turn the input power into thrust gives an important characteristic of the thruster. With all of the data, a lifespan of the thruster can be determined giving an operationally effective limit on these thrusters. Furthermore, knowing the particulate mass helps to understand the contamination potentially expected on the satellite and nearby objects over the lifetime of the thruster.

I.4 End State

The end state of the research will be a rigorous study of the μPPT allowing future space planners the ability to judge the appropriate mission profile and usage of the μPPT. The contamination study will help satellite designers ensure proper placement to limit contamination on solar panels and sensitive instruments.

II. Theory and Previous Research

II.1 Pulsed Plasma Thruster

Most other propulsive devices rely heavily on their geometry to determine their performance characteristics, for example their expansion ratio or burn area. However, PPTs are not so reliant on geometry for their performance. The main requirement is simply the cathode and anode form an arc across the surface of the propellant. Otherwise, there is no set requirement for the propellant feed system or where the arc is formed.

Figure 1 shows the basic design of most PPTs. In this design, a spring feeds the propellant to be even with the cathode and anode. A spark igniter provides the breakdown voltage between the cathode and anode to form the arc. A separate capacitor powers the cathode. For the PPT, there is no nozzle as the Lorentz force accelerates the plasma. The spring then pushes the propellant even with the electrodes for the next firing.

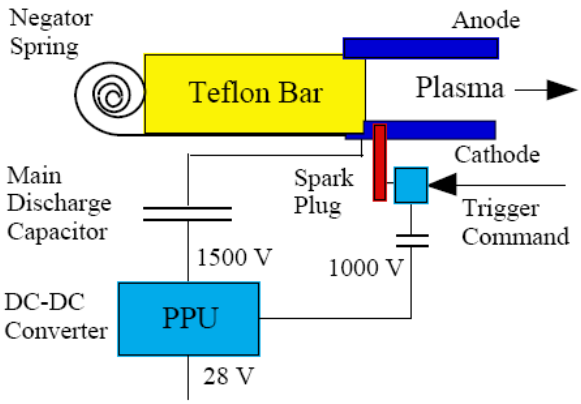

Figure 1: Pulsed Plasma Thruster[3]

Another design option is a side-fed or also referred to as a breech-fed system. In this design, two pieces of propellant enter from the sides forming a channel in the thruster and increasing the surface area the arc covers. The increased amount of propellant ionized with each pulse produces more thrust. Also, the plasma is focused straighter out of the thruster, eliminating sideways movement within the plasma. Focusing the plasma retains any thrust that would be lost by moving out from centerline.

II.2 Micro-Pulsed Plasma Thruster

The µPPT works the same way as the PPT, as stated above, but is much smaller. The small size eliminates need for a propellant feed system. Coaxial central cathodes and outer anodes with propellant set between form the basic design of all µPPTs Figure 2 shows the basic setup of a two-electrode thruster.

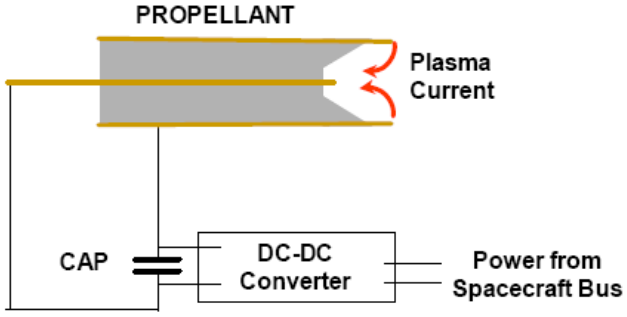

Figure 2: Two-electrode micro-PPT[4]

The design eliminates the need for a propellant feed system as the cathode and anode actually ablate at about the same rate as the propellant. Unlike PPTs requiring a spark igniter, these devices are small enough where the electrode potential overcomes the

breakdown voltage removing the need for the igniter to provide a seed plasma. The two-electrode design often dictates a small, ideal operating range in terms of energy discharge. Operating these thrusters at too high an energy will char the propellant and increase the resistivity across the surface, since charred propellant is electrically insulating. A charred surface will then require higher breakdown voltages.

However, the use of a virtual igniter can ease the formation of the spark. In the three-electrode design, a second electrode, imbedded in the propellant very close to the central anode, forms the virtual igniter or trigger, as in Figure 3.

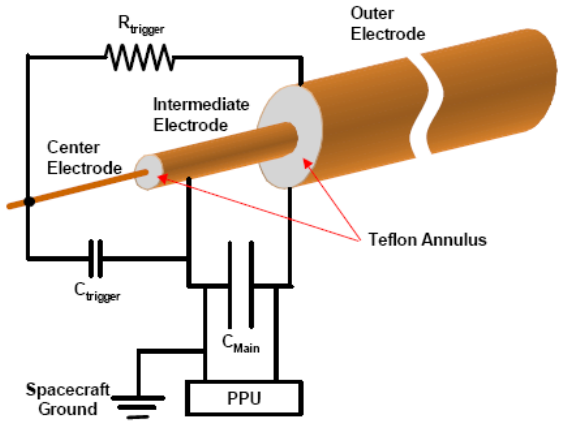

Figure 3: Three-electrode micro-PPT[4]

Placing the central electrodes very close together decreases the required breakdown voltage, lowering the required voltage potentials to form the arc. The arc ablates and ionizes the little bit of propellant between these electrodes. The high-energy seed plasma begins to spread towards the outer high-voltage anode, adding to the electric potential already created by the electric pulse, forming an arc over the larger outer surface area. It is this larger area that produces most of the ablated propellant and thus thrust. By using this seed plasma as an igniter, the overall power requirements of the

thruster can be lowered since not as much power needs to be fed to the outer, very high voltage, electrode to form the arc. This triggered design also improves the reliability and controllability of these thrusters. This is the main design investigated in this paper.

II.3 Pulsed Power and Arc Formation

II.3.1 Circuit Design

A pulsed circuit fires the μPPT providing the power for the thruster to operate at up to 5 Hz. The breakdown voltage for the formation of an arc across the surface of a μPPT is very large, about 1400 V, which is not possible for a satellite power bus to sustain. It is then required to have some sort of generator or transformer that can take a low voltage and create a pulsed, higher voltage discharge.

The circuit starts with a DC-DC power supply providing a low voltage current to the pulse generator. This device uses a transformer (in this case, a Marx generator could be used as well, as discussed below) to convert the low voltage to a very high voltage, but short pulse. The inner anode of the μPPT is set at the high potential. The outer anode receives charge through a separate smaller circuit using capacitors in much the same way. The cathode is kept as close to ground potential as possible. The difference in voltages creates a very large potential in the electrodes. The potential forms the arc as discussed later in this chapter, focusing the discussion for now on each component of the circuit design.

II.3.1.1 Power Supply

The power supply typically provides a voltage of only 1-5 V. This is an acceptable sustained load for a satellite, but well below the required breakdown voltage

of the thruster. The power supplied needs to be a continuous DC voltage in order to charge the transformer, whether it is an induction circuit or a capacitor circuit. No special requirement exists for type of power supply used beyond the DC requirement. The important aspect is the satellite is capable of producing this voltage continuously for the duration of operation of the thruster.

II.3.1.2 Generators

Several generator designs are used to increase the input voltage to a very large output voltage. The simplest design is the Marx Generator[5] as described by Dr. Gennady Mesyats, which creates large voltages by putting capacitors in series.

One design has the capacitors in series connected through switches. Resistors, placed purposefully in the circuit, keep the current flowing towards the next capacitor and not back to the previous one, as seen in Figure 4.

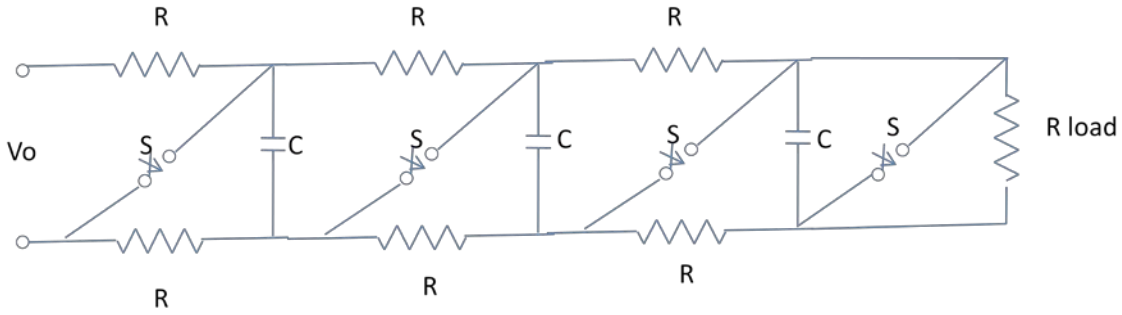

Figure 4: Marx circuit for voltage multiplication[5]

By using this circuit, the voltage can be increased by

$$V_{out} = NV_{in} \qquad \text{Eq. 1}$$

Where N is the number of capacitors, V_{in} is the input voltage and V_{out} is the output voltage. However, the generator has the added complexity of the switches must all be thrown simultaneously in order for the voltage to be multiplied.

This circuit is very simple, but not very efficient. A better version of this generator proposed by Dr. Mesyats involves the use of inductors as well as capacitors. In this circuit, switches, Figure 5, connect each LC circuit.

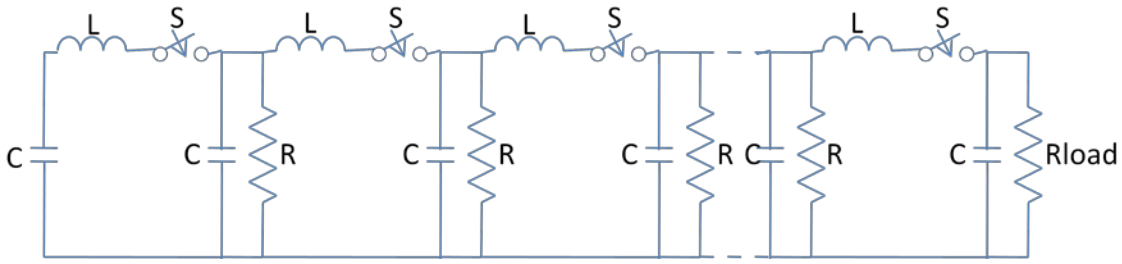

Figure 5: Dr. Mesyats more efficient voltage multiplier[5]

In this case, the switches are fired sequentially, allowing each LC circuit to charge from the discharge of the previous circuit. By firing the switches sequentially removes the complexity of firing them all at once, making this much more reliable circuit. Once the last switch closes, the full charge is then seen across the load resistor, in this case the µPPT. Using this circuit, voltage multiplication is calculated as

$$V_{out} \approx 2^N V_{in} \qquad \text{Eq. 2}$$

V_{out} increases by a power of two as the number of stages is increased. In this circuit, there is a chance the capacitors will not completely discharge into the next capacitor but can actually discharge backwards into the previous capacitor. This loss will decrease the max voltage obtained from this generator. When using this circuit, the design should include a buffer for this effect.

II.3.1.3 Transformers

Transformers are widely used for microsecond pulse creations due to their ability to fire repetitively, and are excellent choices for satellites due to their small size and reliability. Transformers use coupled oscillatory LC circuits. Figure 6 shows an example of a transformer circuit.

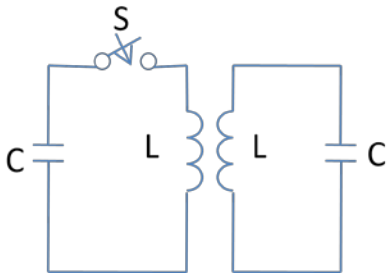

Figure 6: Simple Tesla Transformer[5]

This type of circuit increases the voltage from circuit LC1 to LC2 by passing the current through an inducted magnetic field between the coils of each circuit. The possible output voltage for this circuit given by

$$V_{2max} = V_1\sqrt{\frac{C_1}{C_2}} \qquad \text{Eq. 3}$$

Where C_1 and C_2 are the capacitances of each LC circuit respectively, and the V_1 and V_{2max} are the voltages of each circuit.

Transformers are highly useful for the purposes of μPPTs. They can provide the required voltage multiplication and can create microsecond pulses to create the needed operating conditions for the thruster, perfect for the μPPT.

II.3.2 µPPT Discharge

Once the power supply has charged the transformer and the transformer has created a microsecond pulse at a higher voltage, the power passes to the anode of the µPPT. The cathode feels the high voltage causing electrons to build up at the edge of the cathode since they are attracted to the high voltage. The buildup of electrons forms an electric field in the cathode. If this electric field gets strong enough to reach the necessary breakdown voltage of the cathode, then the needed arc will form across the surface, to ablate, ionize and accelerate the propellant. The creation of this arc is a multistep process, ultimately leading to the breakdown and arcing of the circuit, allowing a current to pass.

II.3.2.1 Discharge in a vacuum

The three main parts to a vacuum discharge are breakdown, spark and finally arc formation. Breakdown is the period of the discharge where the electric field builds up in the cathode. The field strength needs to grow strong enough to cause an explosive electron emission (EEE). The EEEs create a small bit of plasma that grows as more explosions take place eventually forming a spark as this plasma travels to the anode. Once the spark forms the path, an arc creates a low-voltage, high-current path from the cathode to the anode.

II.3.2.2 Electric Field Formation

The first part of breakdown is the formation of an electric field in the cathode. As the anode reaches a high voltage, the potential difference in the gap causes electrons to collect inside the cathode nearest to the anode. The cathode surface is not smooth, but rather is full of divots and micro-protrusions. The micro-protrusions stick up from the

surface like small spikes. Electrons, attracted by the voltage difference, can travel into the micro-protrusions as they try to get to the high-voltage anode. Due to the high-voltage potential, numerous electrons are able to collect in a small area. As the collection of the electrons grows, the electric field in this small micro-protrusion escalates and becomes larger than the average field of the cathode. By enhancing the electric field, these electrons bring the micro-protrusion even closer to reaching the needed electric field to reach the breakdown limits of the cathode.

II.3.2.3 Breakdown Voltage

For every metal, a specific electric field (FE) strength will cause EEEs, irrespective of the gap distance, solely determined by the type of metal. Tungsten, for example, has a breakdown electric field[5] value of 6.5×10^7 V/cm. The FE reaches the required strength as the current density reaches a certain, constant value. This value implies the breakdown voltage is directly proportional to the gap distance. However, experiments have shown there is no direct proportion between the required breakdown voltage and gap distance. The only experimentally verified relation shows the breakdown voltage is exponentially proportional to the gap distance for very small exponents. An EEE occurs when the minimum FE and voltage is reached, then creating a small bit of plasma.

II.3.2.4 Micro-protrusion explosion

An EEE occurs as when the FE reaches the breakdown voltage in a micro-protrusion releasing an ecton, a group of electrons, into the surrounding plasma. The micro-protrusion literally explodes during an EEE. The metal releases an ecton and vaporized metal into the plasma. The occurrence of an EEE appears as a cathode spot in

pictures. The first ecton released begins to spread and surrounds other micro-protrusions. The added plasma full of electrons helps the micro-protrusions reach the needed electric field for breakdown leading to more EEE events, creating secondary ectons. The plasma performs two different important tasks. The first task is forming a plasma sheath over the cathode. The second task is forming a bridge from the cathode to the anode to allow a current to pass.

II.3.2.5 Plasma sheath

As each new ecton forms, they combine into a plasma sheath over the cathode. This sheath plays a very important role in the creation of further ectons. As the sheath spreads over the cathode, it adds to the electric field already present in other micro-protrusions on the surface of the cathode. The micro-protrusions already have enhanced electric fields due to the buildup of electrons. The added enhancement makes breakdown even more likely and easier to achieve. Once these micro-protrusions reach the required levels, they also explode, releasing secondary ectons into the plasma. As these secondary ectons enter the plasma, they begin to spread and surround other micro-protrusions. The spreading in effect leads to a chain reaction along the surface of the cathode that works to increase the size of the plasma forming on the cathode.

II.3.2.6 Cathode ablation

When an EEE occurs, the micro-protrusion becomes very hot. During the explosion, it liquefies the metal forming a droplet. The explosion pushes the droplet from the cathode, creating the ecton. It also leaves a crater on the surface of the cathode. This process slowly removes pieces of the cathode, breaking it down bit by bit. The crater left also forms new micro-protrusions used in the next pulse to form new ectons. Thus

building on this crater and eating away at the cathode, causing the tip of the cathode to recede.

II.3.2.7 Effect on lifetime of thruster

Cathode ablation has a large effect on the performance of the μPPT. The hope in designing these thrusters is the cathode will recede evenly with the propellant. If the cathode recedes faster, it will eventually not be able to see the anode as easily, causing a need for even more power to create the needed voltage for the arc to form from around the propellant, rather than over it. If the cathode recedes slower than the propellant then the arc formation between the cathode and anode could begin to happen far away from the surface of the propellant. With the arc further away, less propellant heats sufficiently to the temperature needed to ablate the propellant. Also decreasing the likelihood the gaseous propellant will pass through the arc and ionize. With less propellant ablated and even less ionized, the thrust of the thruster will drop significantly.

II.3.2.8 Spark

The second task of the plasma is to form a link from the cathode to the anode. As the plasma forms, it develops a negative charge. The positive charge of the high-voltage anode attracts the negative charge. The attraction causes part of the plasma to travel toward the anode. Once reaching the anode, a spark forms over the connection between the cathode and the anode. Spark formation is much like lightning traveling to the surface of the Earth. Many paths will be formed trying to reach the anode, like lighting the spark will have many branches. The first branch to reach the anode forms the spark, just like lighting finally reaching the ground. The plasma also causes a sheath around the anode. Since the plasma has a very high temperature, it can melt parts of the anode. The

melting causes the anode to ablate as well, but for much different reasons than the cathode.

II.3.2.9 Arc formation

Once the spark has formed, an arc is created from the cathode to the anode. The arc forms a constant connection between the cathode and the anode allowing for a high current with low voltage drop to pass between the electrodes. The current heats the propellant but not evenly since the arc is only in a certain place. Firing multiple pulses increases the probability of the spark to cover the entire tip of the thruster. The arc will form at random points and help evenly heat the propellant. Once the capacitors fully discharge, the arc breaks down. When the next pulse occurs, reaching the required breakdown voltage and electric field happens quicker, since typically a remnant of the energy from the last pulse is still present.

II.3.2.9.1 Pulse Shape

Arc formation is not instantaneous, but rather has very distinct steps, as shown in Figure 7, as described by Dr. Bluhm[6].

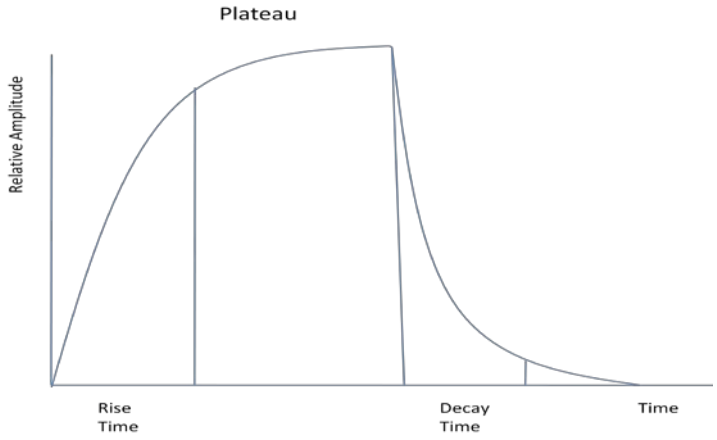

Figure 7: Notional Pulse shape

The rise time is the measure of the time for the pulse to reach 90% the max current amplitude. The plateau is the length of discharge in the pulse. A longer plateau allows for more propellant ablated and ionized. The decay time is the time for the pulse current to drop back down to zero amplitude. It is important the next pulse not occur during or shortly after the decay, but still giving time for residue plasma to move away from the surface of the propellant. In addition, the time gives the propellant a little bit of time to cool, helping in reducing the propellant usage rate. Any leftover plasma can have a negative impact on the next pulse, as there will be seed plasma shorting the circuit before reaching the higher energy levels.

II.4 Propellant Ionization/Ablation

When the arc forms over the propellant, heating occurs, causing the surface of the propellant to evaporate. The electrons in the plasma then collide with the neutral propellant atoms causing an ionization of the particles. The process of ablating and ionizing the propellant is a very detailed process, relative to the pulse length. Many

things must happen in order for the arc to form over the propellant, typically a dielectric substance.

II.4.1 Discharge along surface of dielectric

The presence of a dielectric propellant enhances the spark from the cathode to the anode. Neither the cathode nor the propellant is made of smooth surfaces. Triple points form where the micro-protrusions of each surface meet in the vacuum. The triple point enhances the FE present even more in the cathode micro-protrusion. The enhanced FE leads to an EEE occurring easier and at lower power levels than required for just the cathode. Ecton formation increases, further facilitating spark formation. The EEE also ablates pieces of the propellant. Without the presence of the arc, the propellant is not completely ionized nor is there an electromagnetic field present to accelerate the plasma. Characterization of the loss leads to a better understanding of the performance of the μPPT.

Another loss occurs due to where the arc forms from the discharge. The face of the thruster does not see an even distribution of the arc. In fact, the arc only occurs at a single spot on the surface. The arc heats the propellant directly below, but not the rest of the propellant. The hot propellant beneath the arc ablates the most, with some ablation of the propellant near the arc. Additionally, most of the highly energetic electrons are in the arc. Higher energy electrons may be present in other areas as the ectons spread, but not to the level of the arc itself. The arc ionizes more of the ablated propellant than other areas due to the uneven distribution of electrons. The non-ionized particles contribute significantly to the losses of the thruster. The inherent loss is hard to characterize alone,

as it is hard to tell how much of the propellant is evaporated and not ionized. Once an ion hits a surface, it loses its charge and becomes neutral, so it takes very specialized sensors to determine what portion of the gas is not ionized.

II.4.2 Discharge formed through the propellant

Another loss in the discharge of the μPPT is the electric channel formed through the inter- and intra-molecular chains within the dielectric. A dielectric is normally a non-conductive material due to the separation of molecular chain bands in the material. However, trapped gas or liquids within the dielectric can connect these bands. Electrons can travel along the chains to points where they are either trapped or can make the jump to the next chain. When the electrons are trapped, they can cause heating in a very localized region. If this area gets hot enough, it can cause an explosive expansion due to gasification of the propellant, much like the EEE discussed for the cathode. Since the explosion happens below the surface, it will break off small pieces of the propellant above it. Although the propellant involved in the explosion is vaporized and possibly ionized, the propellant further from the spark is not ionized. Also, this can occur well before a spark is formed. Even if the gas is ionized, there is no electromagnetic field to accelerate it. This phenomenon is also likely the reason the surface of the propellant becomes concave.

The heating of gas below the propellant surface is a major cause of efficiency losses for the μPPT. Contamination increases on nearby surfaces from the large solid particles. In addition, the concave shape of the thruster decreases the lifetime of the thruster. For each pulse, propellant is lost requiring additional propellant over the life

expectancy of the thruster. Also, if the propellant recedes faster than the anode and cathode, the arc formed may not completely contact the surface of the propellant. Thus, not as much propellant is ionized and the amount of thrust can start to drop.

II.5 Lorentz Force

In PPTs, the thrust comes from the Lorentz force[7]. An electromagnetic field interacts with a charged particle accelerating it in a perpendicular direction to the magnetic field.

$$F = qE' = q(E + v \times B) \qquad \text{Eq. 4}$$

Where q is the charge of the moving particles (C), E is the applied electric field (V/m), E' is the effective electric field (V/m). The Lorentz Force is made up of two parts. One part consists of the particle velocity, v (m/s), and B, the magnetic field strength (T). The cross-product gives the direction of the force as well as most of the magnitude. The other part of the Lorentz force, the charge times the electric field, qE, works to accelerate the ions causing a momentum exchange and thus thrust.

Hall Effect and Ion thrusters use the qE component of the Lorentz equation to create thrust. The anode's electric field acts on the charged ions, accelerating the ions and causing the momentum exchange. In this case, only the ions accelerate away from the thruster, requiring the cathode to release electrons into the plume to neutralize the ions.

The PPT and μPPT, on the other hand, use the $v \times B$ component of the Lorentz Force. The changing electric field induces a magnetic field along the surface of the thruster. The ions and electrons move at high speeds along the arc and interact with the

induced magnetic field. The ions and electrons both accelerate away from the surface of the thruster, with opposite spins. The exchange of momentum between the induced magnetic field and the ions causes the thrust. In addition, since both the ions and electrons move in the same direction, the plasma is quasi-neutral. The plasma does not require additional electrons from an outside source to neutralize the plasma. Although a contamination problem exists, the plasma causes the structure to have a net charge.

II.5.1 Magnetic field creation, ion heating and acceleration

As the arc forms, a current passes from the cathode to the anode. The current induces a magnetic field at the surface of the propellant, forming a very strong electromagnetic field at the surface of the propellant. The field pushes the ionized particles away from the surface. Eq. 5 gives the exit velocity of the particles[1]. Here, the exit velocity is a function of the thruster efficiency, η, material permittivity, μ_o, the radius of the anode and cathode, R_a and R_c respectively, as well as the current, J and mass flow, $\dot{m}$.

$$u_e = \frac{F}{\eta \dot{m}} = \frac{1}{\eta}\left[\frac{\mu_o}{4\pi} ln\left(\frac{R_a}{R_c}\right)\right]\frac{J^2}{\dot{m}} \quad \text{Eq. 5}$$

When the electromagnetic field pushes the ions and electrons away, they push back creating thrust (Newton's second law) given by Eq. 6.

$$F = \dot{m} u_e \quad \text{Eq. 6}$$

Due to the mass difference between the ions and electrons, the force from the ions is several orders of magnitude larger than the force from the electrons. These particles are also expelled at very large velocities. This clears the surface of the propellant of a potential difference with the next pulse from electrons and ions. If they were to stay, then

there could possibly be a path for the current to travel and decrease the likelihood of the necessary energy buildup before the spark to ablate the propellant.

II.6 Efficiency

II.6.1 Energy Balance

The efficiency of the µPPT is broken into three different, but related quantities, the overall, thruster and accelerator efficiencies. Dr. Burton, from the University of Illinois at Urbana-Champaign, has worked on finding definitive formulas for these values for the µPPT. One of the problems with the efficiencies of the µPPT is there is so many different ways of describing the efficiency. Dr. Burton lists 22 separate ways[8] of describing the efficiency of the µPPT. He decided the overall efficiency is the product of several other efficiencies, as seen in Eq. 7.

$$\eta_o = \eta_{ppu}\eta_{trans}\eta_{sh}\eta_{heat}\eta_f 8^6 \qquad \text{Eq. 7}$$

Where $\eta_o$is the overall efficiency, $\eta_{ppu}$is the power processing unit efficiency, $\eta_{trans}$is the transfer efficiency, $\eta_{sh}$is the sheath efficiency, $\eta_{heat}$is the heat loss efficiency and η_f is the frozen flow efficiency. Some of these efficiencies combine into broader efficiencies. The terms η_{sh}, η_{heat}, and $\eta_f$are reffered to as the acceleration efficiency, η_{acc}. This new efficiency along with η_{trans}, is also referred to as the $\eta_t$or thruster efficiency. Figure 4 shows the efficiencies, and the relationship of each to the operation of the thruster.

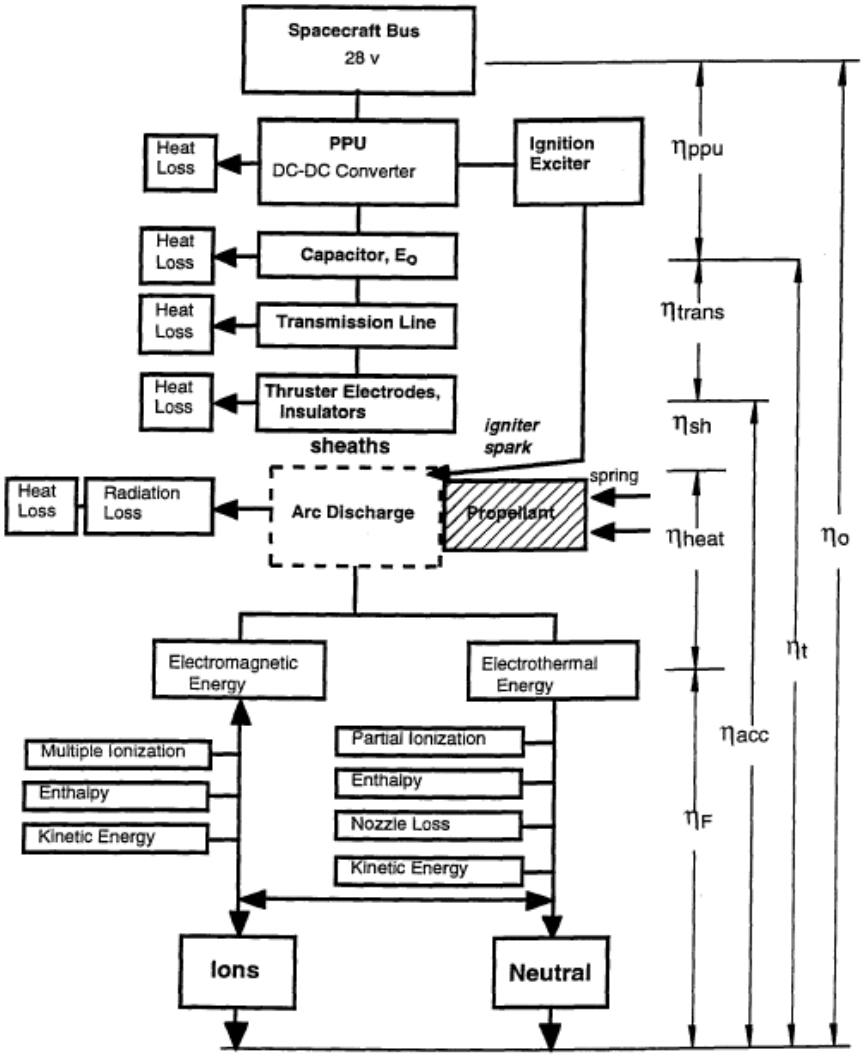

Figure 8: PPT circuit and location of efficiencies[8]

In order to solve for the overall efficiency, each of the terms must be determined to get the individual values. Determining η_t, as the thruster efficiency has most of the other efficiencies buried inside of it, gives the best method to solve for the overall efficiency. Unfortunately, the thruster efficiency is not an easy term to solve for.

The η_t is determined as the ratio of the directed exhaust kinetic energy to the energy stored in the capacitor, E_o. It is the best at giving the thruster efficiency for the

PPT. The stored energy in the capacitor is normally a given quantity, however finding the exhaust kinetic energy is not easy. It involves solving a system of equations to solve for η_t. The exhaust kinetic energy needs to be broken out into two parts, one for the fast moving ionized mass, m^+, and the other for the slower non-ionized, neutral mass, m_n, giving Eq. 8 for the thruster efficiency[8].

$$\eta_t = \frac{\frac{1}{2}m^+{u^+}^2 + \frac{1}{2}m_n{u_n}^2}{E_o} \qquad \text{Eq. 8}$$

The impulse bit from the neutrals and the ions add up to the total impulse bit, with each individual impulse bit being the product of the mass times the velocity for the ion and the neutral[8].

$$I_{bit} = I^+ + I_n \qquad \text{Eq. 9}$$

$$I^+ = m^+u^+ \qquad \text{Eq. 10}$$

$$I_n = m_nu_n \qquad \text{Eq. 11}$$

The ablated mass relation includes the parameter Φ as the late-term ablation factor[8]. If all the mass is ionized, then Φ=1.

$$m^+ + m_n = \Phi m \qquad \text{Eq. 12}$$

This is a system of five equations with 11 unknown variables. Typically an experiment will give you E_o, I_{bit}, and m. Φ is determined through empirical data found in other research. Typically, a value of 0.4 is a good estimate. The other two variables, the velocities u^+ and u_n, are assumed through the Maxwellian distribution for other experiments using a similar thruster. It is this last assumption driving uncertainty beyond acceptable limits for a good estimation. So this term most be solved for in its components.

The η_{ppu} is determined based on the power supply being used, a typical value is about 0.80~0.93. The η_{trans} is found through a simple ratio of the impedance of the PPT and the total impedance of the circuit.

$$\eta_{trans} = \frac{Z_{ppt}}{R_{tot}} \qquad \text{Eq. 13}$$

The accelerator efficiency is the product of the sheath, heat loss and frozen flow efficiencies. The sheath efficiency, η_{sh} can be described by

$$\eta_{sh} = 1 - \frac{V_{sh}}{V_{ppt}} \qquad \text{Eq. 14}$$

Where V_{sh} is the voltage in the sheath and V_{ppt} is the PPT voltage.

The heat loss is from the radiation released by the arc that is not used to heat the propellant as given below.

$$\eta_{heat} = 1 - \frac{E_{loss}}{E_{arc}} \qquad \text{Eq. 15}$$

The remaining energy in the system, not lost anywhere else, is used to accelerate the propellant. This frozen flow efficiency, η_f, can be determined from the speed of sound and the total enthalpy of the ions, which is determined from a lookup table for the material. The equation is shown below.

$$\eta_f = \frac{u^2}{2h_o}$$

The overall efficiency for the thruster can be determined with all the efficiencies known. Using the best available components and assuming best performance, the maximum overall efficiency expected for a coaxial PPT is 60%[8]. The value is an order of magnitude larger than the actual measured values for the thrusters. The number of losses adversely affects the performance of the thruster.

II.6.2 Propellant Temperature Effects

A study completed at the AFRL Propulsion directorate at Edwards AFB[9] to determine the effect of propellant temperature has on the efficiency of the propellant consumption. In this study, the XPPT-1 (Experimental Pulsed Plasma Thruster-1) is tested at various input powers, run durations and initial propellant mass. The measurements taken during the experiments included the thrust, propellant consumption, and propellant temperature.

Thrust measured using a torsional thrust stand developed at NASA-LeRC capable of measuring in the μN range. The propellant consumption is measures by pre- and post-test mass measurements of the propellant bar, using a device with an uncertainty of 0.1 mg. Before the propellant was measured post-test, a period of time, roughly one hour, elapsed allowing the moisture that had boiled off due to the low pressures in the chamber to condense back into the propellant. The temperature is measured by inserting probes from the rear of the bar to various distances from the face of the bar ranging from 1 mm to 26 mm. The probes were placed 0 mm, 4 mm, 7 mm, and 10 mm from centerline[9].

II.6.2.1 Warm-up period

The XPPT-1 fired for over 20,000 discharges[9] with the mass being measured periodically throughout with an emphasis on measuring the mass often early in the experiment and then less frequently as the experiment went on. The data from the 20J, 20W experiment, given in Figure 4 shows the best-fit line with a slope of 26.4 ± .01 μg/discharge apparently for all data points.

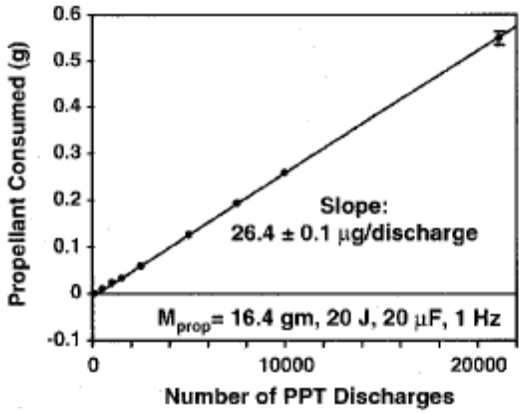

Figure 9: Propellant consumption over 20,000 discharges in AFRL experiment[9]

However if the lower, sub 2,000 discharge, portion of the graph is magnified, as in Figure 5, a noticeable inconsistency between the best fit line and the data can be seen for the points below 1,500 discharges.

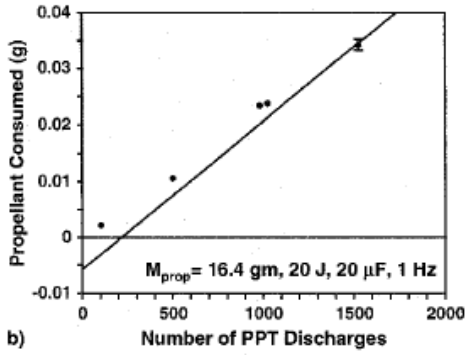

Figure 10: Propellant consumption over 20,000 discharges in AFRL experiment[9], specifically looking at the sub-2,000 discharge region

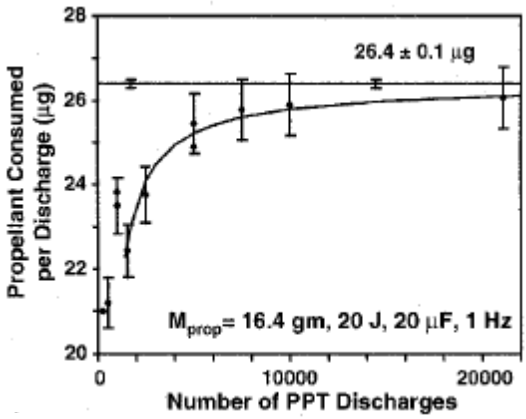

Figure 11: Propellant consumed per discharge comparison between instantaneous and best fit value[9]

Converting the graph to propellant consumed per discharge, Figure 11, the inconsistency noticed in Figure 5 appears again. The constant line on top is the best-fit line showing a constant rate of consumption and the first data points are well below the constant consumption rate. However, for the first several thousand pulses, the instantaneous rate is well below this value.

This difference shows less propellant than expected consumed during the first discharges of the system. The effect is repeated for propellant bars of different masses[9]. At first, the effect is hard to explain, but by looking at the temperature graph, Figure 7, for this test for the various axial locations, it clearly shows the temperature is not constant during the first 5,000 pulses, but grows with each pulse.

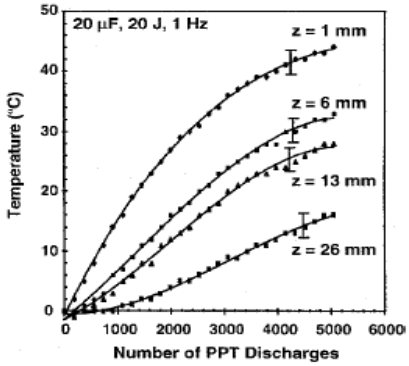

Figure 12: Propellant temperature at various axial locations[9]

The transient effect is known as the warm up period of a PPT. During the first 5,000 pulses, the temperature of the propellant is increasing due to the repetitive pulsing. At roughly 5000 discharges, the temperature of the propellant becomes almost constant, and remains at the constant temperature the remainder of the thrust maneuver.

Arc formation is not the only way to heat the propellant; the input power can also affect the temperature. In this experiment, adjusting the power level shows the effect on temperatures is a rise for all power levels in the first 5000 discharges, however based on the power input the final temperature, and number of pulses to reach it, are quite different shown in Figure 8.

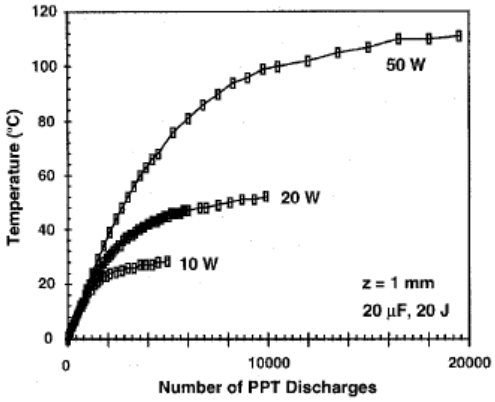

Figure 13: Propellant Temperatures at three different power levels[9]

The figure shows for higher power levels, the PPT warm up period is actually longer than 5,000 pulses. The effect begins to be a major concern for testing devices at this large of a power level and cannot be ignored. However, for flight operations using a 50 W thruster, the behavior is a benefit. The thruster will use less propellant for short duration thrust maneuvers, since the thruster takes longer to heat.

At the lower temperature, the propellant consumed per discharge is actually lower than the steady state value predicted by the best-fit line to the data for a long duration test. This result suggests two conclusions for the PPT. First, an advantage, keeping the propellant temperature low during operation, the better the thruster propellant efficiency. The operational advantage of this fact is space is cold. The propellant is as cool as possible in the space environment, especially placing the thruster hidden from the sun. Second, a disadvantage, for testing purposes the warm up period can drastically affect the results of a test. All tests need well over 10,000 pulses to remove the warm up period in the noise of the data for the test. The other option, used in some experiments discussed below involves operating the thruster for several thousand discharges, before the data collection begins, removing the warm-up period from the data. For example in this experiment, the experimental value of 26.4 μg/discharge and the 1500 discharge instantaneous value of 22.4 μg/discharge (taken from Figure 6) gives the following error in data:

$$\frac{\Delta m}{m} = \frac{\Delta I_{sp}}{I_{sp}} = \frac{\Delta \eta}{\eta} = 14.2\% \qquad \text{Eq. 16}$$

Noise does not account for the warm up period, making the region very important for testing of the PPT. Not known is if the μPPT has this same warm up period effect. In

conduction the research of this paper, the start-up effect will be something important to investigate.

II.6.2.2 Post-pulse Temperature

The temperature of the PTFE is still high enough immediately following the pulse to ablate material off the surface. Since the arc already passed, this material is neither ionized nor accelerated. Dr Spanjers[9] indirectly measured the phenomenon when calculating the propellant consumption rates. However, understanding the temperature gradient on the surface of the thruster as well as the cooling gradient is important in understanding the amount of propellant ablated during this time, affecting I_{sp} and ultimately efficiency.

Dr. Antonsen[10] studied the surface temperature of the μPPT using mercury cadmium telluride photovoltaic detectors, calibrated for PTFE, sensitive to infrared emission[10]. By looking sideways through the plasma, the sensors determined the temperature contribution of the plasma ends as soon as the pulse itself ends, leaving only the temperature of the surface. Temperature measurements of only a small part of the surface were made due to the small area the detectors can see. Since arc formation is unpredictable, leaving no guarantee the arc would form over the sensor measurement region, multiple pulses were used to form a baseline for the temperature profile for the thruster, to ensure the results from pulse to pulse were following the same curve, shown in Figure 14.

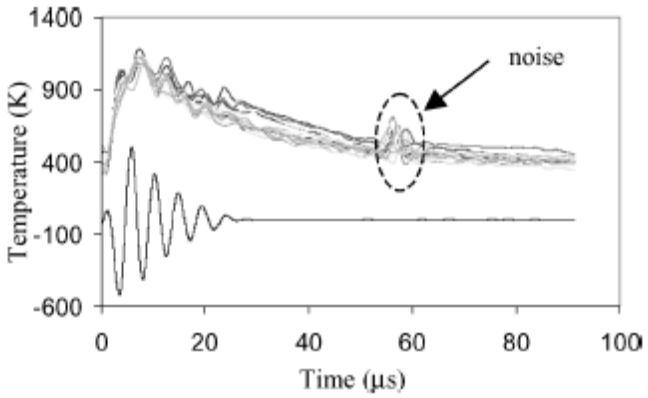

Figure 14: Temperature measurements of several pulses. The bottom line shows the pulse current[10]

The data on the bottom shows the current pulse passing through the arc. Any data during this period is invalid, as the arc has not dissipated. Once the arc stops, the temperature declines for all pulse, until about 60 µs after the initiation there is noise on all pulses, later traced to the spark plug used in the test. Now knowing where the data is valid, each pulse can be analyzed for the post-pulse temperature. For example, pulse 20 shows a linear decay in Figure 15.

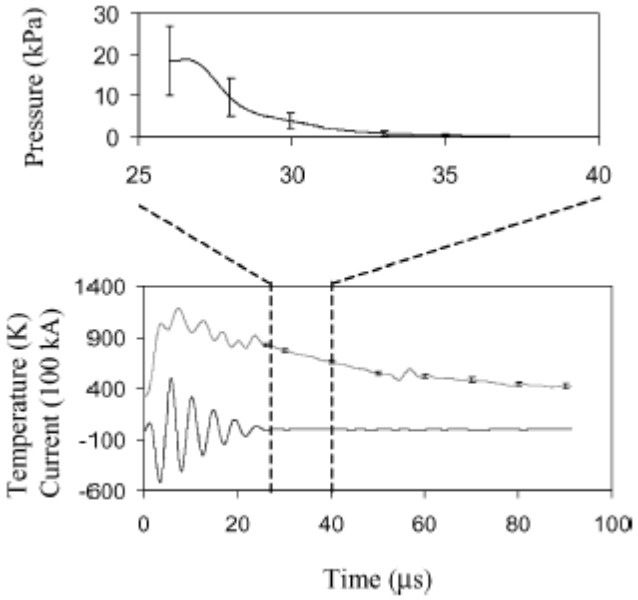

Figure 15: Pulse 20 temperature and PTFE pressure profile[10]

The cutout of this figure is for the time period directly after the arc dissipates, to right before the noise from the spark plug. Using the data in the main graph, along with experimentally determined values, the pressure is inferred in the cutout. As can be seen, the pressure is still high and begins to decay rapidly. The pressure is of the non-ionized, ablated PTFE, providing direct proof of the post-pulse PTFE ablation, causing a loss in the propellant usage efficiency.

II.6.3 Power Effects

The experiment introduced in Section II.6.1, also discussed the power versus thrust performance of the XPPT-1[9]. Using the torsional thrust stand, measurements were taken throughout the experiment for various power levels. Figure 16 shows the thrust for the PPT did not vary much off from a constant value as the power was increased.

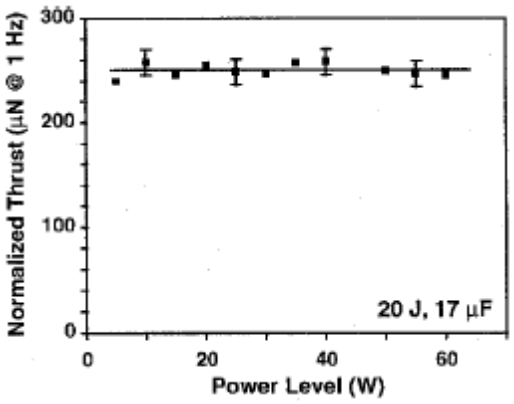

Figure 16: Thrust versus Power Level[9]

Knowing the temperature can affect the amount of propellant being lost per discharge causing the higher power levels will consume more propellant, this constant value for thrust shows the late-term ablation of the propellant has no major effect on the thrust, as can be expected from the results presented in Section II.6.2.2, particle velocity, showed.

Although the thrust is constant, the I_{sp} can be seen declining linearly with the increased power, Figure 14.

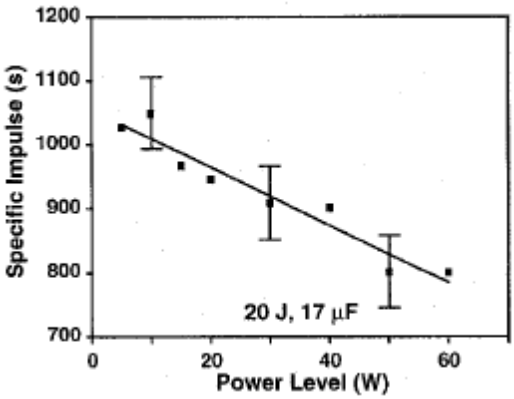

Figure 17: I_{sp} versus Power[9]

I_{sp} is a term used to define the fuel efficiency of the thruster. As the power increases, the temperature of the propellant will increase causing the propellant

consumption per discharge to rise as well. For every pulse, more propellant is being ablated, creating a mass flow, and being used to produce the same thrust, causing the I_{sp} to fall. Eq. 17 shows how I_{sp} is related to thrust.

$$I_{sp} = \frac{F}{\dot{m} g_o} \qquad \text{Eq. 17}$$

The mass flow term, $\dot{m}$, increases while the thrust term, F, remains the same, causing the I_{sp} to decrease as the power level increases. The g_o term is equal in magnitude and units to the gravitational constant of Earth, 9.81 m/s^2, but is not the same thing conceptually; it is merely used here to change the units of I_{sp} to seconds. For the same reasons, increasing the power affects the efficiency of the thruster, as seen in Figure 15.

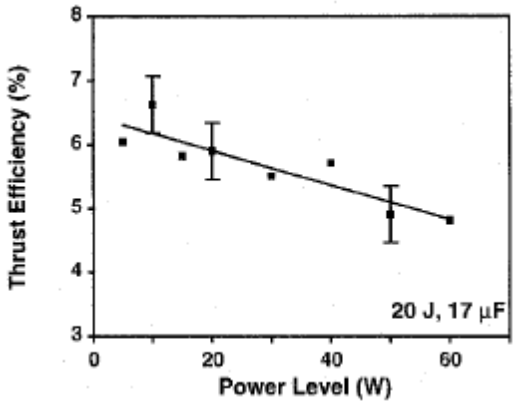

Figure 18: Thrust Efficiency versus Power[9]

II.6.4 Particle Emission

As discussed above, several large particles, emitted by the thruster and not ionized, only add very small bits of thrust to the overall force. However, the impact on the thruster efficiency and the physical impact on the satellite are very important in understanding the µPPT and its possible use on satellites.

II.6.4.1 Material and Size

Research completed by Gregory Spanjers at AFRL on the PPT device determined the size and material type of these particles. In the tests conducted at AFRL[11], the XPPT-1 is used to study the particulate emission material, size and what percentage of the mass is lost as a particle and not ionized. The XXPT-1 placed in a 1.2 m diameter chamber, is pumped down to vacuum pressures. First, the XPPT-1 is preconditioned by firing the thruster over 100,000 times, to make the face of the propellant concave. The experiment involved firing the thruster 6,000 times with pre- and post-test mass measurements, considering moisture evaporation. The mass of the XPPT-1 dropped by 24.9 μg per discharge (averaged value). An error is introduced without waiting for the moisture to re-condense, as the mass of the propellant post-test would also include moisture loss as well as the propellant loss. With the total mass loss now found, the experiment set out to determine how much of the mass was lost as non-ionizing particles. In order to accomplish this experiment, witness plates were setup around the thruster, Figure 4, at various angles 6 cm from the surface face. For this portion of the test, the XPPT-1 fired 1,000 times after having pre-fired the thruster to a steady state temperature, removing the warm up period as a source of error.

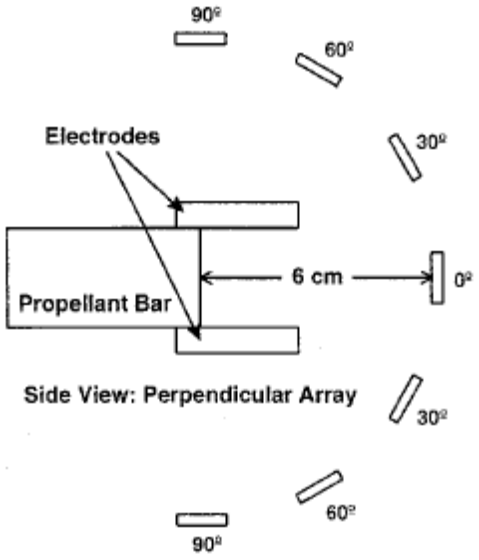

Figure 19: Test Setup done in AFRL test to capture non-ionized particles**Error! Bookmark not defined.**. The plates were setup vertically as shown, as well as horizontally around the face of the thruster (in parallel) [11]

The witness plates are removed after the test, and analyzed for particulate matter using the SEM/EDAX analysis. In analyzing the plates, only particles of 25 μm or larger were counted due to the large number of smaller particles impossible to count by hand. The error from this limitation is analyzed by creating two histograms showing the number of particles of every size and the estimated particle mass of every size for the centerline witness plate. To estimate the mass of the particles, the size of the particle is used as the diameter of a sphere to get the volume. With the known density of PTFE, 2152 kg/m^3, deriving the mass indirectly, eliminating the need to directly measure the mass.

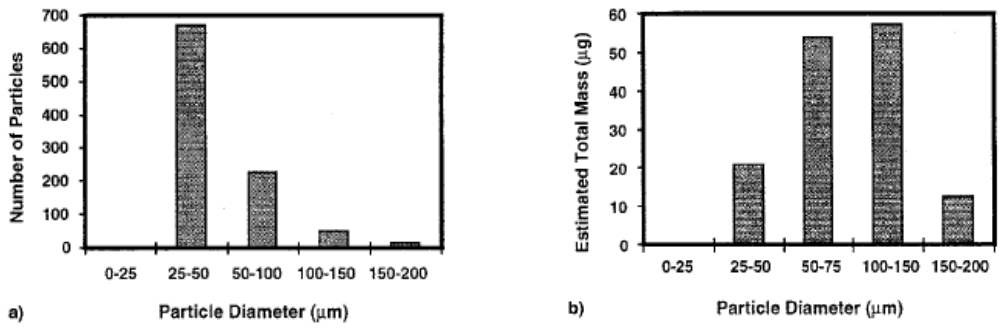

Figure 20: Histograms for witness plate on center-line of the thruster**Error! Bookmark not defined.**. a) size distribution and b) mass distribution [11]

As can be seen in Figure 5a, the number of particles increases as the diameter decrease, thus creating the possibility that not all particles were counted in the experiment. However, Figure 5b shows most of the mass is located in the larger diameter particles, accounting for most of the mass, even without counting most of the particles. The smaller particles only add a very small amount to the mass.

Analyzing the particles after counting to determine the type of material they are made of discovered the existence of two different types of particle populations. One characterized as spherical in shape with diameters of .3 μm, but always smaller than .1um. These particles had strong Fe, Cr and Ni transitions meaning they were from the electrodes and are remnants of the EEE and ecton formation. The other population with strong F transitions, traced back to the propellant, was approximately 200 μm to less than 1μm in diameter. This population did not have a common distinctive shape but rather a large number of random shapes. Since both the electrodes and the PTFE have carbon in them, placing C transition particles in both populations. The results for all of the witness plates shows most of the particulate mass is centered directly in front of the thruster, with the mass density falling off as you move away from center.

The plates did not catch all of the mass emitted since the plates were not continuous. By treating each plate as a point on a graph, a best-fit function retrieved this information. For the perpendicular direction (vertical), the best fit to the data was a $\cos^7\theta$ fit**Error! Bookmark not defined.** and the parallel (horizontal) best fit was exponential, using zero mass density as the boundary conditions at ±90 deg from centerline. Now with functions of mass density versus angle, a simple integration over both gives a particulate mass of 9.8 ± 0.7 mg. With the thruster firing 1,000 times, giving a rate of 9.8 ± 0.7 µg/pulse.

In a single pulse, the XPPT-1 lost 24.9 µg with 9.8 ± 0.7 µg captured by the plates. So 40 ± 3% of the mass lost is not vaporized, leading to a propellant efficiency of less than 60%. This is a leading loss mechanism in PPTs and µPPTs, resulting in very low overall efficiencies for the thrusters. Although understanding the process of particle formation is important to knowing how to limit this loss mechanism, for a practical mission using present technology characterizing this loss to know how much additional propellant is needed for the mission is a driving concern in the design of a thruster.

II.6.4.2 Particle Velocity

In experiments done previously at AFIT, by Capt Seo Myeongkyo[12]**,** high speed stereo photography captured the particulate emission of a µPPT as it leaves the thruster. The photographs were taken with 26 us exposure time at a rate of 25,000 fps. Knowing the relative pixel size to actual distance the velocity could be determined as the distance traveled over a certain amount of time. The stereo photographs also allowed the calculation of the angle of travel of the particles.

The velocity of the particles ranged from less than 100 m/s to just over 300 m/s radially and as high as 1000 m/s axially, with a total velocity magnitude ranging from 50 m/s to 1000 m/s. As can be seen in Figure 21 most particles have a total velocity from 100 m/s to 200 m/s.

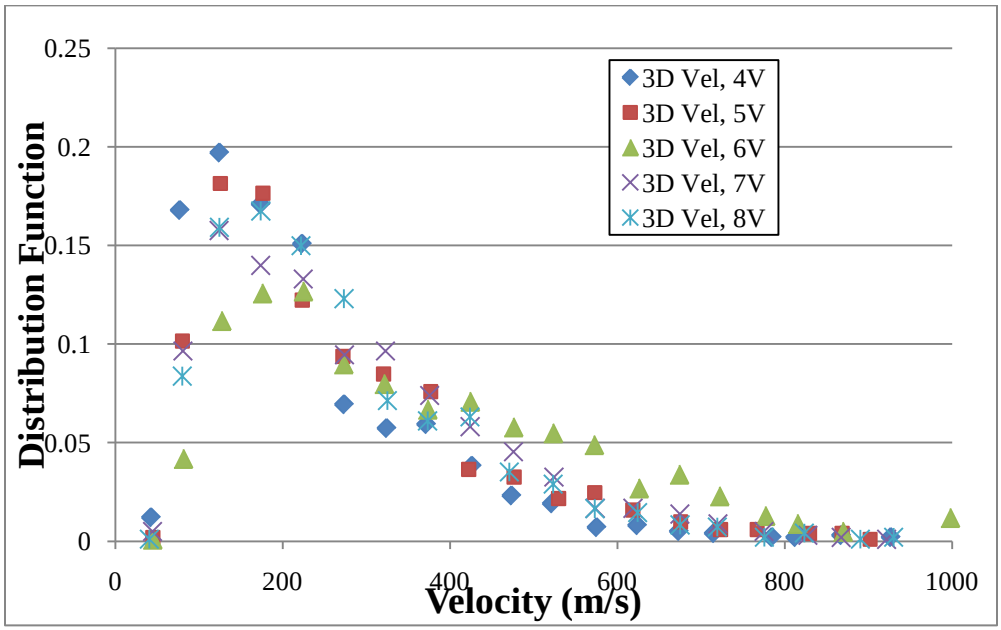

Figure 21: Velocity Magnitude Distribution[12]

The angular distribution of the particles also relates very well with the velocity of the particle. As in Figure 7, the high velocity particles only existed at the small angles from centerline. Slower particles exist in these small angles, but they also exist in increasing numbers at higher angles.

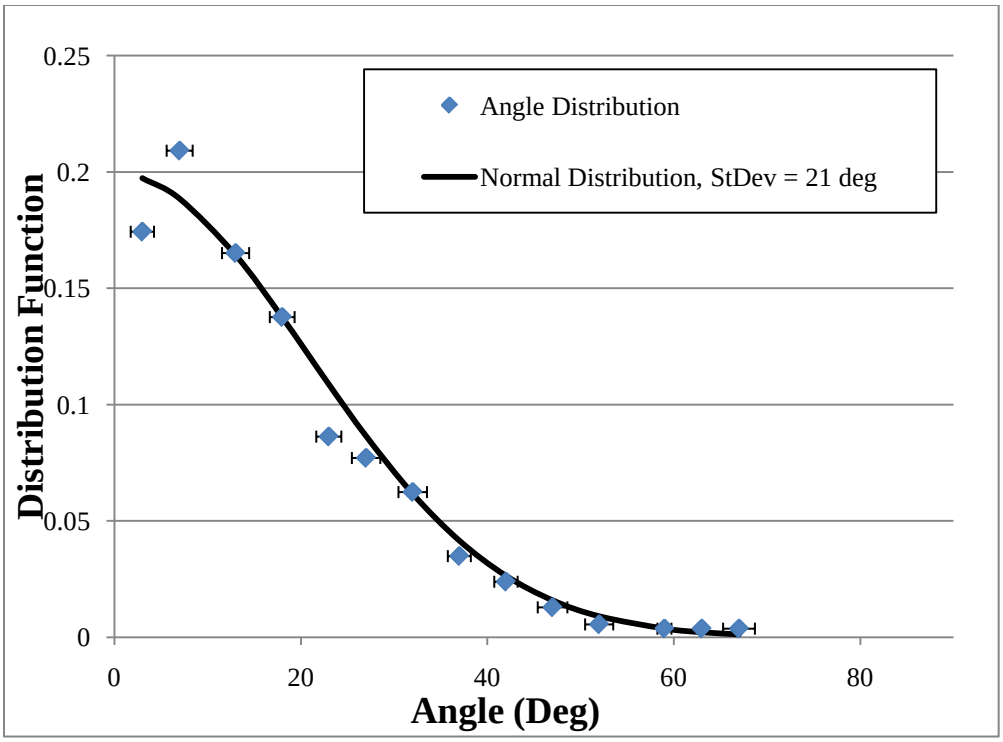

a) Particles slower than 200 m/s (55 % of total particles)

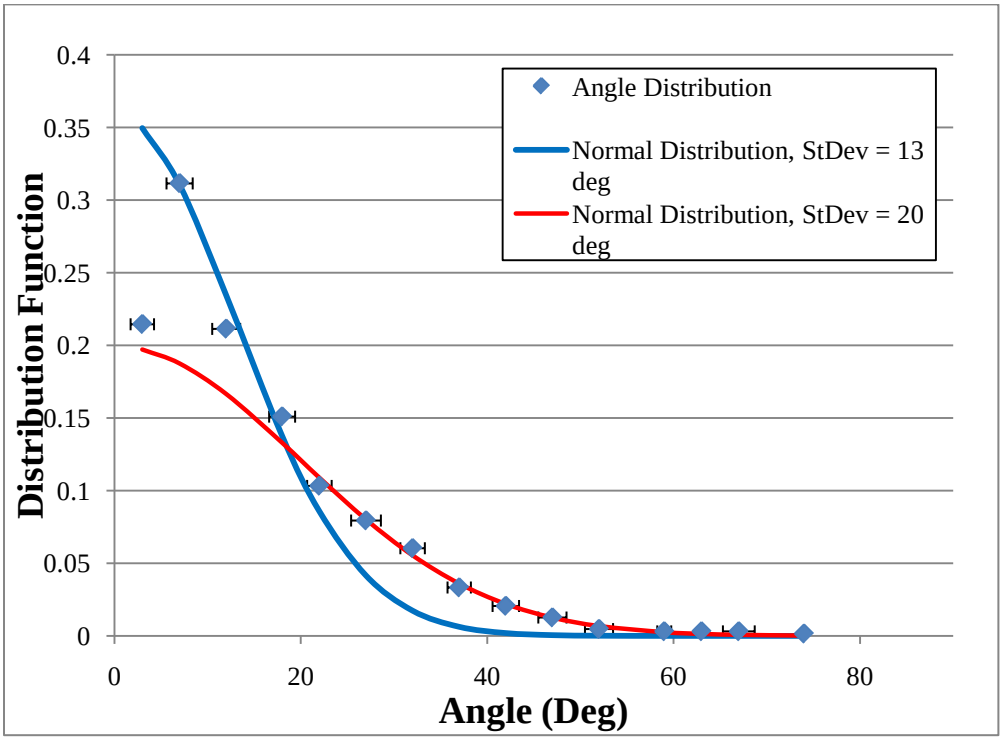

b) Particles slower than 300 m/s (77 % of total particles)

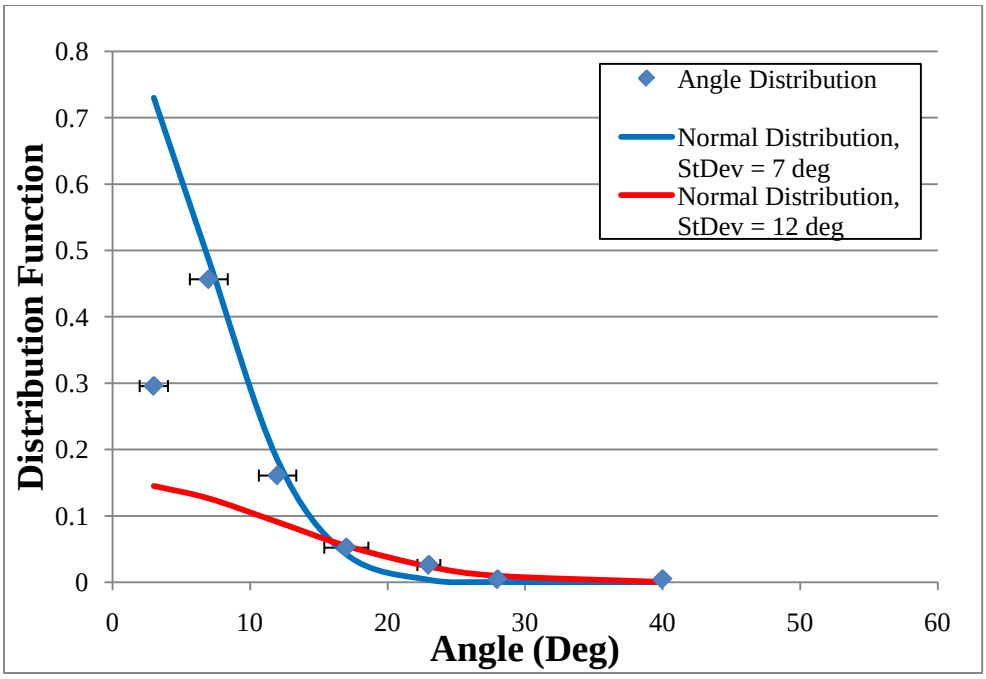

c) Particles faster than 300 m/s (23% of total particles)

Figure 22(a,b,c): Particle velocity distribution for three different velocities[12]

Based on these results, most particles accelerate to high velocities in the same direction as the plasma. When this does not happen and the particles disperse at ever-increasing angles, the velocity decreases. Relating back to the tests done at AFRL, the faster moving particles are the most massive particles since they are moving closer to the centerline. The less massive particles with slower velocities have less momentum, and instead of moving straight ahead with the other, more massive particles, the slower particles are pushed to the side.

II.6.4.3 Particle I_{sp}

The acceleration of the ionized plasma by the induced magnetic field creates the majority of the thrust of a µPPT. A small portion of the thrust also comes from the acceleration of the solid particulates captured in these photos. As can be seen in Table

300, the additional I_{sp} of these particles to the overall thruster is counted in tens of seconds. When compared to a thruster with an I_{sp} near 1000 s, this additional thrust and I_{sp} is negligible, and does little to make up for the loss in efficiency from these particles failing to be vaporized and ionized.

Table 1: I_{sp} Contributions for Each Operating Conditions, max is highlighted[12]

Input voltage (Energy)	4 V (2 J)	5 V (2.7 J)	6 V (3.4 J)	7 V (4.0 J)	8 V (4.4 J)
Ave axial velocity (m/s)	215	256	345	270	258
Isp (sec)	22	26	35	28	26

II.6.4.4 Particle Effect on Efficiency

The thrust of a µPPT is directly related to the amount of propellant ablated and ionized. There more propellant ionized, the higher the thrust. When some of the propellant is then lost as non-ionized particles, the amount of thrust the µPPT is creating drops. By measuring the amount of mass lost to these particles, the amount of lost thrust can also be determined , by comparing this with the actual thrust of the µPPT a propellant efficiency for the µPPT can be found.

The effect of late term ablation of the PTFE propellant is a main source of efficiency loss in the µPPT. Many attempts have been made to determine this effect, some direct, some indirect. A priority research point is solving the problem of late term ablation in order to increase the efficiency of the thruster by any significant amount.

II.7 Satellite Contamination

The μPPT emits a quasi-neutral plasma and a relatively large amount of solid particles. Both of these processes affect the satellite contamination concerns.

II.7.1 Quasi-neutral Plasma

As the plasma accelerates away from the thruster by the Lorentz force, both the ions and electrons accelerate in the same direction. Although the ions and the electrons are each charged, the plasma itself is quasi-neutral, with the same number of ions and electrons present making the net charge of the plasma zero.

This is important for satellites, since the satellite attracts the charged plasma. The satellite could start building a charge under these conditions. If this charge grows large enough, it could begin arcing to nearby components inside the spacecraft, in the same way an arc forms in the μPPT. In addition, a charged satellite could create electro-magnetic interference with the antennas or other sensor equipment onboard the spacecraft. Interference on these systems could lead to loss of mission or even the loss of the satellite completely. The μPPT does not have this concern as it naturally neutralizes the ions through its normal firing process, making μPPTs safer from this form of contamination.

II.7.2 Particulate contamination

Although the μPPT is safer from charging the satellite, it can cause serious problems due to its emission of solid particles. The particles emitted in large enough quantities can coat surfaces and possibly clog joints, or cover a solar panel.

As has been discussed in previously, the μPPT does not ionize all of the ablated propellant. This non-ionized propellant accelerates to lower velocities, but still pushes out from the thruster. If the thruster is located near the solar panels, these particles could build up on the surface of the panel. This covering would block the sensors in the panel from collecting solar energy and lower the efficiency of the panel. This could lead to failure of the satellites power systems.

Researchers have investigated how these particles behave after they leave the thruster. However, more research into how much propellant emitted by the μPPT is required.

III. Test Setup and Apparatus

III.1 Laboratories

AFIT has several laboratories for student research. In these experiments, two separate labs were utilized for their unique equipment, the Geo-orbital Nano-thruster Analysis and Testing Laboratory and the Vibration Laboratory.

III.1.1 Geo-orbital Nano-thruster Analysis and Testing Laboratory

The required equipment for these experiments was spread out between two laboratories. The Geo-orbital Nano-thruster Analysis and Testing Lab (GNAT) where most μPPT work previously was located provided the necessary vacuum chamber for the mass collection and video collection experiments. The vibration laboratory proved useful for its thermal vacuum chamber (TVAC) due to its large size for the torsional balance used to make the thrust measurements.

Located in the GNAT lab is a LACO Technologies vacuum chamber capable of pressures below 10^{-6} torr . It has front and side windows as well as feed-throughs for high voltage lines as well as BNC connections. Due to the small size of the chamber, the time to reach vacuum is less than 45 min and less than 1 min to vent. The quick response time works well for the mass collection experiment since the chamber required repeated pumping and venting as the series of runs progressed. The chamber is computer operated with a minimum amount of user inputs. Once the chamber has been closed and locked, the LabView resets, turning on the roughing pump, which begins to pump down the foreline to the turbo pump. The turbo pump begins to warm up and once the foreline reaches a vacuum and the turbo pump is ready the user can press the “start” button, which

closes the foreline valve and opens the valve between the roughing pump and the chamber. No further input is required from the user to operate the chamber. The roughing pump is capable of taking the chamber to 10^{-2} torr. Once the pressure is below 10^{-2} torr the valve between the roughing pump and chamber is closed, the foreline valve opens and the high pressure valve between the turbo pump and chamber is opened allowing the turbo pump to draw out the remaining air from the chamber. Once the turbo pump is open to the chamber the pressure falls rapidly. Once the pressure drops below 10^{-3} torr the pressure gauge switches to an ion gauge capable of reading pressures well below the required 10^{-5} torr. This gauge, when functioning properly, is very accurate, however during the experiments, the ion gauge was not functioning properly and an accurate reading of the pressure was not possible. The main gauge on the chamber is capable of reading down to $1x10^{-4}$ torr, but not any lower. Therefore, the pressure was below this level, but not known exactly, meaning all work completed in this chamber can only be known to have been completed in a pressure below $1x10^{-4}$ torr, but with no further accuracy. Fortunately, this pressure is sufficient to approximate the space environment for the purposes of these tests.

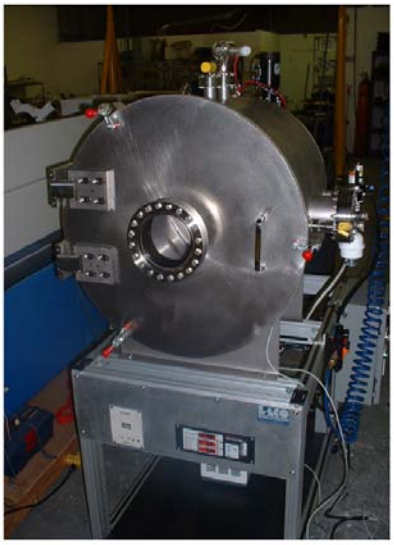

Figure 23 LACO Vacuum Chamber

III.1.2 Vibration Laboratory

The Thermal Vacuum Chamber, or TVAC, is located in the vibration facilty at AFIT. This chamber is a 2 m diameter chamber and 2 m deep. It is capable of pressure below 10^{-6} torr and as the name suggests can cool to below 40deg C and as high as 120deg C. It also has lamps capable of simulating sunlight for testing solar panels in various conditions. The TVAC chosen not for its temperature capabilities though, rather for its size since the LACO chamber is not big enough to hold the torsional thrust balance without interfering with operations. The TVAC is a manually operated chamber requiring user input for every step. First, the user must turn on the roughing pump. Once the chamber reaches 10^{-2} torr, the turbo pump turns on and spins up. Once the turbo pump has had some time to spin up, the valves open and the pump begins to pull on the chamber. Once this is done it takes the chamber approximately 12 hours to pump down to $10^{\wedge-5}$ torr.

III.2 Test Equipment

Beyond the vacuum chambers, numerous other pieces of equipment were required in order for the tests to be completed. The main pieces being the thrusters themselves and the circuits required to operate them.

III.2.1 Three-Electrode µPPTs

For the experiments, two different types of three electrode thrusters were constructed. Fig shows the dimensions of the three-electrode µPPT. The size of the thruster is very small, making construction and handling very difficult.

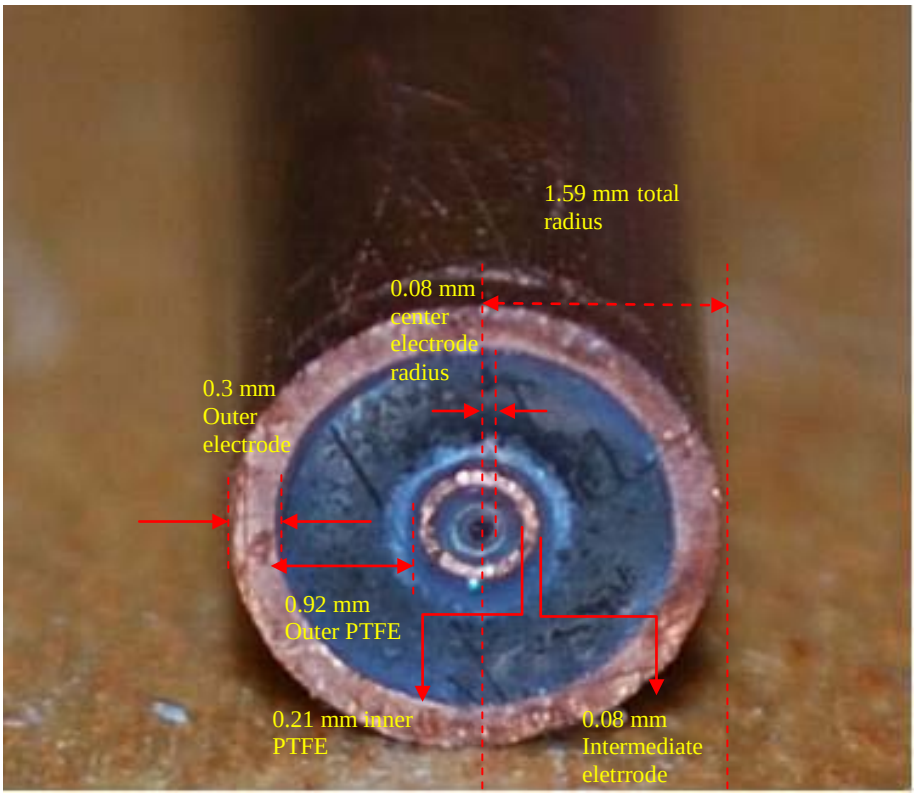

Figure 24 Three-Electrode µPPT Dimensions

The first type was the previously pre-made thrusters received from AFRL and Busek Co Inc. The thrusters made by a private company with all three electrodes and the required PTFE rings, with no construction required by the user.

The second type was built at AFIT. Two tubes were ordered, one being the outer electrode with an inner electrode the size of the trigger and the second tube consisted of what would become the intermediate electrode and the center electrode. With the inner electrode removed from the larger tube, room exists to insert the trigger tube. Appendix A contains a more detailed explanation for this process.

The pre-made thruster proved easier to make for use in these experiments. The center electrode for these thrusters is a thicker diameter of copper making it stronger and easier to connect with the high voltage wires used to connect the thruster to the power circuits. The tube ordered by AFIT had a very thin center electrode that easily broke when trying to connect it to the high voltage wire. The size of the center electrode is very different. Another problem with the AFIT made thruster was a tendency for the PTFE to slide inside the copper rings. The outer tube was heated, making the PTFE more malleable, to remove the original center copper wire to be replaced by the trigger tube. However, pulling on the center wire, the PTFE on occasion would stick to the center wire and slide out of the outer tube. In this case, the thruster at least is cut shorter and on occasion causes the loss of the whole thruster due to certain size requirements based on the connecting wires and the thruster holders described later. In the end, the pre-made thrusters were the most reliable for use on these experiments.

An important aspect of the thrusters for this research is end-of-life situations. Previous research at Busek Co. Inc.[13] showed thrusters lasting into the realm of 100,000

shots before ceasing operation. It is important though to define “ceasing operation” for these thrusters. In this research a thruster is considered to have “ceased operation” when the trigger is no longer controlling when the thruster fires. At this point, several things can be happening, electrodes may be touching or eroded away, the trigger may no longer be able to fire and cause the thruster to not spark at all, or the outer electrode may be able to spark to the inner electrode due to lack of presence of the dielectric PTFE. In any of the cases, the thruster will no longer be firing controllably or at all, and would no longer be suitable for space operations.

III.2.2 Pulsed Circuits

III.2.2.1 Trigger Circuit

The trigger circuit needs to produce voltages up to 10000V at relatively low frequencies, but with pulse-widths in the nano-second range. As discussed in Chapter 2, capacitive circuits are the best for this type of operation. In order to create this high voltage, small pulse-width pulse a pulse generator from HV Pulse Technologies Inc, was used. Below in Figure 23 is a picture of the HV pulse generator and in Table 2 are the capabilities of this device.

Figure 25 High Voltage Pulse, M10k-20

Table 2. HV Pulse capabilities

Parameter	External Load	
	None	10,000 Ω / 40 pF
Amplitude (kV)	0.5 to 10	0.5 to 10
Rise Time (ns)	< 150	< 500
Fall Time (μs)	< 5	< 2
Width (50 %) (μs)	3 to 1,000	1 to 100
Max Repetition Rate (Hertz)	> 6,000	> 600
Maximum Duty (%)	> 2	> 0.2

A frequency generator controlled the HV pulse generator. An Agilent 33120A, Figure 24, was used to input a ramp function of 5V into the HV controller at frequencies for 500 mHz to 2 Hz. The controller then transformed this voltage to the required voltage, from 6000-10000V.

Figure 26 Agilent 33120A Function Generator

The controller was used in the preliminary and setup stages of this research. However, conduction of the actual experiments used an inductor. This circuit uses an agilent power supply to provide an input of 10V into a .7 uF capacitor. The capacitor is hooked into an inductor called a TV backyard amplifier, taking the voltage from 10V to approximately 20,000V.

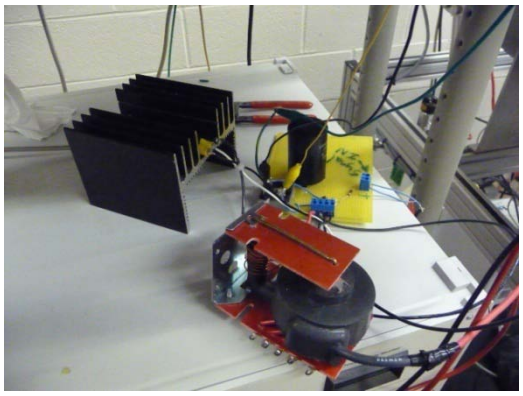

Figure 27 Inductive trigger circuit

III.2.2.2 Outer Electrode Circuit

The trigger and the outer electrode of the thruster received power from different circuits. This circuit did not require a high voltage pulse, only a voltage high enough to allow electric field breakdown and ecton emission to occur with the presence of the plasma from the trigger circuit. Work previously done by Captain Myeongkyo, seen in Table 3, shows that the thruster can operate with as little as 1400V on the outer electrode, only requiring an input of 4V.

Table 3 3 Electrode μPPT operability

Input (V)	1	2	3	4	5	6	7	8
Output (V)	290	760	1100	1400	1640	1840	1990	2110
Energy (Joule)	0.1	0.6	1.2	2	2.7	3.4	4	4.5
Work or not	Not	Not	Work but weak	Work	Work	Work	Work	Work

For this circuit, an EMCO amplifier, Figure 26, takes the input voltage and amplify it to the needed higher voltage, for example, taking a 5V input, from a power supply, to a 1640V output. Once the voltage is amplified, it is sent into two 2 uF

capacitors connected in series. These capacitors charge and hold this high voltage until triggered by the presence of the plasma. The capacitors provide for a small pulse width at a high voltage, which is advantageous for systems operating at micro-second speeds as discussed earlier in Chapter 2.

Figure 28 EMCO amplifier

Once the trigger fires, the high voltage pulse easily tops the electric field breakdown voltage causing ecton emission and the formation of a spark creating the seed plasma, as discussed earlier in Chapter 2. The seed plasma acts as the switch for the outer electrode. Figure 25 shows a picture of the circuit.

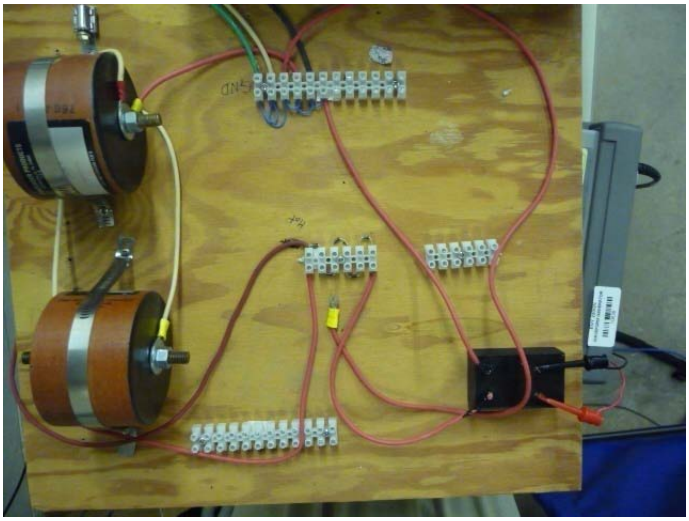

Figure 29 Outer Electrode Circuit

III.2.3 Torsional Thrust Balance

The torsional thrust balance built by Busek Co. Inc. is capable of measuring thrust of approximately 1uN. As mentioned above, the TVAC houses the torsional balance during testing. Due to limitation imposed by the location of feed-throughs, it was necessary to place the balance on a stand to raise it 12 in off the table.

The balance itself has several parts. The most important being the balance arm. The thruster is placed on one end of the arm and a counterweight placed on the other as seen in Figure 27. The counterweight helps to keep the arm balanced and remove any torques from the weight of the thruster itself.

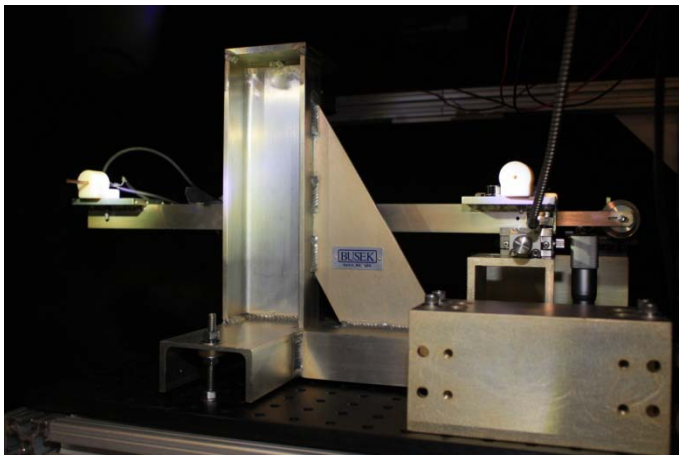

Figure 30 Balance with thruster and counterbalance

In addition, the wires from the back of the thruster are taped down so they leave the arm at the center, minimizing any torque they may add to the arm. The arm itself attaches to the stand by torsional springs and bearings.

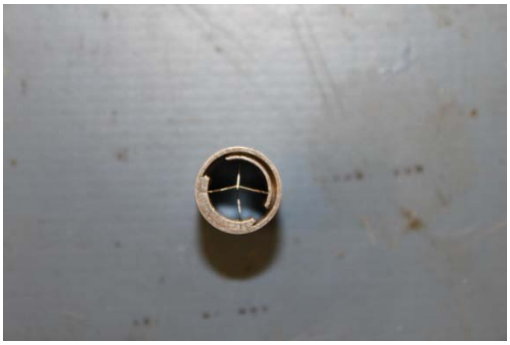

Figure 31 Sample torsional spring used in the balance

There are two adjustable pivots to level the balance for clean data using the provided leveling bubble. Once the stand is level and the arm is balanced, the data collection portion of the stand is ready for calibration. A laser displacement system, or LDS, built by Philtec, Figure 31, collects the data. The LDS uses a fiber-optic sensor to determine the distance of a mirror on the arm from the LDS tip and returns a voltage as the raw data. As the arm moves the voltage also changes in a linear fashion. A magnet placed on a support beam near one end of the balance arm, as a passive dampening system. The magnet pushes back on the arm as it swings close and provides the restoring force to help the arm settle after a test has been completed. The restoring force applied by the magnet is very small compared to the force of the thruster so it can be ignored later during the thrust analysis.

Figure 32 (left) Philtec LDS power supply

Once completing setup of the balance and thruster, the LDS tip was placed within 1mm of the surface of the mirror. Within this distance, the LDS sensitivity is at its best and returns very accurate results. Next, in the procedure calls for determining the ratio of voltage versus the distance the arm moves. A known force, applied through two electrodes on the balance, provides the method to find the ratio. One is a standalone electrode and the other is on the end of the balance arm, as seen in Figure 29.

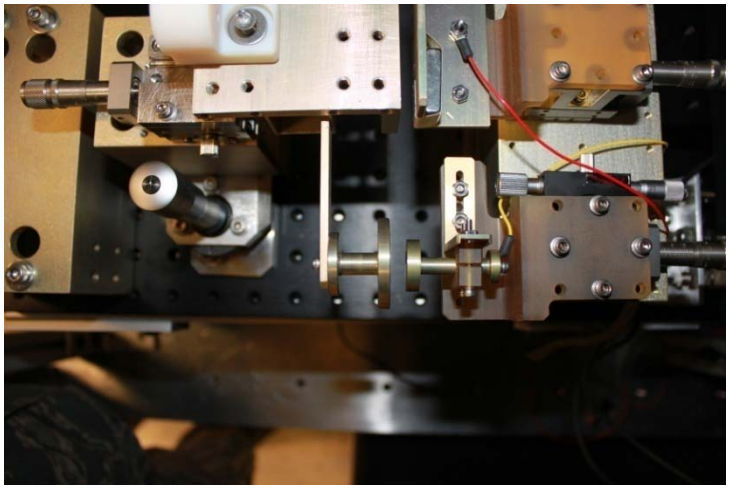

Figure 33 Electrode placement on the Torsional Balance

In the torsional balance setup, the two plates act as parallel plate capacitors. The plates receive a charge, $\pm Q$. Assuming plates of infinite extent, the electric field, E, produced by each plate would have the magnitude of Eq. 18[14], and together would produce the total electric field, E_{tot}, seen in Eq. 19. The plates have an area, A and with a permittivity of free space of ε_o.

$$E = \frac{Q}{2A\varepsilon_o} \qquad \text{Eq. 18}$$

$$E_{tot} = \frac{Q}{A\varepsilon_o} \qquad \text{Eq. 19}$$

The potential difference, V, between the two plates separated by a distance, d, can be seen in Eq. 20. Rearranging and solving for Q leads to the charge of the plates.

$$V = E_{tot}d = d\frac{Q}{A\varepsilon_o} \qquad \text{Eq. 21}$$

$$Q = A\varepsilon_o\frac{V}{d} \qquad \text{Eq. 22}$$

Having an equation for the charge and electric field for each plate, a relationship for the force, F, between the plates can be found, knowing that the force is equal to the charge on one plate multiplied by the electric field from the other. The derivation shown in Eq. 23.

$$F = Q\frac{Q}{2A\varepsilon_o} = \frac{\varepsilon_o AV^2}{2d^2} \qquad \text{Eq. 23}$$

The force equation is for plates of infinite extent, so a correction factor is needed to adjust this force for electrodes of finite size, shown in Eq. 23 for circular plates of diameter D. If the diameter is very large this factor approaches unity, but for finite diameters the effects become larger.

$$F = \frac{\varepsilon_o AV^2}{2d^2}\left(1 + \frac{2d}{D}\right) \qquad \text{Eq. 24}$$

However, the torsional balance presents a very special case wherein the electrodes are not only of finite size, but the electrodes are each different sizes, making the area a very complex part of the equation. The same basic equation is used; however the values of the correction factor will be more complicated. Busek Co. Inc., using a Maxwell modeling software, was able to develop a correction factor and equation specific to the size of the electrodes on the torsional balance and its operating conditions which affects

ε_o. The equation developed from this model for the force between these specific electrodes shown in Eq. 25.

$$F = \frac{1.262\times10^{-9}(1+138.1d)V^2}{d^2} \qquad \text{Eq. 25}$$

Eq. 25 has the same form as Eq. 24. It has a constant out front multiplied by $\frac{V^2}{d^2}$. It also has the correction factor, however instead of being simply $\left(1+\frac{2d}{D}\right)$, it is more complicated due to the differing diameters of the electrodes making the new correction factor $(1+138.1d)$, with the 138.1 replacing $\frac{2}{D}$.

In order to use Eq. 26, the distance between the electrodes must be accurately known. The standalone electrode is on a movable plate controlled by turning a knob with micrometer markings, giving one turn is 50um. The standalone electrode receives a 100 V charge, making it an electromagnet, thus attracting the electrode on the arm. As the arm moves the voltage changes, as seen on the oscilloscope, until the two electrodes touch each other, at this point the voltage on the LDS can be seen peaking and then moving back down. Once reaching the peak, the charged electrode is moved back 1mm from the electrode on the arm. Now that the distance between the electrodes is accurately known, the chamber is ready to be pumped to a vacuum to complete the calibration.

Once at a vacuum, the standalone electrode again receives a 100 V charge. The movement of the arm due to the electromagnetic attraction of the electrode is measured. Using Eq. 25 the force on the balance arm is calculated as 14.46uN. With the displacement of the arm measured, a ratio of μN/V is found. The calibration conducted at AFIT, did not see the displacement measured by Busek, giving a ratio several orders of magnitude larger than previous calibrations by Busek Co. Inc. The original calibration

ratio developed by Busek Co Inc provides more accurate data instead of the calibration ratio determined at AFIT. After discussions with Busek it was determined the calibration tests did not properly model the short pulse duration of the µPPT and therefore was not giving the correct displacement. Using the Busek displacement, a conversion of 3121.7 µN/V was found.

Once the signal from the LDS goes to the control box, the signal splits and is sent to both an Agilent 54622D mixed Signal Oscilloscope, Figure 31, as well as a NI-9205 Data Acquisition Module (DAQ). The DAQ connects through NI-9211 to a laptop with LabView software, Figure 32. This software allows the user to input the data sample rate as well as sample size for a test. Once the data is collected, it can be saved as a text file to the location of the user's choosing. The oscilloscope provided immediate signal feedback, helping to determine proper functioning of the LDS system as well as being used in the force calibration of the electrodes.

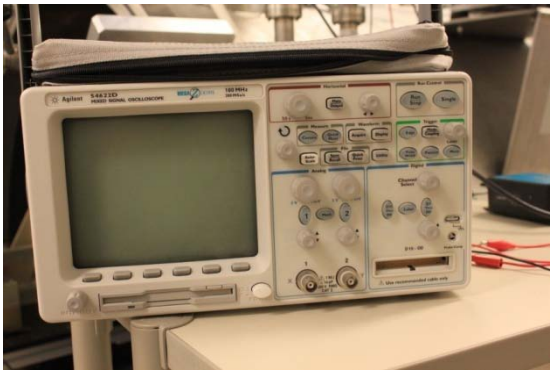

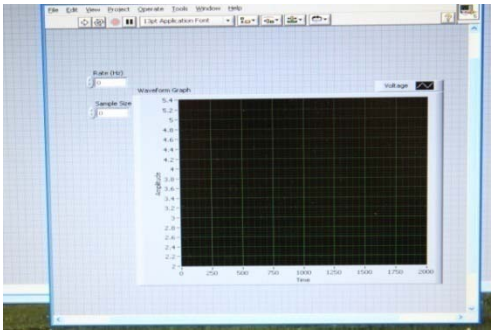

Figure 34 (left) Agilent 54622D mixed Signal Oscilloscope
Figure 35 (right) LabView Software to control DAQ system

The LDS control box and calibration voltage was originally operated by a controller provided by Busek Co Inc, Figure 32. However, the controller ceased to be

reliably operable and work-a-rounds were created. The LDS was left continually powered and hooked directly to the oscilloscope and DAQ. In addition, same power supply as the inductor circuit provided the voltage used for the force calibration, since the functions were not used at the same time.

Figure 36 Busek Torsional Balance Control Box

III.2.4 Shimadzu HPV-2

The high-speed video was taken using a Shimadzu HPV-2 camera. The camera is capable of taking video up to and including 1 million fps. The camera uses a stacked array of CCD chips taking 102 frames, so 1 million fps video captures 102 us of operation. The camera itself is connected to its power supply, a laptop through a USB cable and the same frequency generator as the trigger circuit. The laptop contains all the control software for the camera. Every aspect of the camera can be controlled, from the frame rate, the gain and exposure time as well as setting an internal or external trigger. After camera images a pulse, the video can be viewed instantaneously to determine the integrity of the data collected. Several save options are available including a video file as well as saving each image individually.

Figure 37 Shimadzu HPV-2 Camera

III.2.5 Additional Equipment

III.2.5.1 Photodiode

Several of the experiments relied on accurately knowing the number of pulses the thruster fired. Originally, the frequency of the thruster was controlled and the number of pulses determined by the length of time the thruster fires. The method works well for a new thruster, however as the number of pulses increases, the thruster becomes unreliable in the consistency of its operation and another method of counting shots was required. To meet the counting requirement, a photodiode counted the pulses using the light emitted. The photodiode was powered with 5V and connected to the DAQ. A LabView program counted the pulses using a trigger function. The photodiode, when not in light, returns a sinusoidal with the peaks at the inputted voltage. When in the presence of light, the photodiode voltage increases and holds a higher value. When the voltage increases past a trigger value, the LabView adds an additional pulse to the count. No additional

count is made with the voltage falls. The photodiode proved to be very effective and able to count even the fastest of pulses.

III.2.5.2 Scale

A Voyager Pro scale provides accuracy to +/-1 mg. This provides enough accuracy to measure the change in mass of the thruster during its operation. The scale itself consists of the base plate and digital readout along with a Plexiglas shield to remove any effects from air currents in the room. The balance has a built in level and adjustable rear legs to allow for proper leveling. In addition, the scale has a built in function to let the user know that the scale is stable and able to take a very accurate reading.

Figure 38 Scale

The scale functioned well when allowed to fully warm-up. On occasion, the scale would drastically over or under weigh an object and then slowly approach the correct weight. The error can cause the scale to take close to 15 min to get a single

measurement. In these situations, the best solution was to turn the scale off completely, including pulling the plug, and then restarting the scale and allowing for proper warm up. The problem only occurred when the scale did not warm up causing it to malfunction during operation. When used properly the scale was capable of accurate and repeatable measurements.

III.2.5.3 Stands

Both the mass collection and video experiments required the use of stands to hold the thruster in the proper position. For the mass collection test, a stand was built using the 3D printer to hold the thruster in a vertical position. The stand also had pegs on the legs to hold a bowl to collect the mass coming off the bowl. The material used does outgas, and could cause the chamber to take longer to pump down, however the stand was small enough and pumps efficient enough that no delay was noticed.

Figure 39 Mass Collection Stand

For the video experiment, the thruster needed to be positioned horizontally and level with the center of the main viewing window of the chamber. An aluminum stand, provides the needed height and stability for the camera.

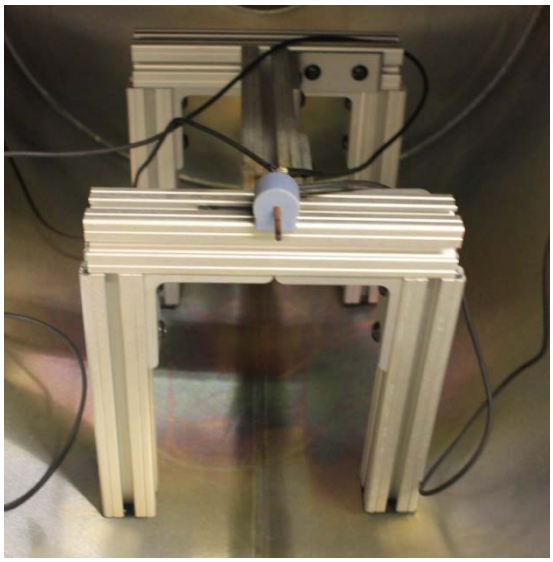

Figure 40 Video Collection Stand

III.2.5.4 Thruster holder

The stand, made of metal, required precautions to remove the possibility of the thruster sparking to the stand. A holder made on the 3D printer held the thruster away from the stand. The holder is nonconductive and thus removes the possibility for the thruster to arc to the stand. The torsional balance required the holder to both hold the thruster and provide counterweight on the other side of the arm.

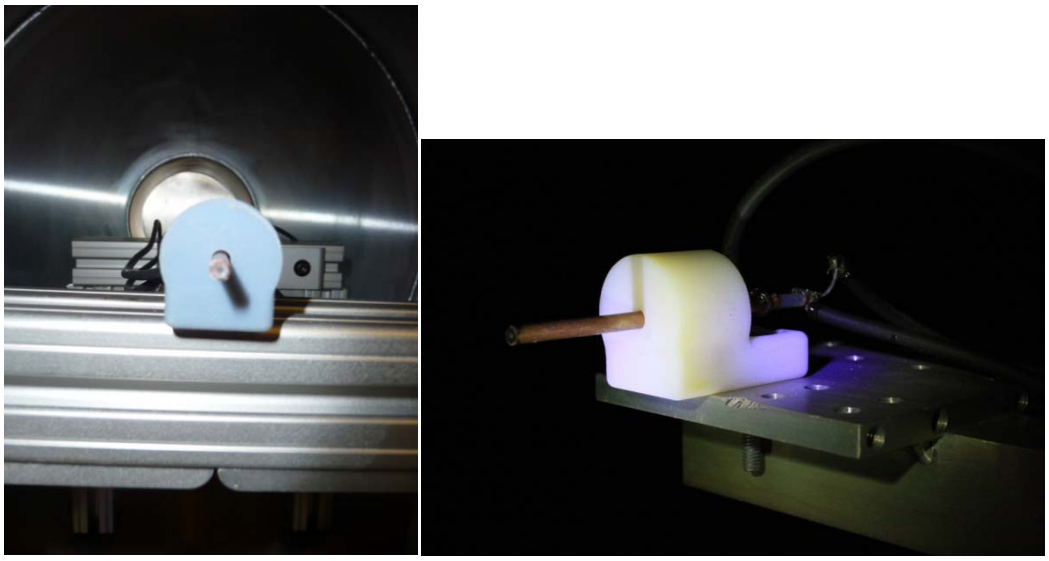

Figure 41 Thruster holder

III.2.5.5 Extension Tubes

The GNAT laboratory does not have a lot of space, requiring the test setup to take up as little space as possible. For the video collection test, the placement of the camera depended on the focal length of the lens. The lenses used, required large focal lengths for the magnification required, forcing the camera to be placed far from the chamber. The extension tubes work by moving the focal point of the lens further from the CCDs of the camera. The extension tubes also magnify the image from the lens, giving a closer look at the tip of the thruster. Figure 36 shows the nine inch and three inch extension tubes.

Figure 42 9 in and 6 in Extension Tubes

The extension tubes are made from aluminum tubing, with Nikon mating surfaces attached. Black paint, sprayed on the inside of the extension tubes, diminished the reflectivity of the aluminum.

III.3 Test Setup

III.3.1 Mass Collection

The goal of the mass collection experiment is to measure the total amount of mass lost by the thruster as well as the mass emitted by the thruster as particulates not ionized to produce thrust. To meet this goal the test was setup to capture the change in mass of the thruster throughout its lifetime performance. The thruster was fired vertically into a plastic bowl used to capture any particles thrown off the thruster. The collection bowl was a plastic to keep the conductivity issues to a minimum without increasing the out-gassing issue. A lid on the bowl to kept the particles from bouncing out of the bowl. The thruster itself was placed so that the tip of the thruster was below the lid so even particles

thrown at an almost 45 angle would also be caught. A newly constructed thruster was weighed to find a starting mass. The collection bowl is also weighed at this point. After the weighing, no changes were made to the thruster or the collection bowl.

The thruster and collection bowl were placed onto the stand and into the vacuum chamber. The chamber was then pumped down to vacuum.

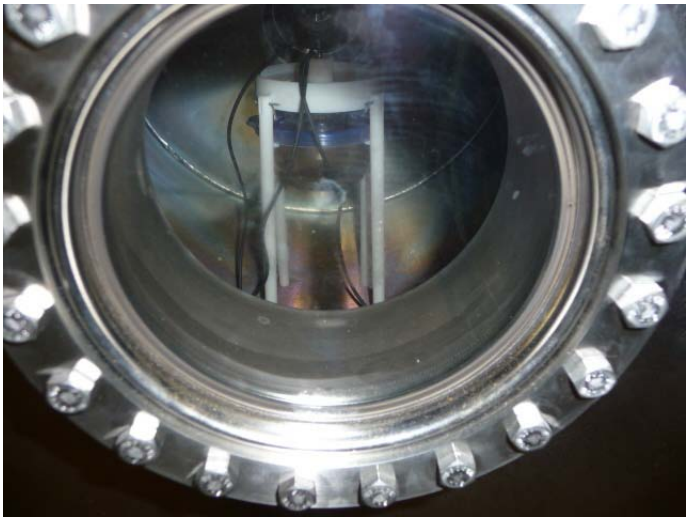

Figure 43 Mass collection setup

The thruster was fired for a predetermined amount of shots, Table 4. In the beginning of life, it is reasonable to use a set time, as the thruster is very controllable and reliable so a known number of shots fired. However later in life the thruster becomes harder to control and less reliable so the photodiode was employed to keep count of the number of shots the thruster fires.

Table 4 Mass Collection Test Plan

Test Series	1	2	3	4	5	6	7	8
Shots	500	1000	1500	5000	10000	12000	35000	36000
#/shots	500	500	500	3500	5000	2000	23000	1000

Once reaching the predetermined number of shots, the chamber is vented and the thruster and collection bowl are removed. At this point, the bowl and thruster need to be given time to absorb moisture and gasses lost when the chamber was pumped to vacuum. Previous tests conducted at AFRL by Dr. Greg Spanjers[9], the PTFE bars for the much larger PPT gained 1mg of mass in the first hour and then remained at a constant value over the next 30 hours. Knowing the µPPT is a much smaller device and based on previous experiences with weighing the µPPT post-test, it was determined at least 15 min ensured the PTFE and plastic had regained lost moisture and gasses.

After the waiting period, both objects were weighed. The weight was recorded as not only the post-test weight but as the pre-test weight for the next run. Neither the thruster nor the bowl were cleaned in any way between test runs. After taking several weight measurements for later error analysis, the thruster and bowl are replaced in the vacuum chamber and the next test in the series was completed.

This test was run until 100,000 shots were reached or the thruster ceased operation.

III.3.2 Thrust Measurements

The thruster was placed in the holder on the opposite side of the arm from the LDS and mirror, due to the concern of contamination from the thruster as it fired.

The chamber is pumped down to vacuum. Once the required pressure, below 10^{-4} torr, is reached the test may begin. To run the test both the roughing and turbo pumps must be turned off. First, the valve between the turbo and roughing pump is closed. Then the turbo and roughing pump, in that order, are turned off. The turbo pump requires

a long period of time to wind down. Unfortunately, the chamber cannot hold pressure for too long, so after a minute of letting the pump wind down testing must begin. The noise associated with the turbo pump is low enough to not affect the results of the test too much.

The thruster was tested at different firing frequencies in an attempt to isolate single shots and also try to capture a constant thrust level. To meet this end the thruster was fired at 500 mHz, 100 mHz and 50 mHz. Using the LabView program to control the DAQ, data was taken at 500 Hz for a preset number of samples based on the particular test being done, as can be seen in Table 5.

Table 5 Test Plan for Thrust Measurements

Test	Length of test (s)	Number of Tests	Sampling Rate (Hz)	Number of Samples
Baseline	30	1 per frequency	500	15000
500mHz	60	2	500	30000
100mHz	60	2	500	30000
50mHz	90	2	500	45000

First a baseline test was completed without the thruster firing. This was required to give a noise baseline of the stand as the force is found by comparing how far the arm moves from a baseline level. Since the turbo pump did not fully wind down, it was important to have a baseline for each test being completed as the noise level was changing as the turbo pump wound down.

Early in the thruster life all tests could be completed before the pressure rose above 1.5×10^{-4} torr. However, as the thruster became older an emitted more extra particles the pressure inside the chamber rose more rapidly. At this point the chamber had to be pumped down between each set of tests for a prescribe frequency.

The test is conducted at preset number of shots based on the results of the mass collection test. It was important to be able to align thrust measurements to points were thruster mass had been measured. In addition, due to the setup of the thruster in the TVAC, it was not possible to directly see how the thruster was operating and if it had met the end of life criteria mentioned earlier. Using the knowledge gained from the mass collection test, the end-of-life was assumed to be about the same, roughly 35,000 shots. Table 6 shows the test plan followed for the thrust measurements, used in combination with Table 5.

Table 6 Thrust Measurement Test Plan

Shot Count	Frequency (mHz)	Shot Count	Frequency (mHz)
0	500 100	15000	500 100 50
1000	500 100 50	20000	500 100 50
1500	500 100 50	25000	500 100 50
2500	500 100 50	30000	500 100 50
5000	500 100 50	35000	500 100 50
10000	500 100 50	30000	500 100 50
		35000	500 100 50

III.3.3 Video Collection

The test plan for the video collection involved collecting videos from a brand new thruster and from a thruster at the end-of-life to compare the resulting pulse characteristics. The mass collection thruster was used as the end-of-life thruster for this data collection.

To conduct the test the thruster was placed in a stand, described earlier, to face the window. The camera was triggered along with the thruster and video was taken at various fstops and gains in the computer to pull out different details seen with different amounts of light.

III.4 Error Analysis

The data collected in this analysis was subject to various errors. In order to account for the error, the error bars are included in all graphs. The error was determined from the standard deviation and the accuracy of the equipment used to collect the data. The number of data points, n, is a major factor as is the standard deviation, σ. In most cases, the standard deviation term far outweighed the error from the equipment, θ. Eq. 27 determined the error for every data point.

$$err = \sqrt{\left(\frac{2.776\sigma}{\sqrt{n}}\right)^2 + (\theta^2)} \qquad \text{Eq. 28}$$

IV. Results and Analysis

As stated in Chapter I, there are several main objectives of this research, including thrust, mass loss and contamination and finally spark formation. The experiments described in Chapter III were specifically designed to investigate these objectives and reach solid conclusions for each. In this chapter, the results of each test are presented and in so doing show how they contribute to reaching the objectives.

IV.1 Thruster Operations

Important to all the experiments conducted was the operation of the thruster throughout its lifetime. A capacitive circuit powered the outer electrode and the inductive circuit and the frequency generator controlled the trigger circuit and the operation of the thruster.

The circuits performed well for the lifetime of the thruster. However, the changing shape of the tip of the thruster caused the operation of the circuits to change throughout the lifetime. As the center electrode eroded away, due to loss of mass from the ecton emission described in Chapter 2, the distance between the electrode and the inner electrode grew larger, increasing the voltage breakdown level. In order for the spark to form, the trigger circuit must exceed the voltage breakdown level, which was ever increasing. The input voltage to the trigger circuit increased continually in order to properly regulate the trigger spark.

The outer electrode also experienced problems due to the changing structure of the thruster. In this case, the spark continually formed over one part of the thruster. The outer electrode may not be perfectly circular and thus closer to the trigger in certain areas,

or any imperfections in the copper of the electrode caused during the cleaning of the tip of the electrode during construction of the thruster. As the spark formed over just one part of the thruster the PTFE© dielectric was eroded in just in this one spot. In so doing a channel was worn into the PTFE©, but since these electrodes are larger they do not erode away as quickly as the center electrode. The PTFE© provided an impedance to the formation of the spark, however with the newly worn channel this impedance is lowered thus lowering the required breakdown voltage. As the thruster fired, it was actually necessary to lower the voltage to the outer electrode. Without taking this action, the outer electrode did not require the presence of the trigger circuit in order for a spark to form. This caused the thruster to fire uncontrollably, and although the photodiode was capable of keeping up with these sparks, it is important to keep the thruster firing normally and at a constant rate. By firing without the trigger circuit, the erosion that would have taken place due to the trigger does not occur. Also, based on previous experiments on the temperature of the PTFE©[10] after spark formation, it is known that it takes time for the temperature to fall back to pre-spark conditions. When the outer electrode is able to fire uncontrollably, it fires almost continuously, keeping the temperature of the PTFE© high. At a higher temperature it does not take as much energy for the PTFE© to be ablated, as a result the spark is able to ablate more of the PTFE© than would be possible at a controlled firing rate.

The thruster successfully operated for approximately 35,000 shots by adjusting the input power to each circuit as the conditions above arose. However, after this point the thruster started to become uncontrollable even using the techniques described above. After 36,000 shots the thruster reached the end-of-life conditions previously described,

the thruster was entirely uncontrollable and even would stop firing all together for long stretches.

For the thrust measurements, there was no window available to watch the thruster and know how well it was operating. The photodiode gave a good idea if it was controlled or not, but could not be relied on for accurate knowledge of the end-of-life conditions. So for the thrust measurement, 35,000 shots was used as the end-of-life to match with the mass collection test.

IV.2 Mass Collection

IV.2.1 Weighing

An important part of this experiment was weighing the thruster and the bowl pre- and post-test. Getting reliable and accurate data from the scale proved more difficult than originally thought. The scale was very finicky in its operation. The scale itself has a warm-up time that varies from 4-10 minutes. Using the scale prior to the scale warming-up caused the scale to take longer to reach the actual weight of the object being weighed, even after the warm-up time has passed. In this condition, the scale would normally overshoot the weight by several tenths of grams. Then the weight would tick down by the milli-gram until it reached the correct weight. This could take up to 20 min for the weight to settle. The rate at which the weight dropped was not constant, nor accelerates or decelerates at a constant rate. Leading the researcher to begin to collect bad data thinking the final weight had been reached, only for the last measurement to suddenly fall several milli-grams from the other measurements. The difficulty of collecting these

measurements caused major concerns in the reliability of the collected data early in the process of completing the experiment.

The warm-up time varied every time the scale was turned on. The only way to determine the warm-up time was to press the calibration button. The scale will not perform a calibration until the scale has warmed-up. If the warm-up time has not been reached, an error message will quickly appear with the warm-up time countdown. The operation of the scale improved significantly after discovering the need to allow the scale to warm-up. The time to take a measurement dropped from 20 min to approximately one min, reducing the overall time to take the required measurements from almost two hrs to 15 min. The reliability and confidence in the measurements also increased with the improved operation knowledge.

IV.2.2 Chamber operations

The LACO chamber operated very reliably for most of this experiment. The chamber routinely was pumped and vented without any serious issue, other than the previously described issue with the ion gauge. The controlling computer caused the only issues with the chamber. On occasion, the computer would freeze or the controlling circuits would fail to open or close different valves. When this would occur the only recourse was to restart the computer. In every case, the computer was able to control the chamber after the restart.

The only unforeseen issue with the chamber was the force with which the chamber vents. The rapid venting of the chamber often caused the stand to fall over due to the violent rush of nitrogen filling the chamber. The collection bowl did have a lid on

it to retain any particles collected. However, any piece of PTFE© resting on the surface on the tip could be knocked off the thruster. This could slightly skew the results, but the small amount of PTFE© that could fall off in this scenario was believed to be too small to skew the results by any significant value, however it needs to be noted and the next stand needs to be built sturdier, removing this error source entirely.

IV.2.3 Data Collection

A successful data run was completed over the course of several days. The thruster, as mentioned previously, was run until the end of its life at approximately 36,000 shots. Following the test plan in Table 4, data was taken and recorded for each step. At each data point the weight was measured at least 4 times to give enough data for a solid error analysis. The raw data for one test point can be seen in Table 7.

Table 7 Sample Raw Data for Collection Bowl after 500 Shots

Collection Bowl 500 shots	
Pre (g)	Post (g)
24.7618	24.7609
24.7615	24.7612
24.7617	24.7612
24.7614	24.761

IV.2.3.1 Thruster Mass Loss

The raw data formed several graphs to show the trend of mass loss of the thruster versus the number of shots fired. Figure 48 shows the mass loss of the thruster throughout the lifetime, with an average error of .12 mg. The graph clearly shows three different trends. Early in the life the thruster is losing mass very quickly as seen by the large negative slope.

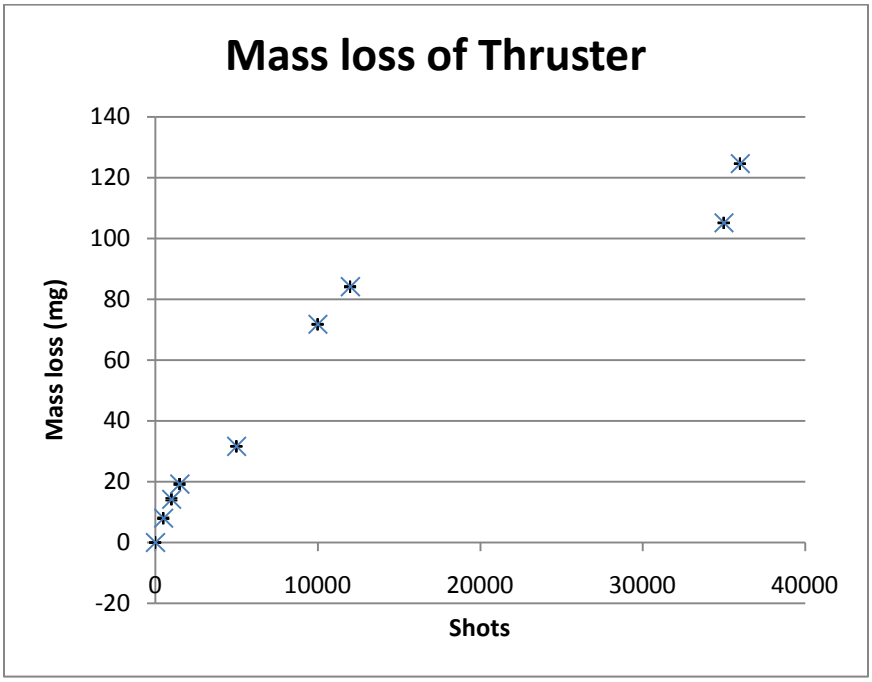

Figure 44 Thruster Mass Loss

A trend line fitted to just this data, Figure 49, shows the slope as 10 μg/shot. In research conducted previously at AFRL[9] showed the first several shots of the PPT fall below the mass consumption rate of the PPT. The first 1,500 shots was considered a warm-up period for the thruster. As seen in Figure 45, the mass loss of the first 1,500 shots is different from the rest of the lifetime of the thruster, with an average error of .25 mg.

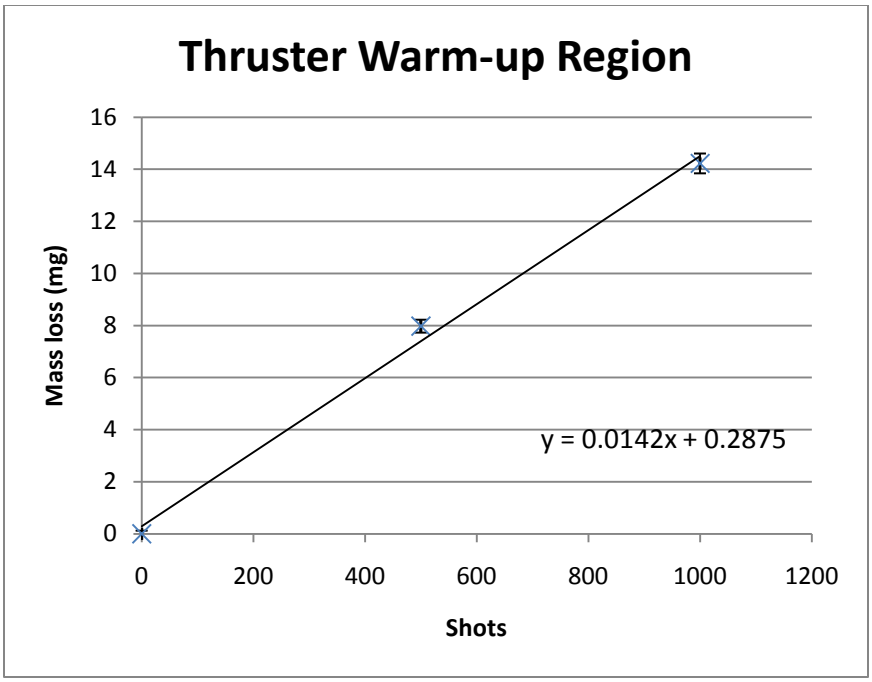

Figure 45 Thruster Mass Loss, shots 0-1,500

However, the μPPT has a greater mass loss in the first 1,500 shots and then the mass loss of the thruster decays as a power function, as seen in Figure 46, with an average error of .21 mg.

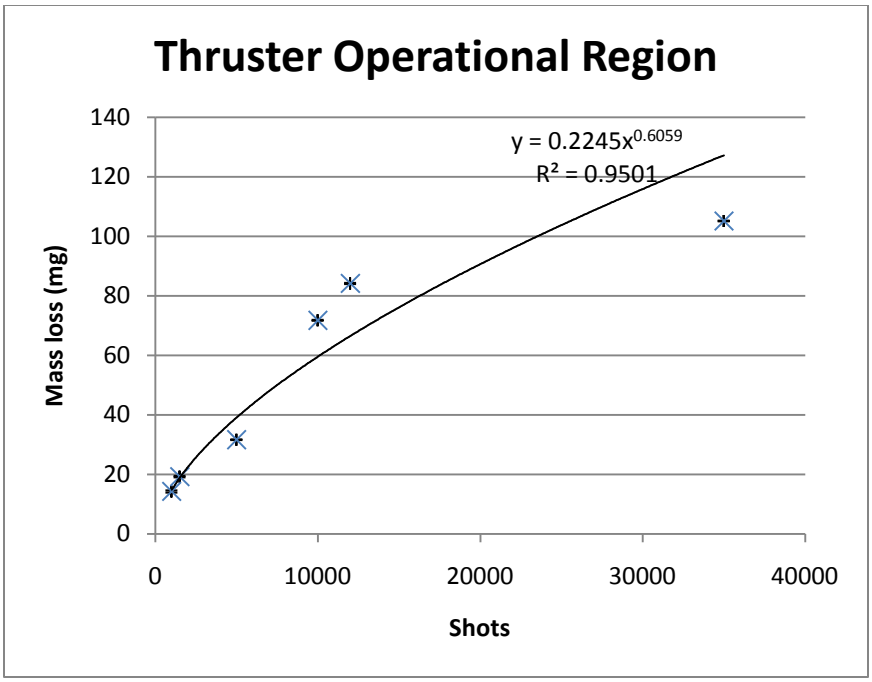

Figure 46 Thruster Mass Loss, shots 1,500-35,000

PPTs have a warm-up period where the mass consumption rate is less than the rest of the thruster, also PPTs follow a very linear curve fit after the first 1,500 shots to have a constant mass loss rate of 26.4 μg/shot[9]. The μPPT also has a warm-up period; however, instead of the gradual rise to the constant mass consumption rate of the PPT, the μPPT's warm-up period consists of a constant maximum mass loss rate of 10 μg/shot, then decays based on a power approximation.

The last data point, at 36,000 shots, is not included in this analysis due to the end-of-life condition of the thruster. Between 35,000 and 36,000 shots, the thruster is no longer operating within the constraints of acceptable operation. At this point, the thruster begins to loss mass at a much larger rate as the thruster sparks at high rates uncontrollably due to the ease with which the spark can form, as discussed before, Figure 51 below.

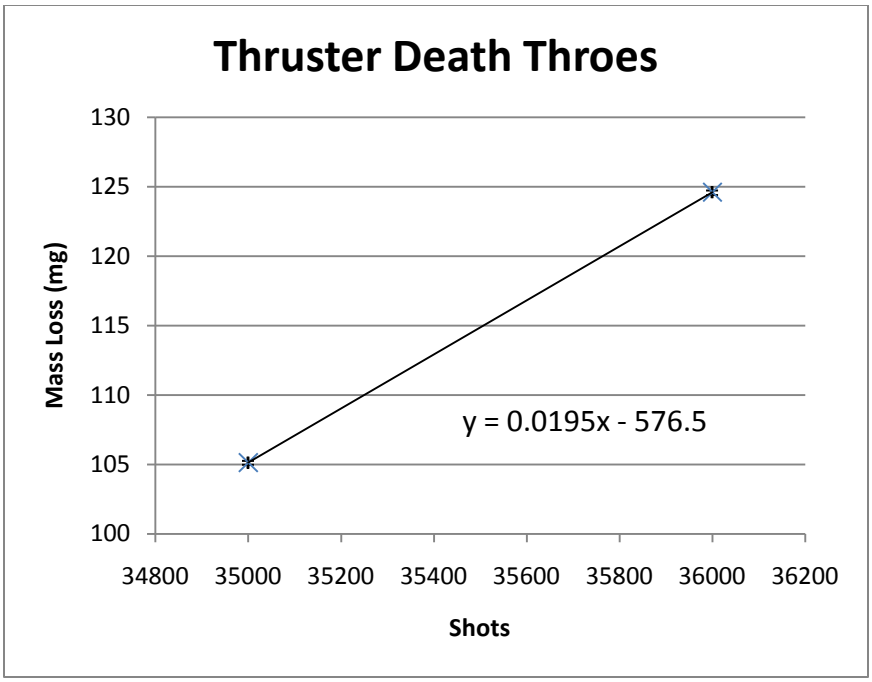

Figure 47 Thruster Mass Loss, 35,000-36,000

At this point the mass consumption rate jumps to 20 μg/shot, with an average error of .125 mg. The mass consumption rate at this point is twice the original mass consumption rate, the thruster mass drops incredibly fast at this point.

IV.2.3.2 Mass Collection Bowl

Also important is the mass collected by the collection bowl during the test. As can be seen in Figure 52, the scale did not have the resolution to pull out the mass collected by the bowl for some of the small shot step sizes, specifically sizes of less 1,000 shots. For the analysis the 500 shot point is removed from the data. The mass of the bowl actually dropped at this point. The data has been thrown out to not negatively impact the trendlines, since it is bad data. The difficulty measuring the very small change in mass demonstrates the very small amount of mass that is lost by the thruster and not

ionized. Not only do these particles add very little I_{sp} to the system[12], but the number of these particles is also very small.

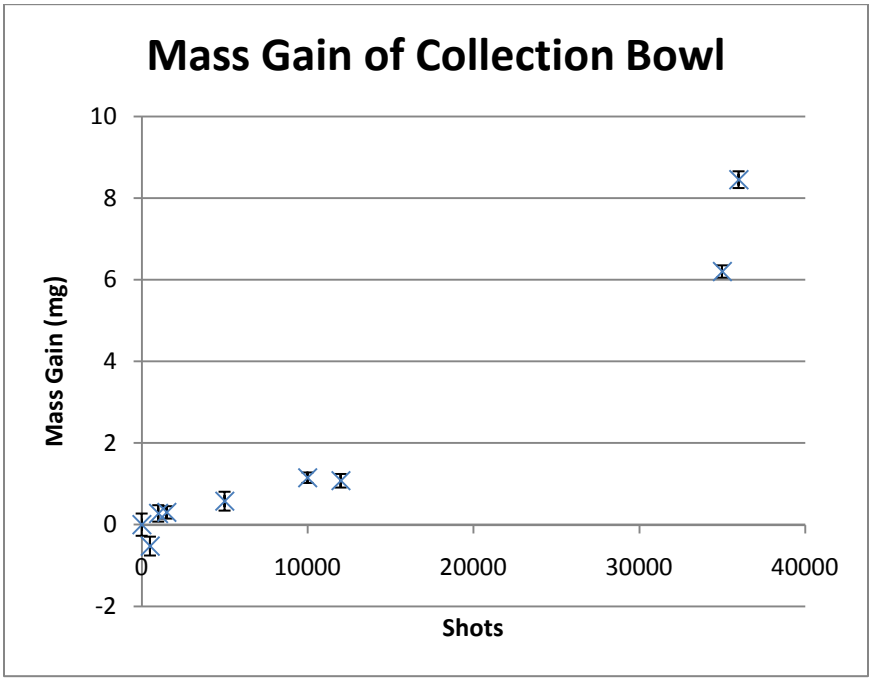

Figure 48 Collection Bowl Mass Gain

Again, there are three trends in this data correlating to the trends for the thruster mass loss, with an average error of .193 mg. The warm-up period, 500-1,500 shots, the operational portion, shots 1,500 to 35,000, and then the end-of-life situation, shots 35,000 to 36,000.

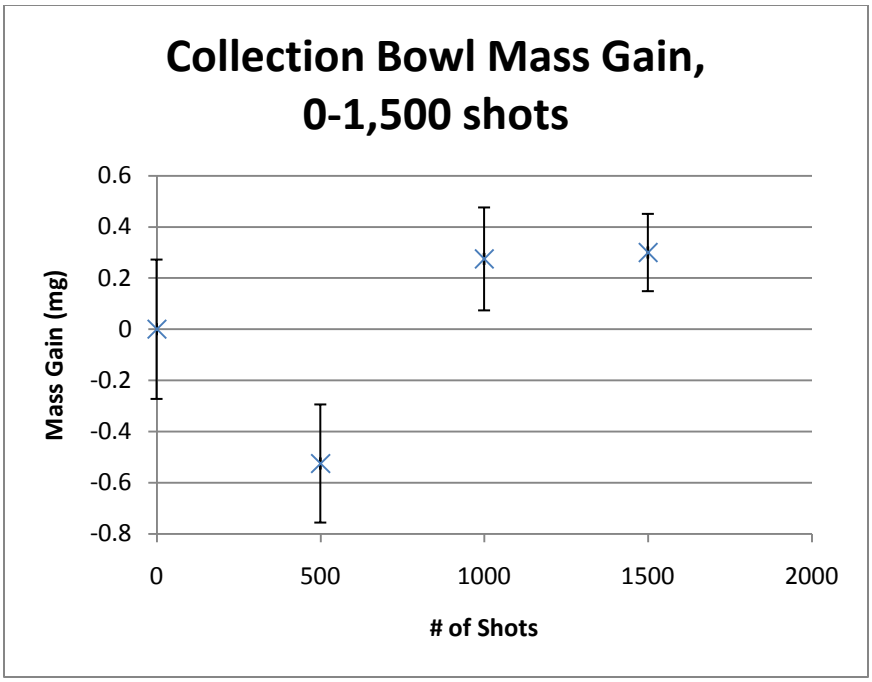

Figure 49 Collection Bowl Mass Gain, shots 0-1,500

During the warm-up period, the mass gain of the collection bowl was .2 μg/shot, with an average error of .23 mg. After this point, the mass gain of the bowl follows a quadratic function. The shape of the curve is very close to the loss of thruster, but it is not an exact match. As the thruster fires, the efficiency of the thruster to ablate and ionize the propellant changes. As seen in Figure 50, with an average error of .13 mg.

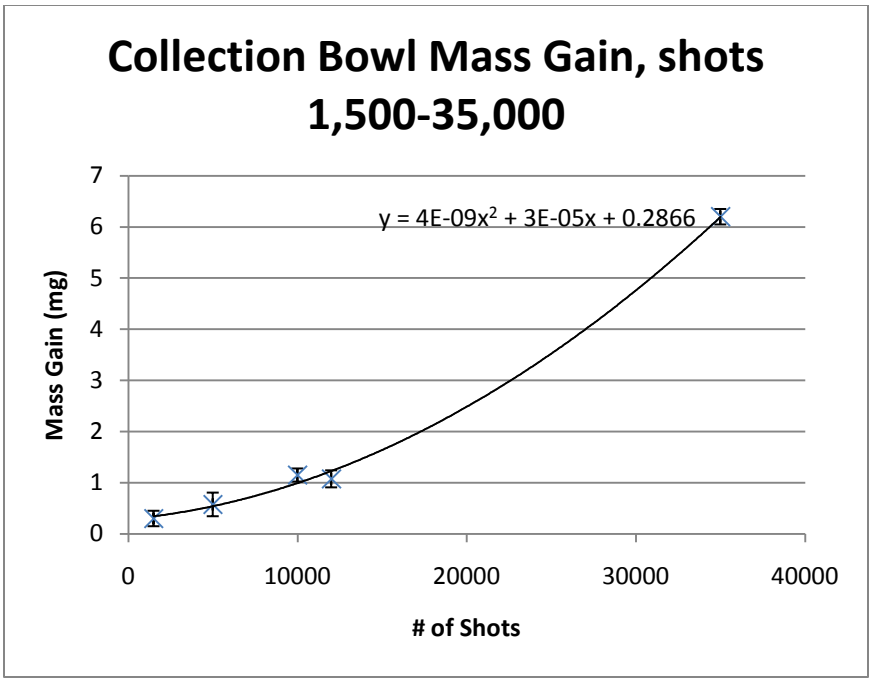

Figure 51 Collection Bowl Mass Gain, shots 1,500-35,000

Again, for the last 1,000 shots from 35,000 to 36,000 shots, the mass gain of the bowl increases by a large amount. Fig shows the mass gain of the collection bowl to be at a rate of 2 μg/shot, with an average error of .178 mg. Once again, the high mass gain shows the propensity of the thruster to discharge large amounts of unionized propellant near the end of the operational life of the thruster.

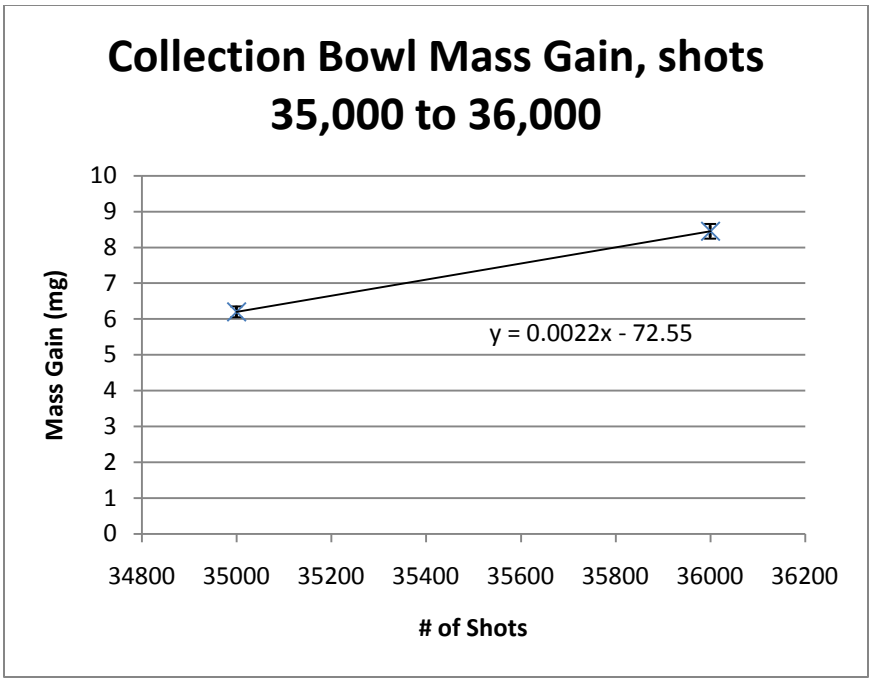

Figure 52 Collection Bowl Mass Gain, shots 35,000-36,000

IV.2.3.3 Propellant Efficiency

The efficiency of the thruster's propellant use is found by knowing the total amount of mass the thruster lost and gained by the bowl. The propellant efficiency is not the total efficiency of the thruster. The total efficiency takes not only the propellant efficiency into account, but also input and output power of the circuits and the losses in the transmission lines. The research presented here is only concerned with the propellant efficiency, η_{prop}.

The efficiency is calculated by equation Eq. 26, where M_t is the mass lost by the thruster and $M_b$is the mass gained by the collection bowl.

$$\eta_{prop} = \frac{M_t - M_b}{M_t} \qquad \text{Eq. 26}$$

The efficiency of the thruster is shown in table Table 8 for each data point. However, due to scale issues, the 500 and 12,000 shot data points are removed. In each

case the bowl lost mass from the previous measurement, once again demonstrating the difficulties of the scale used and the need for a scale with more resolution.

Table 8 Propellant Efficiency of the Thruster

Shots	η_{prop}
1000	95.6
1500	99.5
5000	97.78
10000	98.56
35000	79.90
36000	88.44

The data shows that the propellant efficiency stays above 95% for the first 10,000 shots. Once the thruster nears the end of life the thruster's propellant efficiency drops off to below 90%. The drop in efficiency is due to the increase of mass collected in the bowl.

IV.2.4 Contamination

The μPPT emits a large amount of particulates into the surrounding area when the thruster fires. A clear plastic bowl served as the collection bowl for this experiment to document the effect of the very small particulates can have on the satellite. Throughout the conduction of the test, the bowl slowly changed color. As expected a dark burn ring formed in the bowl directly beneath the thruster early on in the test. Slowly a coating formed over the bowl as the particulates dispersed from the tip of the thruster. Figure 47a shows a clean bowl similar to the one used for the test. Figure 47b shows the actual collection bowl post-test, showing the thick coating the bowl received after only 36,000 shots by this thruster.

Figure 53 a) (left) Clean bowl similar to collection bowl
b) (right) Collection bowl post test

During the test, several large, bright, hot particulates dispersed through the bowl bouncing around inside the bowl. The particulates were most likely pieces of copper from the electrodes thrown off due to the size of the particulate. Since a PPT and μPPt are both made of the same materials, it is safe to assume the same would hold true in this case. Figure 48 shows some of the particulates released from the thruster at the end of a pulse during the mass collection test. Three bright particulates, presumably copper are directly below the thruster, a streak is also visible going at a 45 deg angle from the thruster to the right. The particulates greatly increase the contamination potential of the thruster.

Figure 54 Particulates emitted by the thruster during mass collection test

The particulates seen in Figure 48 increased in frequency later in the life of the thruster, especially between 35,000 and 36,000 shots. The increase in large particulates corresponds to the large drop in mass of the thruster and increase in mass of the collection bowl during the last 1,000 shots. In addition, the large amount of copper particulates correlates with the erosion of the electrodes, especially the inner electrode of the trigger.

IV.3 µPPT Thrust Performance

One of the main objectives of this research is to characterize the thrust of the thruster throughout the lifetime. Testing was completed as described in Chapter III and is analyzed here.

IV.3.1 Test setup and calibration

The thruster was placed in the holder on the opposite side from the LDS mirror. The wires were connected to the appropriate voltage lines and the ground was connected to the chamber itself. The wires were then restrained to the arm and the stand. This kept the wires from hanging off the arm in a location that would cause either an additional torque on the arm or dampening of the motion, as seen Figure 37.

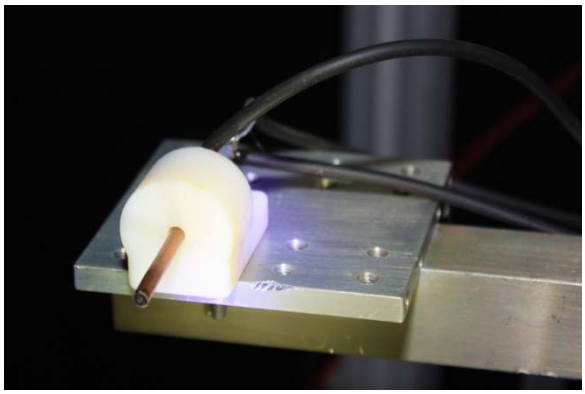

Figure 55 Thruster on Torsional Balance

Once the thruster was in place and an appropriate counterbalance was placed on the opposite arm, the calibration of the stand is ready to be completed. As described before the electrodes needed a separation of 1 mm in order for the proper calibration. The electrodes had a voltage of 100 V applied and following the method described in Chapter 3, thus placing the electrodes 1 mm apart. When turning off the voltage, the balance arm did not return to its original position, it remained slightly torqued from its starting position. Some remaining magnetization in the electrodes could have caused this error, but the exact reason has not been determined.

The next step in the procedure called for the chamber to pump down to a vacuum approximately 10^{-5} torr. At this point, the electrodes again received a 100 V charge. The balance arm electrode reacts to this voltage and the DAQ records the change in the LDS voltage. The LDS showed a voltage change of approximately .00001 V from the baseline before the application of the voltage.

Eq. 25, from Chapter 3, calculates the force from the 100 V calibration voltage as 14.36 μN. Dividing the force by the change in voltage, measured by the LDS, gives a

conversion ratio of over 10000 μN/V. According to the Busek Co Inc[13], a good value of the conversion ratio is approximately 3100-3200 μN/V. The procedure followed in this research placed an error in the data, causing a smaller arm displacement than seen by Busek. Many attempts to fix this error, including re-attempting the procedure and altering the procedure to place the electrodes 1 mm apart when no voltage applied, did not change the resulting discrepancy between the AFIT conversion and the Busek conversion. In order to complete this research, the Busek conversion ratio provided the appropriate force values.

With the conversion ratio determined, collection of the thrust data could begin. The voltage of the current baseline was collected, followed by the collection of the response of the stand to the various inputs as described in Table 6. The wind-down of the turbo pump inserted an error into each of these files. The pumps on the chamber exposed the balance arm to a large vibration environment. The environment caused a torque on the balance arm, shifting the LDS output. Turning off the pumps causes the arm to settle back to its quiet-state position. The wind down of the turbo pump provides a smaller, but a noticeable vibration environment, slowing the settling of the balance arm. Figure 44 shows the response of the balance during the wind-down of the turbo pump.

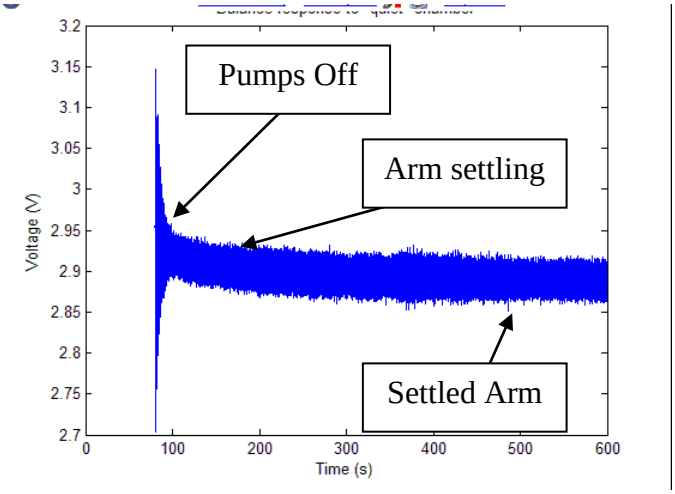

Figure 56 Settling of the balance arm

The response is almost linear, but drops off over a long period. Even though collection of the calibration voltage occurs right before each frequency test, each test is long enough to show an effect of the settling of the arm. A better method of determining the appropriate baseline involved a new procedure for the test. The new procedure involved not only the standard calibration collection, but also turning on the circuit a few seconds after starting the data collection, providing an instantaneous baseline. Completing the test plan with the new procedure created more accurate data for better analysis.

IV.3.2 Analysis Methods

IV.3.2.1 Pulse Amplitude Measurement

The data analysis proved to be more difficult than originally thought. The original method of analysis called for picking out individual pulses within the data and taking the amplitude of the response as the thrust applied. MatLab provided the tool to best analyze the data collected. The code written, first read in each data file and created a

new array for both the time step and the voltage read out. The collected data needed to be cleaned and smoothed for proper analysis. In some data files existed random points well outside the standard deviation of the response, due to random inputs into the LDS. The MatLab code first cleaned the data by removing the random points and replacing the point with the previous point in the data file. Averaging every 25 points into a new data point removed the noise of the signal from the data. Fig shows the raw data and the cleaned and averaged data.

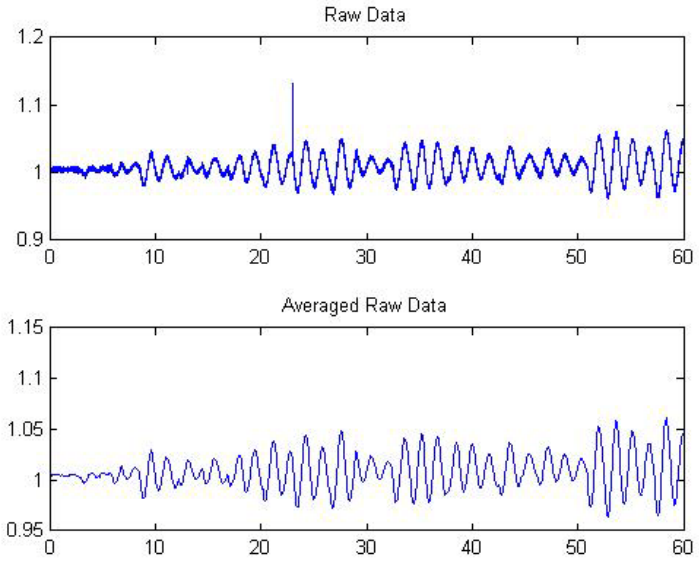

Figure 57 Data for 100 mHz response (above) Raw (below) cleaned and averaged

The next step in the analysis is converting the data from a voltage measurement to a force determine the difference from the baseline for each data set, and then the difference is multiplied by the conversion ratio determined above. The new array showed the force response of the balance arm from the firing. Originally, the method determined the max amplitude of the response after each pulse as the thrust derived from that pulse. However, the response of the balance did not behave as expected. One difficulty

involved determining when the thruster actually pulsed. Since the thruster did not always behave properly and fire consistently, determining when a pulse occurred became a large source of uncertainty. In addition, the response of the balance to a previous pulse seemed to affect the response of the balance to next pulse.

The stand should have a frequency response equal to the frequency of the firing of the thruster. However, every data set shows a harmonic response in the stand beyond the thruster. The harmonics cause the response of the stand to change from the response to a single pulse, to a response of a re-occurring pulse. The response of the stand often grew after a pulse rather than immediately reaching a maximum and then slowly decaying, as seen in Figure 44.

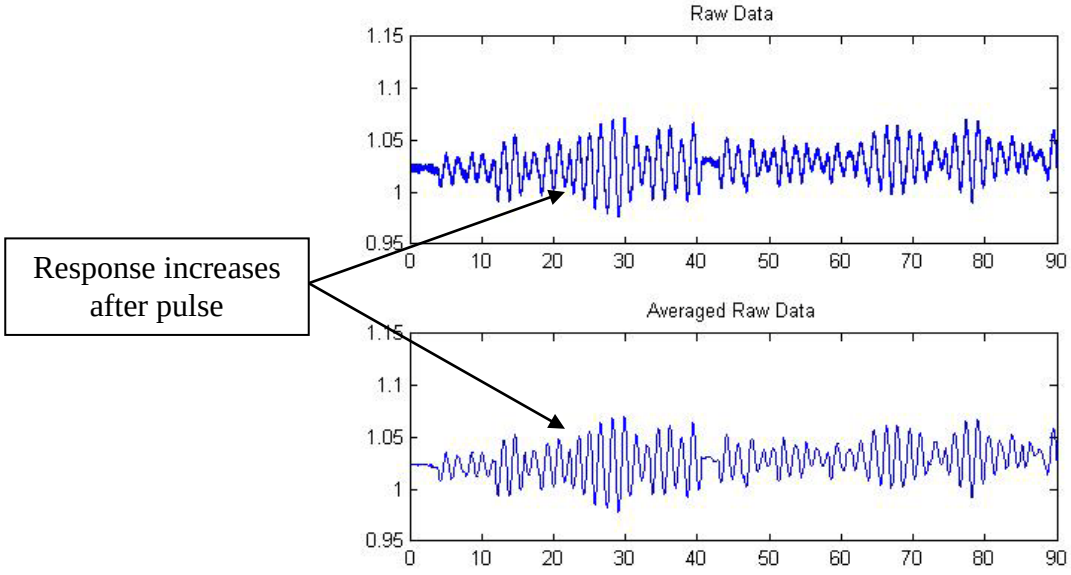

Figure 58 50 mHz Torsional Balance Response

The excited frequencies in the arm response become apparent by conducting a Fourier transform of the data from the time domain to the frequency domain. Again, MatLab provide the necessary tools to complete the transform of the data. The resulting

graphs show the frequencies present in the response of the arm, for a thruster after 100 shots. Figure 45-Figure 47 shows the frequency response during the 500 mHz, 100 mHz and 50 mHz test runs.

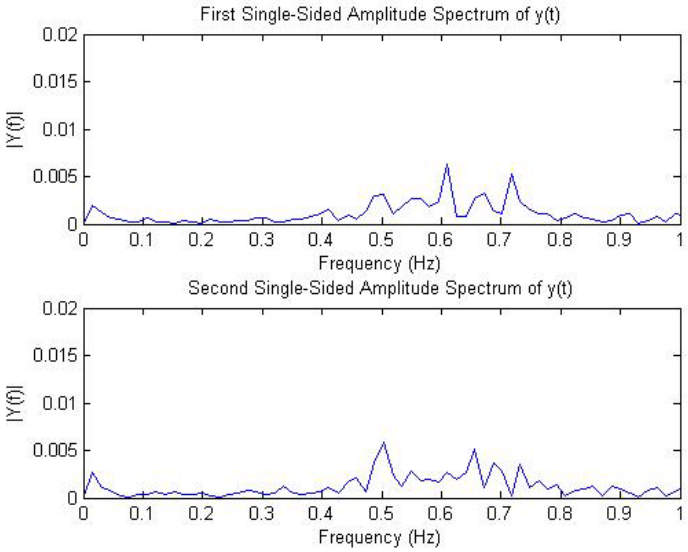

Figure 59 FFT Response for two 500 mHz test runs

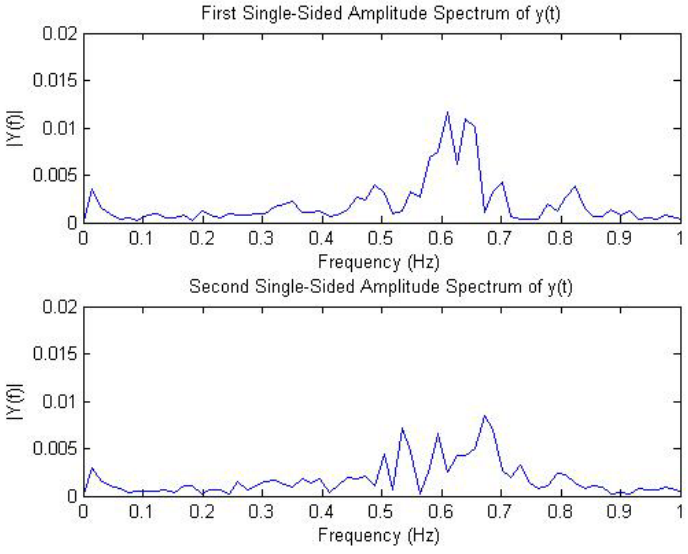

Figure 60 FFT Response for two 100 mHz test runs

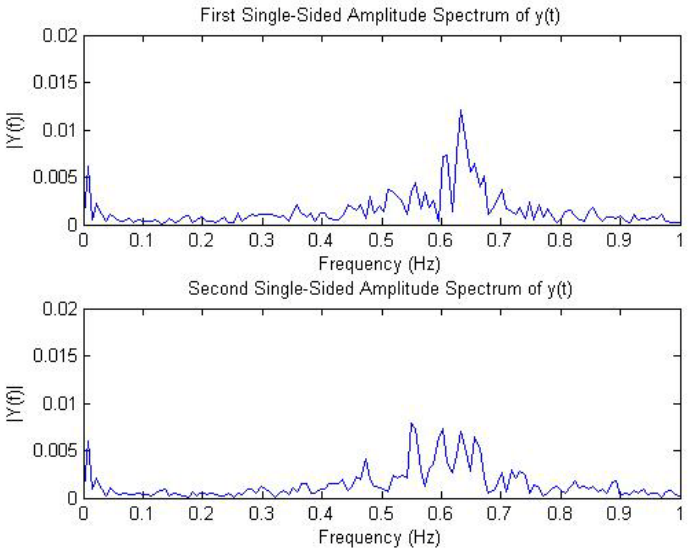

Figure 61 FFT Response for two 50 mHz test runs

The firing frequency of the thruster causes the spikes seen at 500 mHz in Figure 38 and a small spike at 50 mHz in Figure 40. The frequency response of the stand to the 100 mHz firing rate does not have a spike in the correct spot. A very small spike can be seen at about 200 mHz. However, the main spikes to notice are not the firing frequencies, but the other spikes in the response. The stand experiences other, stronger frequencies. A very low frequency of around 10 mHz appears in every file, as does several frequencies from 500 mHz to 600 mHz, except in the calibration file. The 10 mHz frequency is an input from the environment and not from the thrusters, since it is present even when the thruster is not firing. The turbo pump provides the only input to the stand during the calibration runs. However, 10 mHz is too low of a frequency for the spinning of the turbo pump. A third unidentified peak, seen in every data file, provides a better option for the turbo pump, seen in Figure 41.

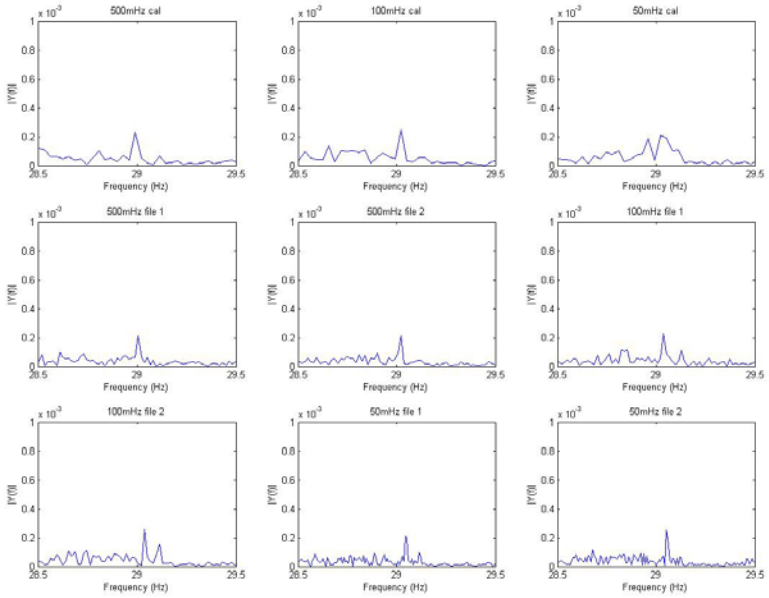

Figure 62 FFT response of each file at 29 Hz

The high speed of the turbo pump will impart a high frequency response into the stand. Either the 29 Hz response seen in Figure 48 is most likely the frequency of the turbo pump or a harmonic thereof.

The thruster must cause 500-600 mHz responses since they are not present in the calibration file. The natural frequency of the stand is very likely the 10 mHz frequency. The 500 mHz, 100 mHz and 50 mHz frequencies providing excitation of the natural frequency caused a growing harmonic response in the arm. The original method to determine force relied on the resulting amplitude from the pulse to be the actual force from the pulse. However, this growing response in the arm, due to the repeated firing of the thruster, invalidates the original method to determine the force.

IV.3.2.2 Equation of Motion Analysis

The equation of motion method for determining the force requires finding the response of the arm to the repeated firings by using the equation of motion for a mass-spring-damper[15], Eq. 29.

$$\theta'' + C\theta' + \omega^2\theta = \sum F(t) \qquad \text{Eq. 29}$$

Where: $\theta = motion\ of\ arm\ in\ radians$
$C = Dampening\ Coefficient$
$\omega = Natural\ Frequency$
$F(t) = Forcing\ Function$

The forcing function in this case is a summation of each firing of the thruster. The dampening coefficient is the amount the arm resists the motion caused by the force due to the stiffness of the springs. The square of the natural frequency is a function of the spring stiffness and the mass of the arm and thruster system. The equations of motion can be solved to provide a model of the system response. Using a numerical solver provided by Mathematica, the model forms the solution for the system response. Several inputs provide the required data to solve the equations of motion, to include the force of each pulse, when the pulse occurs, the natural frequency and the dampening coefficient. However, determining these inputs is the goal of the model. Feeding the data file into the numerical solver, instead of the initial conditions, and attempts to fit the model to the given data. Initial guess for the forces, natural frequency, dampening and pulse time provide a starting point for the solver to step from to find a more exact result.

Before the solver creates the model, the data files require conversion from volts to radians. In certain files, the data showed the thruster mis-firing and producing a larger

voltage change than expected. The large motion range caused the electrode on the arm to impact the calibration electrode, as seen in Figure 47.

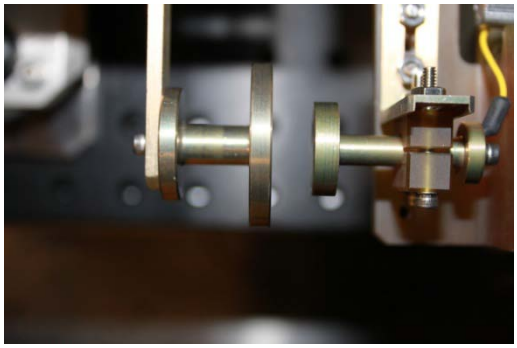

Figure 63 Electrodes on Torsional Balance

The electrodes separation distance is 1 mm, leading to the conversion factor of .4 V/mm. With the distance from the electrode on the arm and the LDS tip to the central axis both known, simple trigonometry gives the angle at the point where the electrodes meet. By combining ratios gives the conversion from volts to radians.

$$A_r = \frac{r_{LDS}}{r_t}$$

$$R = \frac{.4V}{.001m}$$

$$\theta = \frac{l}{r}$$

$$\theta = \frac{\left(\frac{V_{LDS}R}{A_r}\right)}{r_{LDS}} \qquad \text{Eq. 30}$$

A_r= ratio of LDS and Thruster radii
r_{LDS} = radius to LDS tip (m)
r_t = radius to Thruster (m)
R = Given ratio for arm movement to distance moved (V/m)
θ = Angle of arm movement (rad)
V_{LDS} = Measured Voltage (V)

By multiplying the averaged voltage data file by the conversion ratio from into a new array, forming a new data file describing the motion of the arm in radians rather than voltage. Feeding the new file into the Mathematica code provides the data for the model to attempt to match.

The solver steps through the model by preset time steps. At each location the solver attempts to fit the equation of motion to the data provided. The solver uses guessed times for each pulse to determine when the actual pulse occurred and what the force required to match the change in velocity (θ') and the acceleration (θ'') of the response. By iterating dampening coefficient and natural frequency, the solver attempts to slowly approach the actual solution.

IV.3.2.3 Equation of Motion with Single Pulse

The method described above, involves a large number of unknowns for the solver to find. With the large number of unknowns, the possibility the model will diverge increases. In addition, often problems with numerous unknowns can have multiple solutions. However, if the model concentrates on the response due to one pulse, reducing the number of unknowns drastically, the possibility for a single result increases. Given guesses for the initial position, θ, velocity, θ', and acceleration, θ'', of the arm to match the response of the balance to pulses previous to the chosen pulse. The solver tries to match the equation of motion to the data of the chosen pulse by adjusting the initial conditions, the force from the thruster, the dampening coefficient and the natural frequency. The output of the solver gives the input force from the thruster for this pulse. Figure 51 shows the output of the new solver matching a single pulse by estimating the initial conditions to include the force.

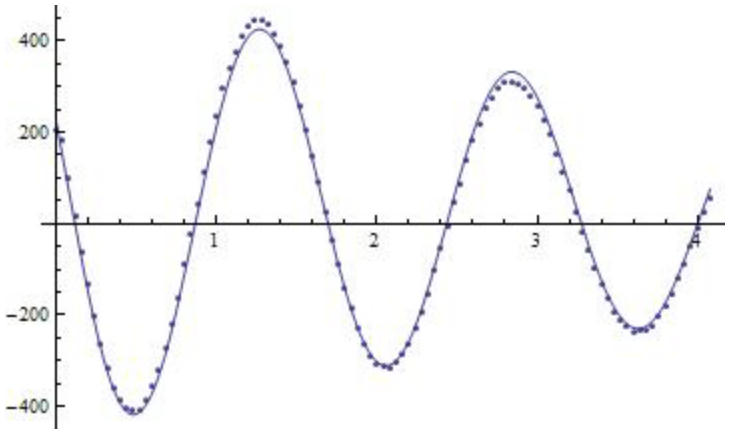

Figure 64 Sample solver response (solid line) fitted to the data (dotted line)

With this method, automation is not possible. The researcher finds the location of a pulse in the file, cuts down the data file to just the length and location of the pulse, and then guesses the initial conditions. To get a statistically accurate result, the solver must generate a result for several pulses. The final method also removes any attachment to the firing frequency greatly reducing the complexity of the analysis. However, the single-pulse method requires a long response to an input force to work. The 500 mHz data files, with a pulse every two seconds, does not give a long enough response for the solver to find a single solution to match the data, because the response is only a single peak. The single-pulse method reduces the complexity of solving for the force, but cuts down on the amount of available data to analyze.

IV.3.2.4 Matching the solution to actual results

The solver is finding the characteristics of the stand to match the data measured from the response. The actual values are already known. By placing the known values into the equation, the force can be found to match these conditions. The found force gives the appropriate order of magnitude for the force of the thruster. In this case, the

data resolved from the single-pulse method is an order of magnitude larger than the actual force level. The resolved forces are multiplied by .1 to retrieve the actual force value. The data shows the response of the arm, the time for the arm's response to travel one period, as approximately 1.5 seconds or .66 Hz. Using the known information of the balance, the torsional spring constant, μ, and the moment of inertia, I, the solver finds the dampening coefficient, Γ. Placing the given values into Eq. 31 gives the calculated frequency response, w_r.

$$w_r = \sqrt{\frac{\mu}{I} - \frac{\Gamma^2}{4}} \qquad \text{Eq. 31}$$

The calculated response is .65 Hz, closely matching the measured results. The solver accurately determined the response of the arm to the given impulse increasing the confidence of the results.

IV.3.3 Thrust Data

The single-pulse analysis provided the tool to glean the thrust data from the response of the arm. Single pulses located in the data files for each data point provided several thrust measurements. For each data point, out of over 200 pulses, at most nine and at least three pulses were clean enough for the analysis method to work, and a thrust value returned by the solver. However, due to the small sample size and error in the solver, the standard deviation for each data point is rather large. Table 9 shows the thrust and standard deviation found at each data point.

Table 9 Lifetime Thrust and Standard Deviation

Shots	0	1000	2500	5000	10000	15000	20000	25000	30000	35000

Thrust	195.40	215.92	180.27	152.83	163.08	186.15	178.16	188.18	158.86	191.73
Standard Deviation	14.20	18.58	47.01	58.11	10.30	30.27	20.44	15.61	12.09	7.41

Shown in Fig the thrust drops during the early part of the life of the thruster and then levels off after 15,000 pulses. However, taking into account the standard deviation of the points the thrust stays relatively constant during the entire lifetime of the thruster.

Work done at AFRL by Dr Spanjers, shows the thrust of the PPT stays constant throughout the life of the thruster[9]. Comparing with the μPPT, the thrust also stays constant throughout the life of the thruster, within the standard deviation of the thruster. When a trend line is fitted to the μPPT data, a line with almost no slope, only -.0003 over 35,000 pulses and a value of 184.87 μN.

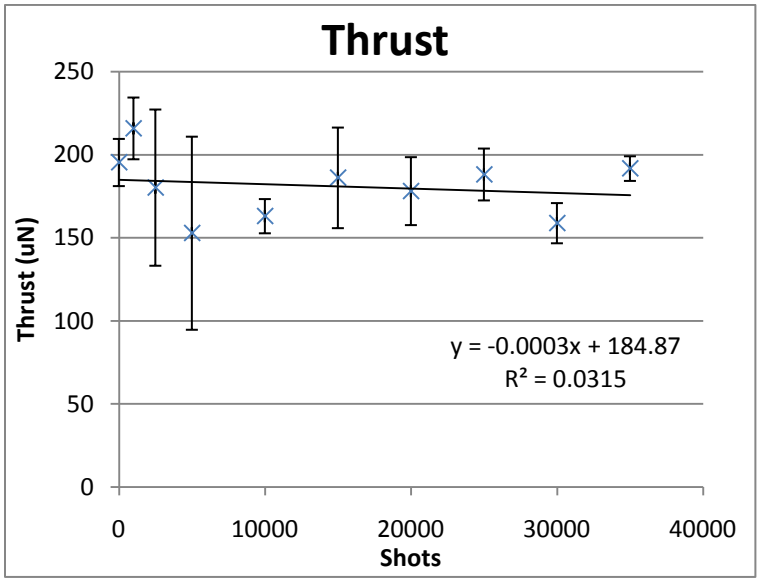

Figure 65 Thrust of μPPT

The constant thrust of the μPPT is interesting since the mass loss rate is changing throughout the lifetime of the thruster. The result implies the spark ionizes the same amount of propellant throughout the lifetime of the thruster. The amount of ablated but

non-ionized propellant and the dispersed particulates must account for the change in the mass loss rate. The result means the propellant efficiency, calculated previously, is not completely accurate. The collection bowl did not capture all of the non-ionized materials thrown off by the thruster. The large particulates account for most of the mass in the collection bowl. Both copper from the electrodes and pieces of the propellant form the particulates. However, some portion of the ablated propellant is not ionized. The collection bowl does not capture the vapor, rather likely sucked out of the chamber by the pumps. The propellant efficiency calculated earlier is therefore not fully accurate. The arc is still ionizing the same amount of propellant, no matter how much is ablated elsewhere, or particulates emitted.

IV.4 Total Efficiency

Comparing the input power to the power outputted by the thruster gives the total efficiency of the thruster. The circuit configuration gives the input power. The output power is a function of the thrust and the mass flow rate, both already measured. The mass flow is the amount of mass lost divided by the number of pulses, giving the mass flow as kg/discharge. Eq. 30 gives the total efficiency, η_t, of the thruster based on the input voltage, V_o, and capacitance, C, along with the thrust, T, fire rate, ν, and mass flow rate, $\dot{m}$. K is a constant to convert CV_o^2 into power.

$$\eta_t = \frac{T^2}{K\dot{m}\nu CV_o^2} \qquad \text{Eq. 30}$$

The mass flow rate from the mass collection experiment, the thrust from the torsional balance and the circuit design give the total efficiency of the thruster at several

points during the lifetime of the thruster. The data points, shown in Table 10, show the efficiency falling drastically during the lifetime of the thruster.

Table 10 Total Efficiency of the μPPT

Shots	1000	5000	10000	30000
Efficiency (%)	68.63	48.19	48.37	29.35

The thruster continues to produce a constant thrust, however at a greater cost to the propellant and power input into the system.

IV.5 Video Collection

IV.5.1 Camera Operation

The Shimadzu HPV-2 camera was very easy to operate and functioned perfectly for this test. The camera was triggered using the same frequency generator as the trigger circuit guaranteeing that the two would trigger simultaneously. The camera successfully operated at 1 million fps, catching the thruster firing every time.

IV.5.1.1 Lenses and Extension Tubes

The HPV-2 camera came with the 180mm lens, with an adjustable f-stop and manual focus, the lens operated very well. However, the very small image produced by the 180mm lens did not provide as much detail as was wanted. The purchase of a 300mm lens, with adjustable f-stop and manual focus as well, provided the close-up images wanted for the research.

The 9 in and 6 in extension tubes combined into one 15 in extension tube (Figure 43), greatly reducing the placement distance of the new 300mm lens from the chamber.

Without the extension tubes, the camera would have been placed on the other side of a wind tunnel to accommodate the focal length of the lens.

Figure 66 15 in Extension Tube

The extension tubes aided the conduction of the experiment with both lenses, greatly reducing the camera placement distance from the chamber; however, the extension tubes did not improve the magnification of the image.

IV.5.2 Results

IV.5.2.1 Spark formation

As mentioned previously the spark had a tendency to form in the same place. The video also showed the spark forming in one location. However, once the spark formed, it did not always stay in the same spot, especially early on in the life of the thruster. The spark moved a few degrees side to side. On some occasions, the spark even jumped to the other side of the thruster.

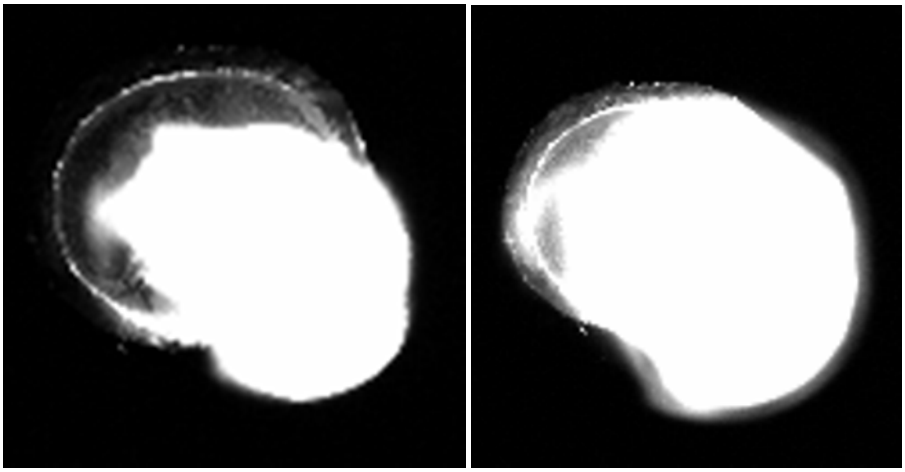

Figure 67 Spark at 20 and 23 μs after ignition

An important effect of the movement of the spark is a possible increase in efficiency. Only the PTFE© vaporized below the spark will be ionized and accelerated. When the spark moves, a better chance exists of ionizing more of the vaporized propellant.

Based on the video, the spark lasted 60-80 μs, though the intensity of the spark did not stay constant, rather it pulsed. The discharge of the capacitor was not even, causing the pulsation in the strength of the spark. This is important to understand as the temperature of the surface PTFE©, as well as the strength of the electric and thus magnetic fields are dependent on the spark. This pulsing can greatly affect the thrust of the device.

At the end of the spark, the thruster throws off large amounts of unionized, heated particulates. As previously discussed, the relatively large particulates do not add to the thrust or I_{sp} of the thruster. Figure 67 shows the thrown off particulates.

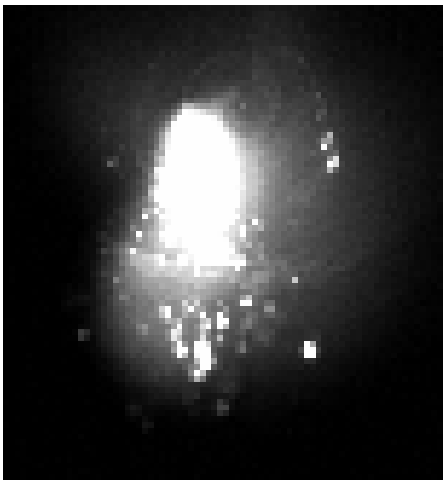

Figure 68 Spark 62 μs after trigger

The end-of-life condition was also interesting. In this condition, the spark did not last as long as at the beginning of life. The total time of the pulse was down to roughly 30-40 μs. In addition, the recurring spark digs a channel and no longer moves but rather stays in one place. One interesting phenomena was seen with the thruster used in the mass loss experiment. The spark dug a very deep channel dug into this thruster, actually eroding the inner electrode down. Due to the inner electrode erosion, the trigger sparked to a different location on the inner electrode and then the spark would "bounce" off and travel down the channel to the outer electrode.

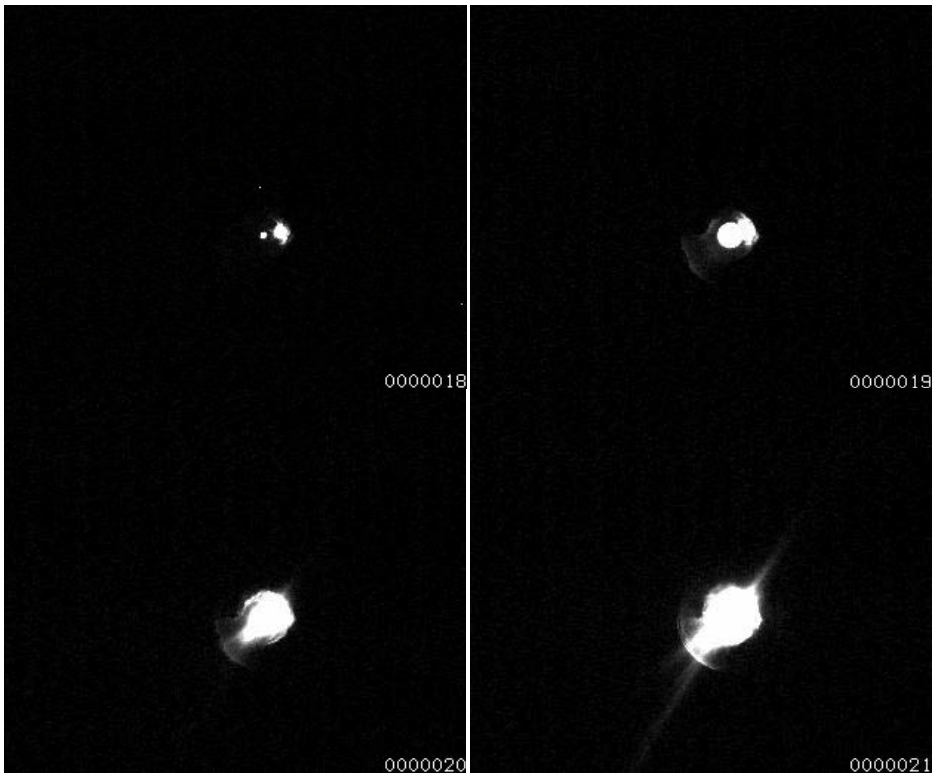

Figure 69 Spark Formation on Mass Collection Thruster

Figure 61 shows the spark formation for the mass collection thruster. In frame 18, the spark is forming to the right of the central electrode. The spark formation of the trigger is seen in frame 19. The spark is building up a large amount of plasma on the right side of the thruster. The plasma bounces off the inner electrode and the right side and flows back to the left, frame 20. The location of the plasma flow is the channel dug by the spark discussed earlier. In frame 21, spark formation is complete over the channel already dug.

Although, the spark no longer moves on the older thruster, unlike the brand new thruster, the release of particulates is still present at the end of a pulse. In Fig, the thruster emits the particulates at the very end of the pulse.

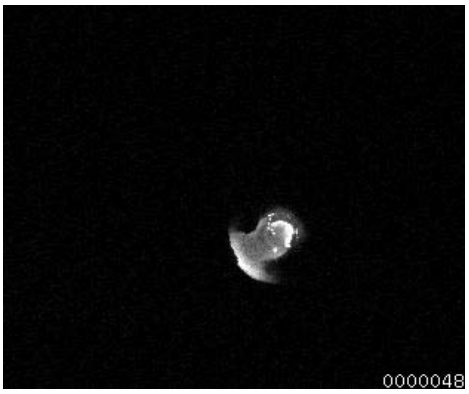

Figure 70 Particulate emission near end-of-life

Overall, the spark formation on the tip of the thruster relies on several different conditions. The shape of the tip of the thruster, the condition of the electrodes, and the voltage applied all change how the spark forms and then acts during operation. Predicting how the spark will form and move during the pulse is very difficult. The condition of the thruster tip is in a constant state of flux as the spark continually shapes the surface.

V. Conclusions and Recommendations

V.1 Thruster Operation

Overall, the thruster performed well, but nowhere near as expected. The objective was to fire the thruster for 100,000 shots, however, the thruster could only reach 36,000 shots before becoming uncontrollable and eventually no longer operating. Further research needs to be conducted to see if the operational limits are really this low or if there were other contributing factors.

To determine this, research is required to find the perfect energy operation level. In this experiment, the energy level was about 2J, and on several occasions charring occurred on the tip of the thruster. A lower energy may reduce this charring and allow for a longer life, but too low and the thruster will not fire at all. In addition, the frequency of firing may be important. The previous research was done at a higher frequency, 2Hz and higher[13], than used in these experiments. A higher frequency would keep the PTFE and the electrodes hotter. Hotter PTFE leads to a higher efficiency and the electron breakdown voltage is easier to reach on hotter electrodes as the electrons are already excited. Firing at a higher energy level and lower frequency, may have damaged the thruster, leading to a shorter operating life. Further research to find the right frequency at the right energy level is required to find the perfect operating conditions combining these two factors.

As discussed in Chapter 4, spark formation and stability is a large unknown in this system, yet is vital to understanding how the propellant is ionized. The images of the spark formation are vital to begin this understanding. The spark is not stationary and

forms randomly based on the current condition of the thruster, although it eventually will tend to form in one spot, following the path of least resistance. As the condition of the thruster tip deteriorated, the length of the pulse decreased.

A better understanding how and why the spark forms where it does may eventually allow control over the spark forcing the spark to form in different areas each time, greatly improving the efficiency and the life of the thruster. By forcing the spark to form over all parts of the surface of the thruster periodically, then the propellant can be ablated evenly and also the ill effects of a channel can be avoided.

Also, more work needs to be done to improve the operating circuit of the outer electrode. The pulsing of the spark can greatly reduce the amount of thrust and the efficiency of the thruster. A circuit that has a solid discharge is needed to ensure the highest efficiency of operation of the thruster.

V.2 Thruster Performance

This research performed in-depth studies of the lifetime performance characteristics of the μPPT. Ultimately, the thruster efficiency determines the performance of the thruster. Finding the efficiency requires first finding the mass loss and thrust of the μPPT. Separate experiments measured the mass loss and thrust.

The mass loss experiment performed two functions, measuring both the thruster mass loss, giving the mass flow rate of the thruster, as well as finding the mass of the particulates thrown off by the thruster. The measurements taken showed the thruster apparently ionizes the ablated mass very efficiently, although later results show flaws in this statement. The thruster showed a propellant efficiency over 95% for the measured

pulses early in life, but falling to below 85% by the end-of-life of the thruster. In addition, the measurements showed the μPPT has a very short warm-up period. The warm-up period of the μPPT is the same length as the PPT. However, during the warm-up period, the mass loss rate of the μPPT is higher than during normal operation of the thruster, whereas the PPT's mass loss rate during the warm-up period was lower than during normal operation. In addition, the PPT showed a constant mass loss rate during normal operation. The μPPT, on the other hand, saw a power law drop in the mass loss rate. The drop continued until reaching the end-of-life conditions. As the thruster ceased operating, the mass loss rate jumped to almost twice the value during the warm-up period.

The thrust gives the other component required to find the efficiency of the thruster. A second experiment was conducted to find the thrust of the μPPT. A micro-Newton Torsional Thrust Stand, designed by Busek Co Inc, provided the perfect setup for the test. Although the response of the stand added difficulty to finding the actual thrust, a method was found by resolving the equations of motion for a single pulse within a file. Using the single-pulse method, although giving good data, proved difficult to implement. The method could not by automated and only gave a handful of data points out of the almost 200 available, especially since the 500 mHz files did not give any useful data for the single pulse method. Pushing past the difficulty of the measurements, thrust data gleaned from the data showed slight variations in the thrust during the lifetime of the thruster. However, with the error included, the thrust is effectively constant throughout the lifetime of the thruster. The constant thrust discounts the propellant efficiency calculated earlier. The thrust should change as the amount of mass loss by the thruster,

but not collected by the collection bowl, changes. The constant thrust, however, means an amount of the propellant is ablated, but not ionized, and lost to the system, most likely through the turbo pump.

V.3 Video Collection

The results of the video collection showed the spark formation and behavior during a pulse. The spark behaved erratically during the pulse. The spark formed randomly on the face of the thruster. The location determined by imperfections in the shape or condition of the surface. As the thruster progressed towards the end-of-life, the spark formed more consistently in one sport, digging a channel in the location. The channel provided less resistance to spark formation during the next pulse, making the spark form in the same location.

The spark did not cover the entire face of the thruster. It is very likely much of the surface of the propellant reached sufficient temperature to ablate some PTFE. However, ionization of the PTFE only occurs below the spark, producing thrust. The rest of the ablated propellant is lost to the system, and not collected by the bowl under the thruster, as shown by the other experiments.

V.4 Contamination

An important objective of this research was to qualitatively quantify the contamination of the satellite due to the thruster. As can be seen in the mass loss experiment, the thruster only emits a very small amount of mass as particulates that could contaminate the satellite. If the thruster is placed near a solar panel for instance, it will not take long for the solar panel to become coated in a thin layer, hampering its

effectiveness. For operational use it is best if the μPPT is placed in a location to minimize any possible contamination of sensors or solar panels.

Future research conducted on μPPTs will require a study on the effect of the μPPT on the satellite. A test with a μPPT firing near and in different relative positions in relation to the solar panels and other sensitive equipment will give more knowledge on the actual effect of μPPT contamination on the satellite.

V.5 Test Recommendations

V.5.1 Vacuum Chambers

Overall, the tests went according to the test plan laid out in Chapter 3. However as noted there and in Chapter 4, several issues arose from the operation of the chambers. The LACO chamber needs a new control card for the LabView system that operates the chamber. A lot of frustration and lost time occurred by continually having to restart the computer. In addition, a better pressure gauge is needed for this chamber. The ion gauge is very accurate, yet it breaks far too often. The chamber requires either a more reliable ion gauge or a new pressure system.

The TVAC chamber needs some modification to improve its performance. The turbo pump and the chamber require a high-vacuum valve between them. When the turbo pump is off, an internal valve opens to atmosphere. A work-around works to close the valve, since without the high-vacuum valve the roughing pump reaches 1 torr and stalls as it is pulling in air from the room into the chamber and then pumping it back out. In addition, the turbo pump on the chamber is extremely small and thus takes several hours to get the chamber down to the required pressure. A larger pump more suited to

the size of the chamber could greatly reduce the time to reach vacuum. The chamber also does have a leak, the chamber cannot hold a pressure for very long without the pumps on. A quick data collection showed that within 20 min the pressure had risen more than one order of magnitude, without the pumps or anything operating in the chamber. For most users of this chamber, the pumps do not need to be turned off, however for the few occasions when the experiment needs low vibration and both pumps are turned off it needs to hold pressure longer.

The chamber was thoroughly checked for leaks and no obvious leaks were found. Most likely there is a leak in a valve or in the several feed lines to the chamber. A possible crack in a weld is a possibility and could create significant repair costs.

V.5.2 Test Equipment

V.5.2.1 Torsional Balance

The torsional balance provided a lot of good data, but improvements can be made to the stand, data collection and the analysis.

The balance itself is very difficult to calibrate. Better placement inside the chamber will help some when calibrating the electrodes to a 1 mm separation distance. The main issue with the calibration though, is not the getting this distance, but rather getting the right response from the balance when the calibration voltage is applied. Calibration attempts in this research were made with a constant force from a 100V power supply. However to better calibrate the balance for the pulse of the thruster; the voltage needs to be applied as a pulse with a similar pulse width as the thruster. In addition,

100V does not apply a large enough force for the motion to show over the noise of the stand. Busek recommends a voltage of 800V for future calibrations of the balance.

Knowing more about the functioning of the LDS can improve the data collection and calibration of the balance. In this research, the tip was roughly placed 1 mm from the reflecting mirror. This distance needs to be better known and more consistent in the operation. A large amount of data was collected in this research at 500Hz for runs times of 30, 60 and 90 seconds. However, smoothing the data by averaging every 25 points, reduces the amount of data. Running the experiments at a much higher sample rate should increase the resolution of the data after completing the averaging.

Analyzing the data from the thrust balance proved to be the most difficult part of these experiments. The tests done attempted to find the thrust of an individual pulse rather than the thrust of continuous high frequency operation. A problem arose from the response of the stand from a previous pulse interfering with the response from the next pulse. The interference meant the established methodology of resolving forces from the balance could not be used and the equations of motion had to be resolved as previously discussed in Chapter 4. Either future research is needed to find a way to measure the thrust, or the response of the balance to a single pulse needs to be better understood in order to find a frequency for the thruster to fire at so the pulses do not interfere with each other.

Interference from one pulse to the next was not the only problem seen. The balance has a very interesting frequency response. It has a natural frequency around 28Hz. Also, when the thruster is fired at 500mHz, 100mHz and 50mHz a response can be seen around 550-600mHz and grows for the lower frequency. A better understanding

of the response of the balance provides more information about the implications to the measured thrust and resulting error. A more detailed study of the frequency response of the balance overall can help determine the right frequency to test at, so as not to hit the natural frequency or any of the harmonics of the stand.

V.5.2.2 Scale

The scale used in the mass loss experiment only read to the fourth decimal. This was not sensitive enough to capture the weight difference of the collection bowl during low pulse number data runs. A more accurate scale can better define the curve of the mass gained and improve the knowledge of the efficiency of the thruster.

V.5.3 9 μPPT Multi-Emitter

The 9 μPPT Micro-Emitter provides the next step in μPPT technology. The Micro-Emitter uses 9 μPPTs fired in sequence to produce a quasi-constant force. The emitter has the potential to greatly improve the performance over the current deployment of a single μPPT. By using 9 μPPTs, the emitter provides more propellant and possibly higher thrust potential with the ability to fire more than one thruster at a time.

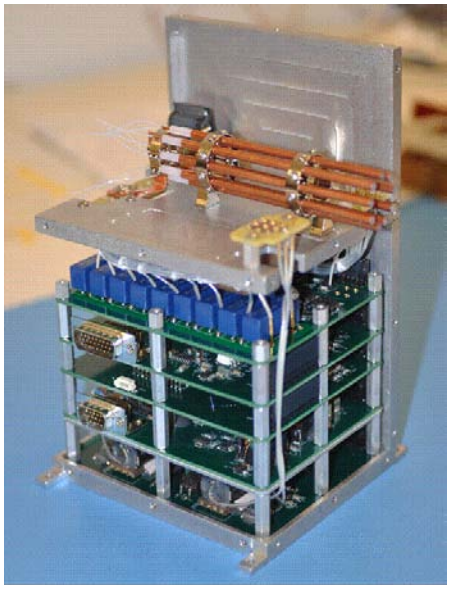

Figure 71 9 μPPT Multi-Emitter

However, the new emitter, based on previous research on single μPPTs, must undergo several tests to characterize the performance of the emitter. The contamination potential of one thruster on another, although unlikely, needs further study. In addition, as seen in this research, the lifetime of the thruster seems to decrease when the thruster is fired at lower frequencies. With the 9 μPPTs fired in sequence, the frequency each thruster fires at is only 1/9 of the actual frequency. Each thruster may actually have a shorter lifetime than one fired continuously at the same frequency as the emitter.

The 9 μPPT Multi-Emitter may lead to new options for small satellite space propulsion, but the emitter requires more research to determine the performance characteristics it possesses.

V.6 Conclusion

The μPPT is a very complex and interesting propulsive device that will allow smaller satellites to successfully complete missions that are more complex. Based on the

research completed here, more research and development is required to improve the efficiency and the reliability of the thruster. Currently the inefficiency of the thruster makes it unattractive to program managers, but with further study in spark formation, proper firing conditions (energy level and frequency) this efficiency can be greatly improved. The reliability of the thruster is also a concern. As seen in this and other research the lifetime of the thruster can greatly vary based on operation conditions and construction of the thruster. More work in these areas can make this thruster more reliable, greatly improving mission success. A major concern is also satellite contamination. The μPPT has the potential to contaminate the surfaces around it with a thin film of PTFE©. Proper placement on the satellite greatly reduces the impact on the satellite and its mission.

Overall, the μPPT can prove to be a valuable resource as the industry moves to smaller and more complex satellites. However, further research is required to fully understand the operation and operational limits of this device.

VI. Appendix A

Thruster Construction

Two different types of thrusters were built for the research conducted. One type, built here at AFIT, required more construction than the μPPTs obtained from AFRL and Busek. The instructions below first describe how to build the μPPT from two different tubes and then moves on to striping the wires and connecting the wires, which applies to both type of thrusters.

A few tools are required to complete the construction of the thrusters, listed below:

- Dremel tool with metal cutting tip
- Wire stripper
- Soldering equipment
- Pliers

Two sizes of tubes were ordered to build the thruster, pictured in Fig.

1. Remove central electrode from large tube
    a. The Dremel is used to cut through the outer copper tube*
    b. Use the pliers to pull the tube casing off the thruster.
    c. Cut through the PTFE* to the central electrode and remove
    d. Remove the central electrode from the large tube
        i. Place the large tube in a 200 deg F oven for 20 min to loosen the PTFE.
2. Prepare trigger tube for placement in the larger tube

    a. Remove the casing on the smaller tube* with the wirecutters
    b. Cut through the PTFE to the central electrode* and remove
3. Slide the trigger tube into the hole of the larger tube
    a. If difficulty arise, reheat the larger tube

For the pre-built thruster, much of the same procedures are followed.

1. The Dremel is used to cut through the outer copper tube*
2. Use the pliers to pull the tube casing off the thruster.
3. Cut through the PTFE* to the central electrode and remove
4. Remove the copper on the central electrode* with wirecutters
5. Cut through the PTFE to the central electrode* and remove

*When cutting down the copper and PTFE, great care must be taken to ensure the proper spacing between connection points is being left to prevent arcing. Enough PTFE should be left between all the copper electrodes, at least ½". The copper needs to be larger enough to solder the wires on later.

Now both thrusters are ready to have the wires connected.

1. Solder wires to the outer and inner electrodes.
2. Twist the central electrode with the wire to form the connection
    a. The central electrode should not be soldered! The wire is too thin and will break from the heat!
3. Coat connections and area between with Super Corona Dope.

a. Corona Dope is a liquid dielectric that, when dry, provides insulation up to 3000 V/mil. At least 3 mil needs to be applied for sufficient protection from arcing. When using Corona Dope there is one simple rule, more is better.

The thruster is now ready for use!

VII. Appendix B

LACO Operation

The LACO tank is computer controlled, requiring minimal input from the user.

To Pump down the chamber:

1. Close the door and all three clamps
2. Open LabView Program
    a. Roughing pump will start automatically pumping down foreline
    b. Turbo pump begins warm-up
    c. If Labview already open press the “Reset” button on the “Shutdown” Tab
        i. Will reset program and start process above
3. When the foreline reaches pressure and turbo pump is ready, the following notice will appear in the message window, “Turbo Pump Ready”
    a. Click the “Start” button on the main page
4. Chamber will complete pumping down with no further input from the user.

To vent the chamber:

1. Press “Stop & Vent” button on main page
    a. Vent valve will open, pumps will turn off automatically
2. Open door clamps
3. When door opens press “Shutdown” button
    a. Closes all valves
    b. Located on “Shutdown” tab

VIII. Appendix C

TVAC Operation

The TVAC is a very complex vacuum chamber that is not fully automated. The procedures below explain the proper operation.

To pump down the chamber:

1. Close the door and tighten door clamps
2. Ensure Turbo Pump valve is plugged in
3. Ensure Valve FV10 and FV02 (both on the screen and the manual valve if still in place) are closed
4. Turn on the roughing pump
5. Open FV06
6. Wait for chamber to reach 10^{-2} torr
7. Turn on the water cooling for the turbo pump
8. Close FV06
9. Turn on the Turbo Pump
10. Open FV02
    a. If the manual valve is still in place, do not open the valve ont eh computer screen! Leave the FV02 on the screen closed and open the manual valve only.
    b. If the manual valve has been replaced, open FV02 normally
11. Chamber will take several hours to pump down

12. If the gauge reads around $7x10^{-3}$ torr for an extended period of time, the gauge has frozen
    a. Remove the connection on top of the gauge to turn it off
    b. Replace the connection and wait for gauge to reboot. The gauge should now read the correct pressure
13. Remove the door clamps
    a. Ensures the door will not break the clamps or get stuck during venting

To Vent the Chamber:

1. Turn off both the turbo pump
2. Close FV02, either manually or on the computer as required
3. Turn off the roughing pumps
4. Unplug the turbo pump valve
5. Open FV10
6. The Nitrogen can be controlled using the dial on the chamber
7. Wait for chamber door to open
8. Close FV10
9. Plug in turbo pump valve

*When venting the second compressor on the Nitrogen generator system needs to be turned on. After venting has completed and the tanks have returned to normal pressure, the second generator should be turned off.

Bibliography

[1] Humble, Ronald W., Gary N. Henry, Wiley J. Larson, "Space Propulsion Analysis and Design", New York, New York: McGraw-Hill Companies Inc, 1995

[2] http://www.nasa.gov/centers/glenn/about/fs23grc.html

[3] Bong Wie, David Murphy, "MicroPPT-Based Secondary/Backup ACS for a 160-m, 450-kg Solar Sail Spacecraft", 41st AIAA/ASME/SAE/ASEE Joint Propulsion Conference & Exhibit 10 - 13 July 2005, Tucson, Arizona

[4] Gregory G. Spanjers, Daron R. Bromaghim, Capt. James Lake, Michael Dulligan, David White, John H. Schilling, Stewart Bushman, Erik L. Antonsen, Rodney L. Burton, Michael Keidar, Iain D. Boyd. "AFRL MicroPPT Development for Small Spacecraft Propulsion", 38th AIAA/ASME/SAE/ASEE Joint Propulsion Conference & Exhibit 7-10 July 2002, Indianapolis, Indiana

[5] Mesyats, G. A. (2005). *Pulsed Power*. New York, New York: Springer Science+Business Media.

[6] Bluhm, H. (2006). *Pulsed Power Systems*. Heidelberg, Germany: Springer.

[7] Jahn, Robert G. (1996). *Physics of Electric Propulsion*. Mineola, New York: Dover Publications, Inc.

[8] Rodney L. Burton, Michael J. Wilson, Stewart S. Bushman. "Energy Balance and Efficiency of the Pulsed Plasma Thruster"

[9] Gregory G. Spanjers, Jamie B. Malak, Robert Lieweke and Ronald A. Spores. "The Effect of Propellant Temperature on Efficiency in the Pulsed Plasma Thruster",

[10] Erik L. Antonsen, Rodney L. Burton, Garret A. Reed, Gregory G. Spanjers. "Effects of Postpulse Surface Temperature on Micropulsed Plasma Thruster Operation", 40th Joint Propulsion Conference 10-14 July 2004, Ft Lauderdale, Florida

[11] Gregory G. Spanjers, Jason S. Lotspeich, Keith A. McFall, and Ronald Spores. "Propellant Losses Because of Particulate Emission in a pulsed Plasma Thruster", Journal of Propulsion and Power, Vol 14, No. 4, July-August 1998

[12] Seo Myeongkyo and Richard D Branam, "Characterizing the Exhaust Plume of the Three-Electrode Micro Pulsed Plasma Thruster", Master's Thesis, AFIT, 2009

[13] M. Gamero-Castano, "A Torsional Balance for the Characterization of Micro Newton Thrusters," Rev. Sci. Inst. 74 (10): 4509-4514, Oct. 2003.

[14] Pasachoff, Jay; Wolfson, Richard, "Physics for Scientists and Engineers", Reading, Massachusetts: Addison-Wesley, 1999

[15] Meirovitch, Leonard, "Fundamentals of Vibrations", McGraw-Hill, 2000

REPORT DOCUMENTATION PAGE

Form Approved
OMB No. 074-0188

1. REPORT DATE *(DD-MM-YYYY)*	**2. REPORT TYPE**	**3. DATES COVERED** *(From – To)*
25-03-2010	Master's Thesis	May 2008 – March 2010

4. TITLE AND SUBTITLE

Thrust and Performance Study of Micro Pulsed Plasma Thrusters

5a. CONTRACT NUMBER

5b. GRANT NUMBER

5c. PROGRAM ELEMENT NUMBER

6. AUTHOR(S)

Selstrom, Jeremy J., Captain, USAF

5d. PROJECT NUMBER

5e. TASK NUMBER

5f. WORK UNIT NUMBER

7. PERFORMING ORGANIZATION NAMES(S) AND ADDRESS(S)

Air Force Institute of Technology
Graduate School of Engineering and Management (AFIT/EN)
2950 Hobson Way, Building 640
WPAFB OH 45433-8865

8. PERFORMING ORGANIZATION REPORT NUMBER

AFIT/GAE/ENY/10-M21

9. SPONSORING/MONITORING AGENCY NAME(S) AND ADDRESS(ES)

Dr. William A. Hargus, Jr
(661)275-6799
william.hargus@edwards.af.mil
AFRL Propulsion Directorate, Edwards AFB, CA 93524

10. SPONSOR/MONITOR'S ACRONYM(S)

11. SPONSOR/MONITOR'S REPORT NUMBER(S)

12. DISTRIBUTION/AVAILABILITY STATEMENT

APPROVED FOR PUBLIC RELEASE; DISTRIBUTION UNLIMITED.

13. SUPPLEMENTARY NOTES

14. ABSTRACT

This research is focused on several areas of the µPPT performance. An important idea studied is the effect of lifetime use on the performance. The thruster is fired for a simulated lifetime of use to see if there is an impact on the thrust of the thruster later in life. Also vital is the efficiency of the thruster. A µPPT performing at max efficiency will ionize all ablated material; however, we know that not to be the case. In this research the effort is made to collect these non-ionized particles in order to measure their mass post-test. With this collected mass and a knowledge of how much the thruster has ablated, it can be determined what percentage of the propellant has been ionized. With the non-ionized particles also comes a concern about contamination. Knowing the amount of particles that can collect at the end of a lifetime of use allows a better understanding of what contamination issues a spacecraft may have and what precautions need to be made.

15. SUBJECT TERMS

Three-electrode micro Pulsed Plasma Thruster(PPT), contamination, high speed video, mass collection, thrust, efficiency

16. SECURITY CLASSIFICATION OF:			**17. LIMITATION OF ABSTRACT**	**18. NUMBER OF PAGES**	**19a. NAME OF RESPONSIBLE PERSON**
a. REPORT	**b. ABSTRACT**	**c. THIS PAGE**			Richard Branam, Lt Col, USAF
U	**U**	**U**	**UU**	148	**19b. TELEPHONE NUMBER** *(Include area code)* (937) 255-6565, ext 7485 (Richard.Branam@afit.edu)

Standard Form 298 (Rev. 8-98)
Prescribed by ANSI Std. Z39-18